

ASTROPHYSICAL IMPLICATIONS OF HYPOTHETICAL STABLE TEV-SCALE BLACK HOLES

Steven B. Giddings^{a,1} and Michelangelo L. Mangano^{b,2}

^a *Department of Physics, University of California, Santa Barbara, CA 93106*

^b *PH-TH, CERN, Geneva, Switzerland*

Abstract

We analyze macroscopic effects of TeV-scale black holes, such as could possibly be produced at the LHC, in what is regarded as an extremely hypothetical scenario in which they are stable and, if trapped inside Earth, begin to accrete matter. We examine a wide variety of TeV-scale gravity scenarios, basing the resulting accretion models on first-principles, basic, and well-tested physical laws. These scenarios fall into two classes, depending on whether accretion could have any macroscopic effect on the Earth at times shorter than the Sun's natural lifetime. We argue that cases with such effect at shorter times than the solar lifetime are ruled out, since in these scenarios black holes produced by cosmic rays impinging on much denser white dwarfs and neutron stars would then catalyze their decay on timescales incompatible with their known lifetimes. We also comment on relevant lifetimes for astronomical objects that capture primordial black holes. In short, this study finds no basis for concerns that TeV-scale black holes from the LHC could pose a risk to Earth on time scales shorter than the Earth's natural lifetime. Indeed, conservative arguments based on detailed calculations and the best-available scientific knowledge, including solid astronomical data, conclude, from multiple perspectives, that there is no risk of any significance whatsoever from such black holes.

CERN-PH-TH/2008-025

November 19, 2021

¹giddings@physics.ucsb.edu

²michelangelo.mangano@cern.ch

Contents

| | | |
|----------|--|-----------|
| 1 | Introduction | 4 |
| 2 | Assessment of pre-existing arguments | 7 |
| 2.1 | Instability of microscopic black holes | 7 |
| 2.2 | Cosmic ray collisions on Earth | 8 |
| 3 | Essentials of higher-dimensional gravity | 11 |
| 3.1 | TeV-scale gravity scenarios | 11 |
| 3.2 | Higher-dimensional black holes | 12 |
| 3.2.1 | Schwarzschild solution | 12 |
| 3.2.2 | Black holes in standard compactifications | 13 |
| 3.2.3 | Black holes in warped compactifications | 13 |
| 3.2.4 | A general perspective | 14 |
| 4 | Black hole accretion in Earth | 15 |
| 4.1 | Accretion basics | 15 |
| 4.2 | Subatomic accretion in Earth | 16 |
| 4.2.1 | Competition with electromagnetic binding | 16 |
| 4.2.2 | Subatomic growth laws | 19 |
| 4.2.3 | Timescales for $r_N \lesssim R_{\text{EM}} \lesssim a$ in $D = 6, 7$ | 20 |
| 4.2.4 | Timescales for $r_N \lesssim R_{\text{EM}} \lesssim R_D$ in $D \geq 8$ | 20 |
| 4.2.5 | Timescales for $R_D \lesssim R_{\text{EM}} \lesssim a$ in $D \geq 8$ | 21 |
| 4.3 | Macroscopic accretion, $R_{\text{EM}} \gtrsim a$ | 22 |
| 4.3.1 | Bondi accretion basics | 22 |
| 4.3.2 | Matching microscopic and macroscopic regimes | 23 |
| 4.3.3 | Time evolution with Bondi accretion | 23 |
| 4.3.4 | Macroscopic time scales: $D \geq 8$ | 24 |
| 4.3.5 | Macroscopic time scales, $D = 6, 7$ | 25 |
| 4.4 | Warped evolution | 26 |
| 4.5 | An Eddington limit? | 27 |
| 4.6 | Summary of growth on Earth | 27 |

| | | |
|----------|--|-----------|
| 5 | Stopping of cosmic ray-produced black holes | 28 |
| 5.1 | Production kinematics | 29 |
| 5.2 | Stopping: neutral black holes | 29 |
| 5.2.1 | Accretion slow-down | 30 |
| 5.2.2 | Coulomb slow-down | 31 |
| 5.2.3 | Slow-down to $\gamma \sim 1$ | 32 |
| 5.3 | Stopping in white dwarfs | 33 |
| 5.3.1 | Nonrelativistic stopping | 34 |
| 5.3.2 | Stopping bounds | 35 |
| 6 | Black hole production on white dwarfs | 38 |
| 6.1 | Magnetic screening | 38 |
| 6.2 | Production rates | 39 |
| 7 | Black hole catalysis of white dwarf decay | 41 |
| 7.1 | Subatomic accretion | 41 |
| 7.2 | Bondi accretion | 42 |
| 7.3 | Generalized scenarios | 43 |
| 7.4 | Summary of white dwarf constraints | 44 |
| 8 | Bounds from neutron stars | 45 |
| 8.1 | Production on neutron stars | 45 |
| 8.1.1 | Production in binary systems | 46 |
| 8.1.2 | Production via cosmic neutrinos | 47 |
| 8.2 | Catalysis of neutron star decay | 47 |
| 8.2.1 | Penetration to core | 47 |
| 8.2.2 | Accretion from within a neutron star | 49 |
| 9 | Summary and conclusions | 50 |
| A | Bondi accretion | 54 |
| B | Effects of radiative transport | 57 |
| B.1 | Subatomic regime | 57 |

| | | |
|----------|--|-----------|
| B.2 | Macroscopic accretion | 58 |
| B.2.1 | Radiative effects in white dwarfs | 59 |
| B.2.2 | Radiative effects in Earth | 61 |
| B.2.3 | Radiative effects in neutron stars | 62 |
| B.3 | Eddington evolution | 63 |
| C | Gravitational scattering of relativistic particles in a Schwarzschild field | 65 |
| C.1 | Classical trajectories and capture | 66 |
| C.2 | Quantum capture | 66 |
| C.3 | Coulomb scattering | 67 |
| D | Nonrelativistic accretion checks | 67 |
| E | Black hole production rates | 69 |
| E.1 | Elementary cross sections | 69 |
| E.2 | Black hole production by cosmic rays | 72 |
| E.3 | Black hole production by cosmic neutrinos | 78 |
| F | LHC production of gravitationally bound black holes | 79 |
| G | Synchrotron losses in magnetic fields | 84 |
| H | Production on background objects | 85 |
| H.1 | On lifetimes and solid angles in X-ray binaries | 85 |
| H.2 | Production on the interstellar medium | 86 |
| I | Useful conventions, conversion factors, and reference quantities | 88 |

1 Introduction

One of the most spectacular manifestations of nature realizing certain extra-dimensional scenarios [1–4] could be the production of microscopic black holes at the LHC [5, 6].³ These are expected to undergo prompt, quasi-thermal, Hawking [9] decay to large multiplicities of elementary particles, leading to very characteristic final states. It has been suggested [10, 11], however, that black hole decay via Hawking radiation may not be a universal feature, and could for example depend on the details of the Planck-scale degrees of freedom. While this suggestion is not based on any complete microphysical picture, and furthermore appears contradictory to basic quantum-mechanical principles⁴, it does raise a possible question about stability of microscopic black holes that might be produced at the LHC, in TeV-scale gravity scenarios. This in turn has led some to express concern about the fate of their evolution: could their accretion pose any threat to the Earth? This is the question addressed in this paper.

The structure of this work, and a succinct summary of our findings, are outlined here. We begin our work by reviewing what are widely regarded as quite convincing arguments for the robustness of the exceedingly rapid decay of microscopic black holes. We then discuss the arguments asserting that macroscopic consequences of new and unknown particles can be ruled out by the lack of evidence for their effects from production by cosmic rays hitting the surface of the Earth or other astronomical bodies. We argue here that charged black holes will lose enough energy to stop when traversing the Earth or the Sun, via standard electromagnetic processes. Since black holes would be typically produced by the collision of quark pairs, whether in cosmic-ray interactions or at the LHC, they would often be initially charged. To the extent that no mechanism leads to their neutralization, the cosmic-ray based argument for their being harmless is therefore robust. Their neutralization through the Schwinger mechanism proceeds according to quantum principles like those underlying Hawking radiation. There is therefore no concrete framework where neutralization occurs without Hawking decay taking place as well, leading to a likely contradiction in assuming that stable black holes must be neutral. We nonetheless make the hypothesis that this odd situation could occur, and analyze the possible effects of such neutral and stable black holes, beginning with a review of some essential features of gravity and black holes in $D > 4$ dimensions, including both large- and warped-extra-dimensions models.

Next, we develop the formalism to describe the evolution of such black holes trapped inside the Earth or inside dense objects such as white dwarfs and neutron stars. We introduce and discuss accretion scenarios that apply within nuclear, atomic and macroscopic matter, evaluating the time scales corresponding to various phases in the evolution of a growing black hole. We establish upper and lower limits to the rate at which accretion can take place, building on very basic principles such as conservation laws and classical and quantum dynamics. This is possible since, in order for accretion to become macroscopic, it is necessary that a black hole exerts its influence over distance scales much larger than its event horizon.

³For reviews with more references see [7, 8].

⁴See, for example, [12].

Such black holes are very small, and their accretion power, if limited to absorbing particles that have impact parameters of the order of the Schwarzschild radius, is typically insufficient to cause macroscopic growth. At large distances the physical processes become independent of the short-distance properties of the black hole, which only acts through its attractive potential, and as a mass sink. In this long-distance domain, classical or quantum dynamics are well-tested, making the study of accretion possible, independently of our detailed knowledge or ignorance about the physics inside the black-hole.

We investigate two concrete scenarios, for various configurations of the extra dimensions: growth of hypothetical LHC-produced stable black holes within the Earth, and growth of such black holes produced by cosmic rays impinging on dense stars, such as white dwarfs or neutron stars. In both cases, we make conservative assumptions, namely fastest possible growth in Earth, and slowest possible growth in a dense star. The first scenario shows that, if the radius of crossover from higher-dimensional gravity to four-dimensional gravity is less than about 200 \AA , the natural lifetime of the solar system is too short to allow significant growth of stable black holes that may be captured inside the Earth. In contrast, in a scenario where the crossover radius exceeds the 200 \AA scale, accretion times could be shorter than the solar time scale. In this case, however, examination of the latter dense-star scenario then produces an argument that, given observational data setting the lifetimes of such objects at a billion years or more, such stable black holes cannot in fact exist for a crossover radius greater than $\simeq 15 \text{ \AA}$.

These arguments thus conclude with the exclusion of any relevant consequences for Earth due to the evolution of black holes possibly produced by the LHC.

While the main line of the argument is relatively straightforward, being based on well-established macroscopic properties of matter, several issues require an in-depth study in order to provide a robust basis to our conclusions. When studying accretion, for example, we need to consider the possibility of effects such as the Eddington limit, where radiation emitted during the infall of matter would slow down the accretion via radiative pressure, constraining the accretion rate of a black hole and thus possibly slowing down its growth inside Earth or a dense star. The estimates of the number of black holes produced by cosmic rays need to rely on a solid understanding of the latter's spectra and composition. Here we therefore consider the worse-case scenarios where, contrary to mounting experimental evidence, the cosmic primaries are dominantly heavy nuclei rather than protons. The loss of acceptance for the highest-energy cosmic ray flux hitting dense stars, due to the intense surface magnetic fields, is also an important element that we analyze. Finally, the slow-down and stopping of relativistic black holes inside dense stars requires a detailed study of energy loss in gravitational scattering and absorption processes.

We note that our bounds are conservative. In particular, at each point where we have encountered an uncertainty, we have replaced it by a conservative or “worst case” assumption. For this reason, our bounds can likely be improved through further work removing such uncertainties. Furthermore, we do not exclude that there could be other independent arguments, based for example on astrophysical or cosmological production of microscopic

black holes, leading to the exclusion of stable black holes, or of their macroscopic effects.

In outline, the next section summarizes existing arguments (and their extension) against risk from TeV-scale black holes, namely the robustness of quantum black hole decay, and constraints from cosmic rays impinging on objects in the solar system. Section three then summarizes aspects of TeV-scale gravity scenarios and the corresponding black holes. Section four discusses black hole accretion in Earth. Section five gives an in-depth analysis of the question of stopping of neutral black holes, via gravitational interactions. Section six describes production of black holes by cosmic rays impinging on white dwarfs. Section seven describes the resulting accretion of a white dwarf, and thus derives constraints on hypothetical TeV-scale scenarios that otherwise might have been of concern. Section eight describes similar constraints arising from black hole production on, and accretion of, neutron stars. A summary and conclusions appear in section eight.

Many of the technical details are treated in a series of Appendices. Appendix A summarizes macroscopic Bondi accretion, which is the canonical framework to deal with the flow of matter into a black hole. For its use in our context, Bondi accretion is generalized here to higher-dimensional gravitational fields. Appendix B discusses the effects of radiation emitted during accretion, and examines the radiative transport conditions relevant to the question of an Eddington limit for the growth of microscopic black holes. In Appendix C we derive the main equations governing the particle scattering and capture in the field of a D -dimensional black hole, and Appendix D proves few facts required by the study of stopping by white dwarfs. Appendix E reviews the formalism for the calculation of black hole production at the LHC and in the collisions of cosmic rays, including the case of high-energy neutrinos. Here we discuss the impact of different assumptions about the composition of the high-energy cosmic rays, we evaluate the production rates under the various assumptions, and establish the most conservative lower limits on such rates. We also discuss the production properties of black holes produced by cosmic rays, to serve as initial conditions for their slow-down in dense stars. In Appendix F we calculate the probability that black holes produced at the LHC are trapped in the Earth's gravitational field. We argue that, independently of our general conclusion that trapped black holes would not accrete macroscopically, the velocity spectrum of black holes produced during the LHC lifetime in allowed extra-dimensional scenarios is such that they would typically escape the Earth's attraction. Appendix G discusses the impact of magnetic fields on the penetration of cosmic rays down to the surface of dense stars. Appendix H addresses the production of black holes by cosmic rays hitting "background" objects, such as neutron star companions, the interstellar medium, or even dark matter. Here we discuss the conditions for the companion of a neutron star in X-ray binary systems to efficiently act as a beam-dump for cosmic rays, leading to the production of black holes and their capture in the neutron star, unimpeded by the presence of magnetic fields. A final Appendix contains useful conversion factors and physical constants that are used throughout the paper.

2 Assessment of pre-existing arguments

We begin by assessing the strengths and weaknesses of previously existing arguments regarding risk from black hole production.

2.1 Instability of microscopic black holes

One of the most profound steps so far towards the yet-incomplete unification of quantum mechanical and gravitational principles was Hawking’s discovery [9] that black holes evaporate. This provided an important missing link in the pre-existing laws of black hole thermodynamics, by explicitly calculating the temperature that characterizes a radiating black hole.

While Hawking’s result has become nearly universally accepted, it is certainly true that elements of the original derivation of black hole radiance rely on assumptions that are apparently not valid. Notable among these is the use of modes of ultra-planckian frequencies at intermediate steps in the derivation. This naturally raises the question of the robustness of the result.

Belief in the robustness of Hawking’s prediction of nearly thermal evaporation has been boosted by arguments for the result which have now been produced from several different directions. These derivations have the virtue of either facing head-on the issue of the trans-planckian modes, or being independent of them, and the basic effect has survived a number of important consistency checks.

One early approach relying on the trace anomaly and avoiding explicit reference to trans-planckian modes was pioneered by Christensen and Fulling [13]. In this approach, the stress tensor describing the Hawking radiation is found by combining the known trace anomaly in two dimensions, and the constraint that the stress tensor be conserved. This approach has been used to give explicit models of evaporating black holes [14], and has also recently been generalized to higher dimensions in [15] and a number of followup works.

Another approach is to modify the short-distance physics to remove the offending trans-planckian modes. One summary of such a prescription appears in [16], where it is argued that despite a different origin for the modes, this approach supports the statement that Hawking radiation persists. This approach is also related to analog gravity models.⁵ These are models based on condensed matter systems, where a horizon for sound waves occurs, and exhibits a precise analog of the Hawking effect. For example, the abstract of a recent overview talk [18] on the subject of Hawking radiation states “analog models of gravity have given us a clue that despite the shaky derivation, the effect is almost certainly right.” These models illustrate various detailed features of the corresponding radiation in the analog systems.

One of the puzzles of Hawking radiation stems from the fact that it appears to lead to loss of quantum coherence, when followed to the end state of evaporation [19], and this has

⁵For a review, see [17].

led to the “black hole information paradox.”⁶ Many workers feel that the resolution will be that there are subtle corrections to Hawking’s thermal spectrum, that lead to unitary evolution. Thus while very few question that black holes Hawking evaporate, it is clear that there are detailed aspects of the evaporation process that we do not understand.

Indeed, the basic result, that black holes evaporate, appears quite robust from a very general perspective. Nature is quantum-mechanical, and basic quantum-mechanical principles dictate that any allowed decay will occur. Thus, stable (or nearly-stable) objects must be “protected” by conservation laws, examples being baryon number, lepton number, *etc.* There is no such conserved charge carried by a black hole that is not carried by ordinary matter, if a black hole can be produced in collisions of partons at the LHC. Thus by basic quantum principles such a heavy black hole should decay into light, ordinary matter, and the only question is the time scale. Since such a black hole can have mass at most around ten times the higher-dimensional Planck mass, $M_D \sim 1$ TeV, the only relevant dimensionful parameter is the corresponding time scale, $t_D \sim 1/M_D \sim 10^{-27}s$, and there are no other small dimensionless parameters to suppress decay. Thus, on very general grounds such black holes are expected to be extremely short-lived, as is indeed predicted by the more detailed calculations of Hawking and successors.

Despite these very strong arguments for black hole decay, the possibility of manufacturing microscopic black holes on Earth suggests that one conduct an independent check of their benign nature. For that reason, this paper will test the hypothesis that the statements of this subsection are false, by investigating possible consequences of hypothetical black holes that do not undergo Hawking decay.

2.2 Cosmic ray collisions on Earth

Cosmic rays hit Earth with energies known to exceed 10^{20} eV, corresponding to center-of-mass (CM) energies exceeding 100 TeV. Thus, anything that can be made with Earth-based accelerators up to this energy is already being made by nature. This argument can be used to effectively rule out the existence of particles predicted by some speculative scenarios, or to exclude possible macroscopic consequences of high energy collisions, as discussed for example in [23, 24].

This argument requires however more attention if the large momentum imparted to the produced particles by the cosmic-ray kinematics has an impact on how they evolve after production. Consider the cosmic-ray collision producing the black hole (or any other particle), at the parton level. E_1 is the energy of the parton inside the cosmic ray nucleon, and $E_2 < m_p$ the energy of the parton inside the atmospheric nucleon, where m_p is the nucleon mass. To produce a particle of mass M , we need $E_1 \geq M^2/2E_2$, and therefore the minimum energy of the produced black hole in the Earth rest frame is given by $E_1 > M^2/2m_p$, or, for

⁶For reviews, see [20–22].

the maximum value of $M = 14$ TeV allowed at the LHC,

$$E_1 \sim p_{BH} > 10^8 \text{GeV} \quad , \quad (2.1)$$

where p_{BH} is the momentum of the resulting black hole. Any argument that such black holes, should they be stable, would undergo macroscopic accretion, must be based on the proof that, while traversing the Earth, they slow down enough to get trapped by the Earth's gravitational field. Most such TeV-scale black holes should initially have color or electric charge, since the incident partons (quarks, gluons) are charged. In the usual picture, where Hawking radiation is present, these rapidly discharge through the Schwinger mechanism [25] of particle-antiparticle pair creation in an intense (chromo-)electric field, or through breaking/absorbing a QCD string. The timescale for the neutralization is proportional to the black hole Schwarzschild radius R . While there is no known example of a consistent microphysics such that Schwinger discharge occurs and Hawking radiation does not, one can point out one difference between them. Specifically, the Schwinger effect can be described in terms of pair production in the gauge field outside the horizon, but Hawking radiation is a trans-horizon effect. In the unlikely event that our understanding of the horizon misses some critical element forbidding black hole decay (an assumption that, in our view, appears to contradict the basic quantum principles outlined above), one might imagine that Schwinger discharge nevertheless takes place. (One could parameterize such a scenario by imposing rather artificial boundary conditions at the horizon.)

Thus, we will consider collisions on Earth in two contexts – those which produce hypothetical stable charged black holes, and those which produce hypothetical stable black holes that rapidly neutralize.

Passage of a high-energy charged particle through matter leads to well-understood energy loss [26, 27]. This is due to long-range electromagnetic effects, that have nothing to do with the microphysics associated to the particle itself. Therefore, a muon, or a black hole with the electric charge and the mass of a muon, would be subject to the same energy loss through radiative processes as they move through matter. Since at high energy the radiative properties are mostly determined by the value of the Lorentz γ factor of the charged particle, we describe the energy-loss properties of a singly-charged black hole by rescaling the energy loss of muons to the equivalent γ value. For relativistic velocities, below the threshold for e^+e^- pair production in the field of nuclei, the energy loss is described by the Bethe-Bloch equation. The energy loss in this regime depends on the velocity, with a slow growth proportional to $\log \gamma$. The stopping power for black holes is therefore similar to that of muons, of the order of $2 \text{ MeV cm}^2/\text{g}$ up to $\gamma \sim 10^3$ [26, 27]. For the average composition of Earth, this means an energy loss of about 11 MeV/cm . Above $\gamma \sim 10^3$ (which is the case at the time of production for black holes of mass larger than 1 TeV) pair production, bremsstrahlung and nuclear dissociation appear. These grow approximately linearly with energy (or γ), with an energy loss of the order of 60 MeV/cm at $\gamma \sim 10^4$, for the average Earth density. With Earth-like densities, the distance scale necessary to slow down from the production energy $E \sim M^2/m_p$ to $\gamma \sim 10^3$ is thus of order $M/(6\text{keV}) \text{ cm}$, or, for $M \sim 14 \text{ TeV}$, more than 10^4 km , larger than the radius of the Earth. The subsequent slow-

down below $\gamma \sim 10^3$ takes place with the constant energy loss of 1 GeV/m, corresponding to $\gtrsim 10^4$ km. The stopping distance grows with M , and a more careful estimate shows the Earth provides enough stopping power for black holes with unit electric charge up to a mass of the order of 7 TeV. For larger masses, one can appeal to the stopping power of the Sun. With a core density of about 150 gr/cm³, over a radius of the order of 0.2 solar radii, namely 1.4×10^5 km, the Sun column density can stop black holes of mass well in excess of 100 TeV. Notice also that our estimates are based on a black hole with unit electric charge. Any minor addition to $Q = 1$, due for example to accretion of a net charge, would further increase the stopping power. The continued health of the Sun on multi-billion year time scales – during which many such black holes would have been produced and stopped – thus apparently immediately rules out any risk from charged TeV-scale black holes.

The above arguments apply to any elementary charged particle. In particular, they apply to possible magnetic monopoles. The stopping power for monopoles moving through matter is about 100 times larger than that of a charged particle [28], since their magnetic charge is at least $1/\alpha$ times greater than the electron electric charge. This means that the Earth itself can stop magnetic monopoles of masses much larger than those that can be produced at the LHC.

Let us next turn to the hypothesis that such black holes are stable, but rapidly neutralize via Schwinger production or another mechanism. In this case, the only interactions of a black hole with matter are through its gravitational field. We will give a more careful treatment of such interactions below, but a rough cross-section is the geometric size, $\sigma \sim 1/\text{TeV}^2$. Again using the average density of Earth, we find of order one scattering event expected in its transit for this cross section. The maximum momentum loss in a collision with a parton of energy E_p is of size $\sim \gamma^2 E_p$. This is achieved when particles are scattered with significant momentum transfer in the black hole frame, for example in a head-on elastic collision, where the target particle is significantly deflected. Since $\gamma \sim M/E_p$, this would correspond to a loss of a fraction of order 1 of the initial momentum (2.1). However, this is clearly not necessarily typical: due to the short-distance character of the D -dimensional gravitational potential, the impact parameter range for hard elastic scattering is restricted, and typically we shall either have a small-angle scattering, or the target particle can be captured by the black hole, leading to a large inelasticity and to a reduced velocity loss. We shall discuss these issues in more detail in Section 5. The more careful analysis presented there also indicates that the stopping power of the Sun is likewise insufficient.

To summarize, hypothetical stable charged black holes should stop in the Earth for masses up to about 7 TeV, and in the Sun if heavier. The multi-billion year longevity of Earth and Sun apparently provides a good safety guarantee. We have no concrete example of a consistent microphysics such that black holes neutralize via Schwinger discharge but don't Hawking radiate, but our present state of knowledge of quantum black hole processes doesn't strictly rule out such a possibility. Thus, we will seek alternative bounds on such a scenario, which will also serve the purpose of improving the stringency of the bounds for charged black holes.

3 Essentials of higher-dimensional gravity

In this section we quickly review some features of higher-dimensional scenarios realizing TeV-scale gravity, and of the black holes that exist in these scenarios. A brief overview discussing more aspects of these scenarios and black hole production in them is [7].

3.1 TeV-scale gravity scenarios

The basic idea of TeV-scale gravity is that either via large extra dimensions [1, 2] or large warping [3], the true Planck scale is lowered to the vicinity of a TeV. To summarize, let the D -dimensional action be

$$S = \frac{1}{8\pi G_D} \int d^D x \sqrt{-g} \frac{1}{2} \mathcal{R} + \int d^D x \sqrt{-g} \mathcal{L} , \quad (3.1)$$

where G_D is the D -dimensional gravitational constant, \mathcal{R} is the Ricci scalar, and \mathcal{L} is the matter lagrangian. We consider a general compact metric $g_{mn}(y)$, possibly together with warp factor $A(y)$,

$$ds^2 = e^{2A(y)} dx^\mu dx_\mu + g_{mn}(y) dy^m dy^n . \quad (3.2)$$

Here the non-compact coordinates are x^μ , and the standard model fields are typically taken to lie on a brane spanning these dimensions. Then the relation between the higher-dimensional Planck mass,⁷

$$M_D^{D-2} = \frac{(2\pi)^{D-4}}{8\pi G_D} \quad (3.3)$$

and the four-dimensional Planck mass, defined via the four-dimensional gravitational action

$$S_4 = \frac{M_4^2}{2} \int d^4 x \sqrt{-g_4(x)} \mathcal{R}_4 , \quad (3.4)$$

is

$$\frac{M_4^2}{M_D^2} = M_D^{D-4} \int \frac{d^{D-4} y}{(2\pi)^{D-4}} \sqrt{g_{D-4}} e^{2A} \equiv M_D^{D-4} \frac{V_w}{(2\pi)^{D-4}} . \quad (3.5)$$

This equation defines the “warped volume” V_w .

Current lower bounds [26] on M_D are around 1 TeV. In order for M_D to be in the TeV vicinity, one must have a large warped volume. This can be achieved by large volume and moderate warping, by large warping, or by some combination of the two. A simplified version of the relationship (3.5), assuming the scale of all extra dimensions is set by a radius R_D , is

$$\frac{M_4^2}{M_D^2} \approx (M_D R_D)^{D-4} e^{2\Delta A} , \quad (3.6)$$

⁷In this paper, we use the conventions of the “Extra dimensions” minireview by Giudice and Wells, in the *Particle Data Book* [26].

where ΔA is a measure of the relative difference in warping between the region of maximal warp factor and the region in which standard-model physics resides.

One can solve for the characteristic D -dependent size of the extra dimensions,

$$R_D \approx M_D^{-1} \left(\frac{e^{-2\Delta A} M_4^2}{M_D^2} \right)^{1/(D-4)}. \quad (3.7)$$

Of course, larger warping and fixed M_D means that R_D is smaller for a given D . In particular, for unwarped scenarios R_5 is macroscopic and thus ruled out, but with sufficient warping one finds viable scenarios, such as that of [3].

For $M_D = 1$ TeV and with no warping, we find the following radii:

$$R_D = 4.8 \times 10^{-2} \text{cm}, \quad \text{for } D = 6 \quad (3.8)$$

$$R_D = 3.6 \times 10^{-7} \text{cm}, \quad \text{for } D = 7 \quad (3.9)$$

$$R_D = 9.7 \times 10^{-10} \text{cm}, \quad \text{for } D = 8 \quad (3.10)$$

$$R_D = 2.8 \times 10^{-11} \text{cm}, \quad \text{for } D = 9 \quad (3.11)$$

$$R_D = 2.7 \times 10^{-12} \text{cm}, \quad \text{for } D = 10 \quad (3.12)$$

$$R_D = 4.9 \times 10^{-13} \text{cm}, \quad \text{for } D = 11. \quad (3.13)$$

For higher M_D and/or in the presence of warping, these numbers should be multiplied by a factor

$$\left(\frac{M_D}{\text{TeV}} \right)^{(2-D)/(D-4)} e^{-2\Delta A/(D-4)}. \quad (3.14)$$

3.2 Higher-dimensional black holes

3.2.1 Schwarzschild solution

We next turn to properties of black holes in these scenarios. We begin with the D -dimensional Schwarzschild solution with mass M , which takes the form

$$ds^2 = - \left[1 - \left(\frac{R(M)}{r} \right)^{D-3} \right] dt^2 + \frac{1}{1 - \left(\frac{R(M)}{r} \right)^{D-3}} dr^2 + r^2 d\Omega^2. \quad (3.15)$$

Here the Schwarzschild radius $R(M)$ is

$$R(M) = \frac{1}{M_D} \left(\frac{k_D M}{M_D} \right)^{1/(D-3)}, \quad (3.16)$$

where the constant k_D is defined as

$$k_D = \frac{2(2\pi)^{D-4}}{(D-2)\Omega_{D-2}}, \quad (3.17)$$

and where Ω_{D-2} is the volume of the unit $D - 2$ sphere,

$$\Omega_{D-2} = \frac{2\pi^{(D-1)/2}}{\Gamma[(D-1)/2]} . \quad (3.18)$$

One can likewise write down the higher-dimensional version of the Kerr solution [29].

3.2.2 Black holes in standard compactifications

Nonrotating black holes with radius much less than the curvature scales and the sizes of the extra dimensions are well approximated by the Schwarzschild solution (3.15). When the Schwarzschild radius reaches a size comparable to that of an extra dimension, one expects an inverse Gregory-Laflamme [30] transition to the lower-dimensional black hole, extended over the extra dimension. In this case the solution will be given by the lower-dimensional version of the solution (3.15), with trivial dependence on the compact coordinates.

For the purposes of computing forces due to a black hole, we will need its gravitational potential. In the weak-field regime this is given by

$$\phi = -(g_{00} + 1)/2 , \quad (3.19)$$

leading to the force on a mass m :

$$F_G(r) = -\frac{\tilde{k}_D}{M_D^{D-2}} \frac{Mm}{r^{D-2}} , \quad (3.20)$$

where

$$\tilde{k}_D = (D-3)k_D/2 = \frac{D-3}{D-2} \frac{(2\pi)^{D-4}}{\Omega_{D-2}} . \quad (3.21)$$

The attractive gravitational force matches between the lower and higher-dimensional expressions in the region $r \sim R_D$. Specifically, by equating the D -dimensional force law to that of $4D$, we find that the forces match at a crossover radius

$$R_C = (8\pi\tilde{k}_D)^{1/(D-4)} R_D , \quad (3.22)$$

whose values are of size $5 - 6 R_D$ in cases of interest.

3.2.3 Black holes in warped compactifications

As an example of a broad class of warped compactification scenarios, consider a metric of the form

$$ds^2 = dy^2 + e^{2y/R_D} dx_4^2 + R_D^2 ds_X^2 , \quad (3.23)$$

where $e^{2y/R_D} dx_4^2$ describes the $D = 4$ part of the metric. Here R_D is both the characteristic curvature radius associated with the warping, and the radius of the remaining extra dimensions, compactified on some compact manifold X , whose metric ds_X^2 we have taken to have

radius $\mathcal{O}(1)$. The coordinate y is taken to have range $(0, L)$. The form (3.23) is representative of many known examples of warped compactifications, such as the truncated AdS_5 solutions of [3] and the warped flux compactifications of [4, 31], although more generally one expects for example the metric of X to vary with y .

For these compactifications, a black hole whose radius satisfies $R \ll R_D$ is well-described as the D -dimensional Schwarzschild solution (3.15). On the other hand, a sufficiently large black hole is expected to be described by a four-dimensional Schwarzschild solution, represented by (3.23) with dx_4^2 replaced by the four-dimensional Schwarzschild metric. Between these extremes the solutions are not known.

However, approximate forms for the linearized gravitational potential, appropriate to describing the weak field regime of a concentrated mass such as a black hole, have been derived in [32]. In the region $R_D \lesssim r \lesssim L$, one finds the linearized perturbation of dx_4^2 given by

$$\phi = \frac{\hat{k}_D M}{M_D^{D-2}} \frac{e^{-j_D r/R_D - (D-1)y/R_D}}{R_D r^{D-4}}. \quad (3.24)$$

Here $j_D = j_{(D-3)/2,1}$ is the first zero of the relevant Bessel function, and \hat{k}_D is a constant. Thus, the radial gravitational force at $y = 0$ is

$$F_{D,w} = -\frac{\hat{k}_D M}{M_D^{D-2}} \frac{e^{-j_D r/R_D}}{R_D r^{D-4}} \left(\frac{j_D}{R_D} + \frac{D-4}{r} \right). \quad (3.25)$$

An important question is at what specific radius R_C does the gravitational force from (3.24) match onto that for four-dimensions. This can be found by equating $F_{D,w}$ to $-G_4 M/r^2$. This yields the relation

$$\frac{R_C}{R_D} = \frac{1}{j_D} \left\{ \ln \left[\frac{M_4^2}{M_D^2 (R_C M_D)^{D-4}} \right] + 2 \ln \left(\frac{R_C}{R_D} \right) + \ln \left(8\pi \hat{k}_D \left[j_D + (D-4) \frac{R_D}{R_C} \right] \right) \right\}. \quad (3.26)$$

From this, we see that if R_C is significantly smaller than the radius given by the unwarped version of (3.6), this correspondingly increases the size of the region between R_D and R_C where warping is significant.

3.2.4 A general perspective

We close this section by outlining a broader perspective on TeV-scale gravity and black holes. Note that a general feature of the above discussion is that below the value R_C the potential (3.19) crosses over from the four-dimensional form to one that grows more rapidly as r decreases. The flat and warped cases give both power law and exponential growth laws. Moreover, the gravitational potential is proportional to the mass. In order to have a TeV-scale model, note that the potential corresponding to a TeV-scale mass should reach the value $\phi \sim 1$ by the time r reaches the value $r \sim 1/\text{TeV}$. We assume that while the gravitational

potential is modified at short distances, the dynamics of other forces is four-dimensional, as in brane-world models, in order to agree with experiment.

Moreover, as we will see, many features of the accretion process only depend on the long range potential, since it is at such long scales that gravity begins to compete with other effects. From this general perspective, a very general definition of a black hole is as an object with such a long-range gravitational potential, and which is allowed to accumulate mass at $\phi \sim 1$.

One could postulate more general forms for the potential, but clearly the cases we have described are representative of a very wide class of potentials that become strong at the TeV scale.

4 Black hole accretion in Earth

4.1 Accretion basics

Our interest is in accretion of black holes trapped inside astronomical bodies such as planets, stars, neutron stars, *etc.* One parameter governing this accretion is the effective capture radius $r_c(M)$ of the black hole, for a given mass. This is the radius out to which the gravitational field of the black hole succeeds in attracting matter that will eventually be absorbed. The other parameter is the flux of mass towards the black hole, F . Specifically, the black hole mass grows as

$$\frac{dM}{dt} = \pi r_c^2 F . \quad (4.1)$$

This formula neglects reradiation of incident energy, which is discussed in Appendix B, and, if present, can lower the growth rate. The flux can arise either from the motion of the black hole relative to the body, or from the motion of the constituents of the body relative to the black hole. In the case where the dominant effect is the velocity v of the black hole, we have

$$F = \rho v \quad (4.2)$$

where ρ is the mass density near the capture radius. This produces an evolution equation

$$\frac{dM}{dt} = \pi \rho v r_c^2(M) , \quad (4.3)$$

The capture radius r_c is frequently different from the Schwarzschild radius R , and depends on the size and state of motion of the black hole, as well as on properties of the surrounding medium. For example, free particles with velocity v with respect to a black hole have capture radii

$$r_c \approx R/v \quad (4.4)$$

Black holes whose production is accessible at the LHC have an initial radius of the order TeV^{-1} . As they absorb matter, their physical and capture radii grow.⁸ In atomic matter, there are three possible domains where the properties of black hole interactions with matter vary. The first phase is that where r_c is smaller than the nucleon size, $r_N \sim 1 \text{ fm}$. A second phase is that where $r_N \lesssim r_c \lesssim a$ (where $a \sim 1 \text{ \AA}$ is the atomic radius). The third phase is $r_c > a$. Similar phases are present for growth inside a white dwarf, but in the case of growth inside nuclear matter of a neutron star, the two latter phases are replaced by a single phase with $r_c \gtrsim r_N$. The details of the evolution during these phases will vary, depending on where r_c is relative to R_D and R_C , the distances characterizing crossover from the D -dimensional force law to that of four-dimensions.

This section will discuss evolution, first at the atomic level, and then, for larger-scale black holes, from macroscopic matter. The latter is described by Bondi evolution; we also briefly discuss, and argue against, the presence of an Eddington limit, which would be relevant if emitted radiation were sufficient to slow accretion. Our goal will be to estimate, under the most pessimistic assumptions, namely of fastest possible growth, the timescale required for accretion of black holes to macroscopic size. In subsequent sections, we will also perform similar calculations for accretion of white dwarfs and of neutron stars.

4.2 Subatomic accretion in Earth

4.2.1 Competition with electromagnetic binding

As is described in Appendix F, most LHC-produced black holes would be produced with large velocity as compared to the Earth's escape velocity, $v_E = 11 \text{ km/s}$, due to imbalanced kinematics of the initial-state partons, initial and final state radiation, etc. However, those that are downward directed will accrete matter and slow down while passing through the Earth. Appendix F estimates this effect based on closely related calculations for black holes created by cosmic rays in section 5. For present purposes, we will simply make the most conservative assumption that some of these black holes do become gravitationally bound to Earth. Given the escape velocity and that the minimum mass of such a black hole would be $\mathcal{O}(\text{TeV})$, typical kinetic and gravitational potential energies would thus be $\gtrsim \mathcal{O}(\text{keV})$. This means that on the occasions where a black hole and nucleus bind, the black hole's energy overcomes the (atomic) binding energy of the nucleus to the surrounding material, and the combined system continues to fall. Thus the black hole's motion should initially be dictated by the net gravitational field of the Earth.

In a collision of the black hole with a nucleus, binding depends on the size of the impact parameter b ; we will largely neglect separate capture of electrons since their capture rates are much smaller due to their smaller masses and higher velocities. The black hole's effects are significant at impact parameters where its gravity competes with the electromagnetic

⁸They also may have significant initial angular momentum. However, as they absorb matter, with negligible average angular momentum, they become increasingly well-approximated as non-spinning black holes.

binding forces of the surrounding medium. The latter are estimated by noting that if a nucleus is displaced from its equilibrium position by a small displacement d , one will find a restoring force of the form

$$F_E(d) = -Kd \quad (4.5)$$

for some constant K . This is justified, for example, by considering the force acting on an ion⁹ of charge Z' as it is displaced by a distance d from the center of charge of its electron cloud:

$$F_E(d) \simeq -\alpha \frac{Z'}{d^2} Z' \frac{d^3}{a^3} = -\alpha \frac{Z'^2}{a^3} d, \quad (4.6)$$

where we assumed the electron charge to be uniformly distributed in the atomic volume. The black hole will exert a competing gravitational force which is maximum at the point of closest approach. For a D -dimensional force law (3.20), and with the nucleus displaced by d towards the black hole, it is

$$F_G(d) = -\frac{\tilde{k}_D M m}{M_D^{D-2} (b-d)^{D-2}} \quad (4.7)$$

where the nuclear mass is given in terms of the mass number and proton mass as $m \simeq A m_p$. The nucleus can become bound to the black hole if this force dominates F_E for all d over the range $(0, b)$. This amounts to the condition that, for all d ,

$$\frac{\tilde{k}_D M m}{K M_D^{D-2}} > d(b-d)^{D-2}. \quad (4.8)$$

Maximizing the right-hand side with respect to d , we find the binding condition:

$$b < (D-1) \left[\frac{\tilde{k}_D M m}{(D-2)^{(D-2)} K M_D^{D-2}} \right]^{1/(D-1)} = R_{\text{EM}}, \quad (4.9)$$

which defines the *electromagnetic capture radius* R_{EM} . To simplify subsequent expressions, we rewrite this as

$$R_{\text{EM}} = \frac{1}{M_D} \left(\frac{\beta_D M}{M_D} \right)^{1/(D-1)} \quad (4.10)$$

where we define

$$\beta_D = \frac{(D-1)^{D-1} \tilde{k}_D M_D^2 m}{(D-2)^{D-2} K}. \quad (4.11)$$

The ratio of electromagnetic to Schwarzschild radii is given by

$$\frac{R_{\text{EM}}}{R} = \frac{\beta_D^{1/(D-1)}}{k_D^{1/(D-3)}} \left(\frac{M_D}{M} \right)^{2/(D-3)(D-1)}. \quad (4.12)$$

⁹Here we account for the fact that the inner electrons are typically strongly bound to the nucleus, and so move with it.

Since K is governed by atomic scales, $\beta_D \gg 1$, and R_{EM} exceeds R for subatomic R .

For low relative velocities, nuclei entering this radius can become bound to the black hole. Note that this will not be the case for sufficiently high relative velocity v , as the free-particle capture radius R/v is smaller than R_{EM} for large v . However, we will consider sufficiently small velocities that $R_{\text{EM}} < R/v$, where competition with electromagnetic binding described by F_E dominates.

While subsequent total absorption of a captured nucleus is not guaranteed,¹⁰ the most conservative assumptions for the purposes of discussing accretion on Earth are those that lead to the fastest accretion. We will thus assume that all of the mass of the nucleus is absorbed. In the absence of other effects, this black hole would also have the charge of the nucleus. This charge may discharge through the Schwinger mechanism, or be retained, depending on assumptions. If it is retained, the next time that the black hole encounters a nucleus within R_{EM} , this charge is insufficient to prevent absorption, but with sufficient charge buildup repulsion could become an important effect. A positively-charged black hole will also have an enhanced absorption rate for electrons, which works toward neutralization. So, while charge effects could possibly somewhat slow the absorption rate, we will make the conservative assumption that they don't, and that sufficient neutralization is automatic.

To determine actual capture sizes, one needs the parameter K . There are different ways of estimating a typical K . One approach is to estimate the dipole force when one separates an ion in a crystal from the electron cloud of the bonding orbitals, as suggested earlier by eq. (4.6). Assuming there that all but the outermost electrons move coherently with the nucleus, yields the value

$$K \sim \frac{\alpha}{a^3} \sim \frac{14 \text{ eV}}{\text{\AA}^2}, \quad (4.13)$$

where a is the atomic radius, $\sim 1 \text{ \AA}$. Another method is to use the relation to the Debye frequency ω_D ,

$$\frac{K}{m} = \frac{\omega_D^2}{\chi}, \quad (4.14)$$

where χ is an $\mathcal{O}(1)$ constant that depends on the material. Corresponding Debye temperatures, $T_D = \omega_D$, fall in the range 300-600K for typical materials forming the Earth's interior ($T_D^{\text{Fe}} = 460\text{K}$, $T_D^{\text{Si}} = 625\text{K}$, $T_D^{\text{Mg}} = 320\text{K}$). In this case, one finds a typical K of size:

$$K = \frac{12 \text{ eV}}{\chi \text{\AA}^2} \left(\frac{m}{40\text{GeV}} \right) \left(\frac{T_D}{400\text{K}} \right)^2 = 1.20 \times 10^{-27} \frac{m}{\chi} \left(\frac{T_D}{400\text{K}} \right)^2 M_0^2, \quad (4.15)$$

consistent with (4.13). Here we have introduced the TeV mass scale,

$$M_0 = 1\text{TeV}, \quad (4.16)$$

which frequently provides a useful normalization scale. In Earth one also has semi-solid or semi-fluid layers, but these have characteristic values of K/m , given by pairing potentials, of similar size to those of solids.

¹⁰In particular, (chromo-)electrostatic effects apparently slow accretion early in this phase.

Since K/m is directly related to T_D , we will in fact parameterize results in terms of this temperature. For example,

$$\beta_4 = \chi \frac{27M_4^2}{32\pi T_D^2} = 1.30\chi \times 10^{57} \left(\frac{400K}{T_D} \right)^2 . \quad (4.17)$$

With this prelude, we are now prepared to discuss the subatomic phase of accretion.

4.2.2 Subatomic growth laws

As we have described, in principle there can be three regimes depending on the size of the capture radius relative to nuclear and atomic scales. The capture radius in atomic matter is given by R_{EM} ; let us estimate this for the minimum size black hole, with $M \sim M_D$. For $D = 11$, we find from (4.10), (4.11), and (4.14) that

$$R_{EM}(M = M_D, D = 11) \sim 3\chi^{1/10} \times 10^{-14} \text{cm} , \quad (4.18)$$

with larger values for smaller D . Thus the subnuclear growth phase is nearly negligible, and we will (conservatively) set the corresponding time to zero.

We therefore turn directly to evolution from $R_{EM} \sim r_N$ up to the atomic radius, $a \sim 1 \text{ \AA}$. Combining the general evolution equation (4.3) with the expression (4.10) for the electromagnetic radius, the growth law for a black hole moving with velocity v takes the form

$$\frac{dM}{dt} = \pi\rho v R_{EM}^2 . \quad (4.19)$$

This expression integrates to give a distance

$$d = d_0 \left(\frac{M_D}{M_0} \right)^3 \frac{D-1}{(D-3)\beta_D} \left(\frac{\beta_D M}{M_D} \right)^{(D-3)/(D-1)} \quad (4.20)$$

for growth to a mass M , where we introduce the characteristic distance, given via TeV units (4.16)

$$d_0 = \frac{M_0^3}{\pi\rho} . \quad (4.21)$$

Using the average density for Earth, $\rho_E = 5.5 \text{ gr/cm}^3$, one finds $d_0 = 3 \times 10^{11} \text{cm} = 9s$, which is much bigger than the Earth's radius. The distance (4.20) is governed by the upper limit of the mass, and the lower limit has thus been dropped. The expression (4.20) can also be written in terms of the final R_{EM} , using (4.10), as

$$d = d_0 \left(\frac{M_D}{M_0} \right)^{D-2} \left(\frac{D-2}{D-1} \right)^{D-2} \frac{1}{(D-3)\tilde{k}_D} \frac{K}{mM_0^2} (R_{EM}M_0)^{D-3} . \quad (4.22)$$

From eqs. (3.8)–(3.13) we see that this evolution applies to all values of $R_{EM} < a$ if $D \leq 7$. For $D \geq 8$, instead, the radius R_D of the extra dimensions is smaller than a , and

therefore as R_{EM} grows larger than R_D the dimension governing the force law changes, and one should then set $D = 4$ in eq. (4.22). We therefore must treat these cases separately.

In performing the following estimates, using the formula (4.22), we will assume that the black hole uniformly travels at the escape velocity v_E . Were its velocity higher, it would not be gravitationally bound to Earth. This is clearly a conservative assumption, as the black hole will slow down as it accretes; if needed one could model this slowdown by integrating the evolution of the mass and potential energy over the lifetime of the black hole. (We expect that the bounds of this paper might be tightened by a more complete treatment of this slowdown.) We will also assume a uniform density ρ_E for Earth. Of course, if the black hole spent most of its time near the center of the Earth, one should use a higher central density. But, correspondingly, the black hole velocity would be lower, scaling linearly with the distance from the Earth's center. Since the Earth's density in the deep core is at most a factor of 2–3 higher than its average value, the estimates using the average density and the escape velocity should tend to (conservatively) overestimate the accretion rate.

4.2.3 Timescales for $r_N \lesssim R_{\text{EM}} \lesssim a$ in $D = 6, 7$

The relevant time scales for growth to atomic sizes for $D = 6, 7$ can be found by setting $R_{\text{EM}} \sim 1\text{\AA}$ in in eq. (4.22), assuming constant velocity v_E , and substituting the values of the other parameters. This results in the following timescales:

$$t \sim 4.5 \times 10^3 \frac{1}{\chi} \left(\frac{T_D}{400K} \right)^2 \left(\frac{M_D}{M_0} \right)^4 s \quad , \quad D = 6 \quad (4.23)$$

$$t \sim 3.0 \times 10^{11} \frac{1}{\chi} \left(\frac{T_D}{400K} \right)^2 \left(\frac{M_D}{M_0} \right)^5 s \quad , \quad D = 7. \quad (4.24)$$

These times are quite short, compared to geologic time scales, and this phase for $D = 6, 7$ will therefore be regarded as negligible.

4.2.4 Timescales for $r_N \lesssim R_{\text{EM}} \lesssim R_D$ in $D \geq 8$

For $D \geq 8$, the black hole would first evolve from $R_{\text{EM}} \sim r_N$ up to $R_{\text{EM}} \sim R_D$ via the evolution law (4.19). The relative timescales can be obtained by equating R_{EM} in eq. (4.22) with the expression of R_D given by eq. (3.7), and assuming the uniform velocity v_E , resulting

in:

$$t \sim 5.4 \times 10^6 \frac{1}{\chi} \left(\frac{T_D}{400K} \right)^2 \left(\frac{M_0}{M_D} \right)^{3/2} \text{ yr} \quad , \quad D = 8 \quad (4.25)$$

$$t \sim 2.0 \times 10^4 \frac{1}{\chi} \left(\frac{T_D}{400K} \right)^2 \left(\frac{M_0}{M_D} \right)^{7/5} \text{ yr} \quad , \quad D = 9 \quad (4.26)$$

$$t \sim 2.2 \times 10^2 \frac{1}{\chi} \left(\frac{T_D}{400K} \right)^2 \left(\frac{M_0}{M_D} \right)^{4/3} \text{ yr} \quad , \quad D = 10 \quad (4.27)$$

$$t \sim 4.8 \frac{1}{\chi} \left(\frac{T_D}{400K} \right)^2 \left(\frac{M_0}{M_D} \right)^{9/7} \text{ yr} \quad , \quad D = 11 \quad (4.28)$$

The corresponding times are short compared to *e.g.* the solar lifetime, and become shorter in higher dimensions, since the values of R_D in these cases become smaller and smaller, approaching r_N and reducing the available evolution range. As we show next, this however means that there will be more range for the 4-dimensional evolution, which is typically slower because of the weaker gravitational coupling in 4 dimensions.

4.2.5 Timescales for $R_D \lesssim R_{EM} \lesssim a$ in $D \geq 8$

Once R_{EM} reaches $\mathcal{O}(R_D)$, the distance at which the black hole's gravity competes with electromagnetic binding forces is in the region where the black hole's field transitions to the lower dimensional form. For concreteness, let us first neglect warping and assume that all radii are the same so that this is a transition to the four-dimensional regime. One reaches this regime at the crossover radius given by (3.22).

The distance required to reach a given $R_{EM} > R_C$ is then, from the distance (4.22) and using the formula (4.17) for β_4

$$d = \frac{32\pi d_0}{9\chi} \left(\frac{M_4}{M_0} \right)^2 \left(\frac{T_D}{M_0} \right)^2 (R_{EM} M_0) \quad (4.29)$$

We are interested in the corresponding time scale to reach $R_{EM} = 1 \text{ \AA}$, where evolution begins to cross over to “macroscopic.” Introducing the numerical values for our parameters, along with the escape velocity v_E and taking $R_{EM} = 1 \text{ \AA}$, we then find a time of the order of hundred billion years

$$t = 9.9 \times 10^{18} s \frac{1}{\chi} \left(\frac{T_D}{400K} \right)^2 = 3.1 \times 10^{11} \frac{1}{\chi} \left(\frac{T_D}{400K} \right)^2 \text{ yr} \quad , \quad (4.30)$$

for evolution to the “macroscopic” crossover.

In the case of $D = 8$, R_C is close to 1 \AA . One may therefore fear that, should the effective R_C be an underestimate by a factor of 2-3, there will be no room for this phase of evolution. However, notice that, aside from the factor $(D - 1)/(D - 3)$, the distance

(4.20) is the characteristic distance for one e-fold growth of the mass. Since the higher-dimensional evolution law must match onto the four-dimensional one in this region (as can be seen explicitly), and since the growth of the radius over a single e-fold in the mass is small ($e^{1/(D-1)}$, or $e^{1/3}$ in four dimensions), the e-fold time for $R_{EM} \sim 1 \text{ \AA}$ sets a lower bound on the evolution time.

4.3 Macroscopic accretion, $R_{EM} \gtrsim a$

4.3.1 Bondi accretion basics

Once the electromagnetic capture radius of the black hole, R_{EM} , grows beyond the atomic radius a , accretion becomes a macroscopic process, with multiple atoms falling in, and with the gravitational range of the black hole exceeding the mean free path. In this regime, two effects counter the free fall of matter: the cohesion forces that keep atoms together, and matter's finite compressibility. We shall not attempt to provide a simple model to describe the effect of cohesion forces on a macroscopic scale, due to the varied composition of matter inside the Earth, with crystalline, semisolid, and liquid phases at various depths. Moreover, it is possible that once the accretion rate reaches a certain threshold, radiation emitted from the accreting matter can melt the surrounding material. (This reradiation effect is discussed in Appendix B, where it is found not to be important until $R_{EM} \gg 1 \text{ \AA}$.) Since our aim is to be conservative and consider the fastest conceivable evolution, we shall neglect the slow down due to cohesion forces, and treat the inside of the Earth as a non-viscous fluid, free to fall into the black hole, subject only to the general laws of hydrodynamics, such as the continuity equation and energy conservation. The compressibility of the medium, which limits the amount of matter that can be funnelled towards the black hole, is accounted for by macroscopic hydrodynamic properties of the medium, such as its sound speed.

The description of accretion under these conditions was developed by Bondi, Hoyle and Lyttleton [33]. We review the derivation of the resulting evolution equation and extend it to incorporate the D -dimensional force law in Appendix A; it is

$$\frac{dM}{dt} = \pi \lambda_D c_s R_B^2 \rho, \quad (4.31)$$

where we define the *Bondi radius* in terms of the black hole radius R ,

$$R_B = \left[\frac{(D-3)}{4c_s^2} \right]^{1/(D-3)} R, \quad (4.32)$$

λ_D is a numerical constant depending on D and on the polytropic index Γ , given in (A.20), which can range between $3 < \lambda_D < 18$, and ρ and c_s are the density and sound speed within the matter asymptotically far from the black hole.

4.3.2 Matching microscopic and macroscopic regimes

Before estimating corresponding time scales, let us first compare the sub- and super-atomic regimes of growth at the transition point, $R_{EM} \sim a$.

Using eq. (4.14) and the relation between Debye frequency and sound velocity $c_s \simeq \omega_D a = T_D a$,¹¹ we can rewrite the expression for R_{EM} given in eq. (4.10) as

$$R_{EM} \simeq a \Delta \left(\frac{M}{M_{a,D}} \right)^{1/(D-1)}, \quad (4.33)$$

where

$$\Delta = \frac{D-1}{D-2} \left[(D-2)(D-3) \frac{\chi}{2} \right]^{1/(D-1)}, \quad (4.34)$$

$$M_{a,D} = \frac{c_s^2 (a M_D)^{D-3}}{k_D} M_D. \quad (4.35)$$

From equations (4.32) and (3.16), we also find:

$$R_B = a \left[\frac{D-3}{4} \right]^{1/(D-3)} \left(\frac{M}{M_{a,D}} \right)^{1/(D-3)}. \quad (4.36)$$

The evolution equations for the two regimes can therefore be equivalently rewritten as:

$$\left(\frac{dM}{dt} \right)_{EM} = \Delta^2 \pi \rho v_{EM} a^2 \left(\frac{M}{M_{a,D}} \right)^{2/(D-1)} \quad (4.37)$$

$$\left(\frac{dM}{dt} \right)_B = \lambda_D \left[\frac{D-3}{4} \right]^{2/(D-3)} \pi \rho c_s a^2 \left(\frac{M}{M_{a,D}} \right)^{2/(D-3)}. \quad (4.38)$$

As before, we use $v_{EM} \sim v_E$; notice that c_s inside the Earth has a comparable value. So, up to an overall factor of order 1, $M_{a,D}$ turns out to be the mass value at which the two evolution rates are the same, and the capture radii for the subatomic and the Bondi accretion regimes coincide. The subatomic growth is faster when $M < M_{a,D}$, while Bondi's growth is faster when $M > M_{a,D}$. This means that for the purpose of being conservative, it is justified to use the former accretion model below $M_{a,D}$, and the latter above $M_{a,D}$.

4.3.3 Time evolution with Bondi accretion

We can split the numerical analysis for the Bondi accretion into the case of $R_D < a$ ($D \geq 8$), where all the evolution for $R_{EM} > a$ is four-dimensional, and the case with $R_D > a$ ($D \leq 7$), where we need to consider both phases.

¹¹Using $T_D = 400$ K and $a = 1$ Å, we obtain $c_s \simeq T_D a \sim 5.2$ km s⁻¹, which is consistent with the sound velocities of typical Earth materials. E.g. $c_s^{Fe} \sim 5$ km s⁻¹ at atmospheric pressure; sound velocities in the liquid forms of a metal are just 20-30% smaller.

The D -dimensional Bondi evolution equation (4.31) is straightforward to integrate. Since we are interested in times for evolution to given radii, it is most useful to convert it to an equation for the Bondi radius R_B , using (4.32). This gives the following times, for evolution from an initial Bondi radius $R_{B,i}$ to a final Bondi radius R_B :

$$t = d_0 \frac{4c_s}{(D-5)\lambda_D k_D} \left(\frac{M_D}{M_0}\right)^{D-2} (M_0 R_B)^{D-5} \quad , \quad D > 5 \quad (4.39)$$

$$t = d_0 \frac{4c_s}{\lambda_5 k_5} \left(\frac{M_5}{M_0}\right)^3 \ln(R_B/R_{B,i}) \quad , \quad D = 5 \quad (4.40)$$

$$t = d_0 \frac{4c_s}{\lambda_4 k_4} \left(\frac{M_4}{M_0}\right)^2 \left(\frac{1}{M_0 R_{B,i}} - \frac{1}{M_0 R_B}\right) \quad , \quad D = 4 \quad (4.41)$$

Recall that d_0 was defined in (4.21). A transition from the D - to 4-dimensional Bondi behaviour will occur when R_B is in the range of $R_{D,C}$. It is easy to check that this transition is continuous, namely the values of the D - and 4-dimensional Bondi radii coincide, when $R_B = R_C$. At this radius, the mass is given by

$$M_B = 16\pi c_s^2 [4\pi k_D (D-3)]^{1/(D-4)} \left(\frac{M_4^2}{M_D^2}\right)^{(D-3)/(D-4)} M_D \quad . \quad (4.42)$$

The evolution time to the slightly smaller radius $R_B = R_D$ is found from (4.39),

$$t = d_0 c_s \frac{4}{(D-5)\lambda_D k_D} \left(\frac{M_D}{M_0}\right)^{(D-2)/(D-4)} \left(\frac{M_4}{M_0}\right)^{2(D-5)/(D-4)} \quad . \quad (4.43)$$

4.3.4 Macroscopic time scales: $D \geq 8$

We start with the case $R_D < a$, so that evolution for $R_B > a$ is purely four-dimensional Bondi accretion. When the black hole enters the macroscopic regime, $R_B \approx a$, eqn. (4.32) implies that its mass is of order 10^{11} gr, therefore still small in geologic terms. Thus by this time it should have settled deep within the Earth. The quantity $c_s d_0$, relevant to the Bondi evolution formulae, can be estimated from the approximately linear relation, known as Birch's law [34], between sound speed and density. This has been tested experimentally for Fe [35, 36] up to the the densities of 12 gr/cm^3 found in the Earth's core, giving :

$$d_0 c_s \approx 1.33 \times 10^{-4} s \quad , \quad (4.44)$$

which is then density independent. (One also finds values comparable to this using, *e.g.*, sound speeds and densities for materials such as iron at low pressure.) Eq. (4.41) then gives the following time to double the radius from $R_B \approx a$ to $R_B \approx 2a$ (and the mass from $M \approx 10^{11}$ gr to $M \approx 2 \times 10^{11}$ gr):

$$t = \frac{8\pi}{\lambda_4} d_0 c_s \frac{1}{a M_0} \frac{M_4^2}{M_0^2} \sim 1.2 \times 10^{12} \frac{1}{\lambda_4} \text{ yr} \quad . \quad (4.45)$$

As shown in Appendix A, the value of λ_4 is in the range 4-18; for $\Gamma = 5/3$ (namely the adiabatic index of a non-relativistic electron gas), $\lambda_4 = 4$. Notice that the parameter dependence of (4.45) is identical to that of eq. (4.29), once we use $c_s \simeq T_D a$. This is also reflected in the similarity of the timescales, eqs. (4.30) and (4.45).

As a side note, we remind the reader of discussions of the possibility that primordial black holes remain from the early universe; in the standard quantum scenario only those with masses $\gtrsim 10^{15}$ gr would have not yet evaporated. With the present formalism, we can provide a bound on the lifetime of Earth, should a minimum-mass primordial black hole be captured within its gravitational field. Using the parameters in this section, and the evolution law (4.41), we find a bound on the accretion time $t \gtrsim 47$ Myr, with shorter times for higher-mass black holes. These, and corresponding accretion times we will find for white dwarfs and neutron stars, may allow one to set limits on galactic densities of primordial black holes.

4.3.5 Macroscopic time scales, $D = 6, 7$

In the cases $D = 6, 7$, $R_D > a$ and so we have D -dimensional Bondi evolution up to $R_B \sim R_D$, and then four-dimensional Bondi evolution from $R_B = R_C$ up to infinity. To be conservative, we model the phase with $R_D < R_B < R_C$ by assuming D -dimensional evolution with a constant Bondi radius, with $R_B = R_C$, until the black hole mass grows to the point that the respective R_B exceeds R_C . For $D = 7$ the mass at $R_B \approx a$ is of order 10^4 gr; for $D = 6$ it is much smaller. For our approximate estimates, we again use the value of $c_s d_0$ given in (4.44).

The times for the evolution up to R_D are thus given by (4.43), leading to:

$$t = 5.5 \times 10^4 \frac{1}{\lambda_6} \left(\frac{M_D}{M_0} \right)^2 \text{ yr} \quad D = 6 \quad (4.46)$$

$$t = 8.6 \times 10^8 \frac{1}{\lambda_7} \left(\frac{M_D}{M_0} \right)^{5/3} \text{ yr} \quad D = 7. \quad (4.47)$$

The following phase, between R_D and R_C , then has a time scale given by:

$$t = d_0 c_s \frac{16\pi}{[4\pi(D-3)k_D]^{1/(D-4)} \lambda_D} \left(\frac{M_D}{M_0} \right)^{(D-2)/(D-4)} \left(\frac{M_4}{M_0} \right)^{2(D-5)/(D-4)}, \quad (4.48)$$

The subsequent evolution to large sizes has a time scale determined by the initial radius, $R_B = R_C$ in (4.41), and results in an expression identical to (4.48), with λ_D replaced by λ_4 . The timescales for these two phases are given by:

$$t = 9.7 \times 10^4 \frac{1}{\lambda_{6,4}} \left(\frac{M_D}{M_0} \right)^2 \text{ yr} \quad D = 6 \quad (4.49)$$

$$t = 1.28 \times 10^{10} \frac{1}{\lambda_{7,4}} \left(\frac{M_D}{M_0} \right)^{5/3} \text{ yr} \quad D = 7. \quad (4.50)$$

The $D = 6$ time is short as compared to geologic time scales. Using $\lambda_7 = 4$ (independent of Γ) and $\lambda_4 = 4$ (for $\Gamma = 5/3$) we obtain in $D = 7$ a combined time scale of approximately (6.4, 20, 40, 65, 94) billion years for $M_D = 1, \dots, 5$ TeV. Since, as we discuss in Appendix E, a conservative threshold for black hole formation is $M_{min} = 3M_D$, these values correspond to minimum black hole masses $M_{min} = (3, 6, 9, 12, 15)$ TeV.

4.4 Warped evolution

In order to parameterize more general evolutions, we consider the case of a warped scenario, as described in section 3.2.3. In this case, we have D -dimensional evolution up to capture radius R_D , then a warped evolution up to R_C , then four-dimensional evolution from then on. These scales are related by an expression of the form (3.26). Combining this with the maximum value of the warping, found from (3.6) by taking R_D to be the minimum possible value, M_D^{-1} , we find that

$$R_C/R_D \lesssim 10^2, \quad (4.51)$$

so there is still not wide disparity between these scales.

As the preceding discussion has illustrated, a key question is the location of R_C with respect to the atomic scale a . Macroscopic evolution in the the four-dimensional regime is dominated by the timescale from the lower endpoint at $R_B = R_C$, and if $R_C \lesssim 200\text{\AA}$, this, via (4.41), yields a safe time scale in excess of 3×10^9 yr. The warped growth below R_C should also yield a similar time scale, as in the preceding discussion.

On the other hand, accelerated growth is possible for R_C significantly larger than 200\AA . We particularly saw this in the case $D = 6$. Warped evolution presents another extreme (but finely-tuned) scenario. Specifically, consider the case $D = 5$ with radius just below the experimental bound, say $R_C \approx 0.2\text{mm}$. In this case, one finds five-dimensional evolution through subnuclear, subatomic, and Bondi phases. If, in line with our discussion of scales, we take $R_D \approx 0.02\text{mm}$, the evolution time up to this radius follows from (4.40). This yields an estimate $t_{B,5} \approx 5 \times 10^{-3}s$. At this point, the black hole has a mass $M_{B,5}$ around 0.1gr. Next, one evolves through the warped regime. The precise form of the evolution in this regime is not completely understood. The form of the linearized potential [32] suggests that the radius grows as the logarithm of the energy, but ref. [32] also points out that the corresponding solutions are possibly unstable and instead spread out more widely on the visible brane. Ref. [37] worked out details of a possible picture of the resulting solution, which would be the gravitational dual of a plasma ball of QCD. Whatever the precise evolution law is, it is quite slow, since at the end of this phase the mass is of size $M_{B,4} \approx 2 \times 10^{17}\text{gr}$ while the radius has only changed from R_D to R_C . Conservatively, one can take the fastest time scale for evolution, namely that with a *constant* capture radius $R_B \approx R_C$. Finally, the time for the four-dimensional evolution from $R_B = R_C$ to the mass of the Earth has time scale given by (4.41). Both of these phases yield time scales

$$t \sim 3 \times 10^5 \text{ yr} . \quad (4.52)$$

While this time scale as well as that of the $D = 6$ case only represent *lower* bounds on the accretion time, since we have made various conservative assumptions such as that of accretion from a fluid, these times are too short to provide comfortable constraints.

4.5 An Eddington limit?

If evolution is sufficiently rapid, as is particularly exhibited by the $D = 6$ case and the extreme $D = 5$ warped case, and in four dimensions, one is naturally led to question whether there is an Eddington limit. This would occur if radiation from the rapidly accreting matter produced sufficient pressure to inhibit accretion.

In particular, one can parametrize the total luminosity of the outgoing radiation in terms of the rate of mass accretion by an efficiency parameter η ,

$$L = \eta \frac{dM}{dt} . \quad (4.53)$$

If this radiation is in photons, it will exert a force on the infalling atomic matter of Earth which can be approximated as given by the Thomson cross section σ :

$$F_L = \frac{\eta \dot{M} \sigma}{4\pi r^2} . \quad (4.54)$$

The question is whether this can balance the force of gravity pulling the matter inwards.

We examine this question in more detail in Appendix B. In short, we do not find evidence for such an Eddington limit; this is connected to the known result (see e.g. [38]) that spherical accretion onto a black hole is inefficient at producing a large luminosity.¹² Nonetheless, we note that if a mechanism to produce such an Eddington limit *were* found, this would lengthen the shorter accretion time scales considerably. In particular, as we review in Appendix B, four-dimensional Eddington evolution produces exponential growth of the mass with time, with time constant

$$t_{Edd} = \eta \frac{\sigma}{4\pi m G} , \quad (4.55)$$

where m is the average atomic mass per electron, $m \approx 2m_p$. This produces an e-fold time scale of size $t_{Edd} \approx 2.3\eta \times 10^8 \text{yr}$.

4.6 Summary of growth on Earth

This section has modeled growth laws on Earth, using conservative assumptions.

The resulting growth times for $D \geq 8$ are bounded below by the many-billion-year time scales given in eqs. (4.30), (4.45); these arise from the subatomic and superatomic regimes,

¹²In certain low-collisionality astrophysical contexts, different from conditions dealt with here, magnetic fields alter this story; see *e.g.* [39].

respectively, and are times that are long as compared to the expected natural lifetime of the Sun. At these times, the black holes masses are still in the range of 10^{11} gr, and have a growth rate of the order of 300 kW, which gives a bound on possible power output that is totally negligible in the geologic context.

The case of $D = 7$ also gives times longer than the Sun's lifetime, with an overall timescale for the evolution, eq. (4.50), ranging from 6 to over 80 billion years. At such time scales, the growth rate reaches approximately 10 GW, about 10^{-7} the solar flux on Earth, and much smaller than the ~ 40 TW heat flow from the interior of the planet; this bounds any possible thermal impact to be negligible. The case $D = 6$, with time scale (4.49), even though very long by human standards, is much shorter than the natural lifetime of the solar system. As we saw, certain warped scenarios are also similarly potentially problematic. Therefore, in order to constrain these scenarios we turn to their consequences for other astronomical bodies, particularly white dwarfs and neutron stars.

5 Stopping of cosmic ray-produced black holes

Collisions with center-of-mass energies comparable in energy to LHC occur frequently in the universe. The best known and directly measured process is the collision of high-energy cosmic rays (CRs) with the nucleons in the Earth's atmosphere. For the collision of a CR of mass Am_p to exceed the nucleon-nucleon center of mass (CM) energy of $E_{LHC} = 14$ TeV, the CR energy should be at least $E_{min}(A) = A E_{LHC}^2 / 2m_p \sim (10^{17}A)eV$, well below the maximum value of measured CR energies. A simple estimate of the number of nucleon-nucleon interactions above LHC energies can be obtained from an approximate flux relation, derived from the current data [40–42]:

$$\frac{d\Phi}{dE} \sim 10^6 (E/\text{GeV})^{-3} \text{ m}^{-2} \text{ s}^{-1} \text{ sr}^{-1} \text{ GeV}^{-1}, \quad (5.1)$$

which provides a lower bound to the measured CR spectra in the interesting region $E_{CR} > 10^{17}eV$, up to the GZK cutoff [43, 44] of $E_{GZK} \sim 5 \times 10^{19}$ eV. Confining ourselves to the part of the spectrum below the GZK cutoff, we obtain the following integrated flux:

$$N(\sqrt{s} > E_{LHC}) = A \int_{E > E_{min}(A)} \frac{d\Phi}{dE} dE \sim \frac{1.6 \times 10^3}{A} \text{ yr}^{-1} \text{ km}^{-2} \text{ sr}^{-1}, \quad (5.2)$$

where \sqrt{s} is the CM energy of a nucleon-nucleon collision. This corresponds to about $1/A \times 10^{22}$ collisions above the LHC energy at the surface of the Earth during the course of its existence. This number greatly exceeds the total number of collisions in the course of the LHC operations at its highest intensity (about 10^9 s^{-1} over a 10^8 s period), even assuming a cosmic ray flux dominated by Fe nuclei.

If black holes can be produced at the LHC, they will therefore be copiously produced in such CR-induced collisions with astronomical bodies. Thus, stability of such bodies on

astronomically long time scales offers the prospect of ruling out rapid accretion scenarios. In order to provide such bounds, one needs to check that a CR-produced black hole will slow sufficiently to be trapped in such an object, so that it begins accreting. After that, one needs to check the relevant accretion time scale. This section will focus on the former question. We will find that while, as briefly described in section 2.2, we cannot guarantee that Earth is an efficient target for trapping hypothetical CR-produced black holes in all scenarios, white dwarfs and neutron stars do provide very useful targets.

5.1 Production kinematics

Let E be the energy of a cosmic ray nucleon hitting an astronomical target. Black hole production would arise from collisions of two partons, with center-of-mass momentum fractions x_1 and x_2 for incident parton and target parton, respectively. The mass M of the resulting black hole is given by

$$M^2 \approx 2 x_1 x_2 y^2 E m_p \quad (5.3)$$

where $y \leq 1$ is an efficiency factor, parametrizing inelasticity (energy loss) due to radiation in the collision process, and m_p is the proton mass. The bulk of the production is at $x_1 \sim x_2 \sim x = M/(y\sqrt{2Em_p})$. After being produced, the black hole in the fixed-target frame will carry energy $x_1 y E \sim M\sqrt{E/2m_p}$, and thus has a Lorentz γ factor

$$\gamma \simeq \sqrt{\frac{x_1}{x_2}} \sqrt{\frac{E}{2m_p}}. \quad (5.4)$$

Since $x_1, x_2, y \leq 1$, eq. (5.3) gives

$$\gamma = \frac{M}{2x_2 m_p y} > M/2m_p. \quad (5.5)$$

The black hole will therefore be highly relativistic. These boosts range up to typical values of size $\gamma \sim 3M/m_p$; for example, in the extreme case of interest for the LHC, $M = 14\text{TeV}$, fig. 7 shows significant production at $\gamma \lesssim 4.5 \times 10^4$.

If the black hole is very weakly interacting, it could travel across the object unimpeded, thus preventing limits from being set. We therefore concentrate first on this issue.

5.2 Stopping: neutral black holes

In line with our discussion of section 2.1, we will explore the assumption that black holes interact only via their gravitational field. Collisions can slow such a black hole via two mechanisms. First, in a typical collision the black hole will gravitationally scatter a particle in its asymptotic field, thus losing some of its momentum. We henceforth refer to this gravitational mechanism as Coulomb slow-down. Second, for smaller impact parameters, a black hole can absorb a particle, in the process possibly emitting some radiation, and

typically increasing its mass. This also slows the black hole, and will be referred to as accretion slow-down. In what follows we denote by E_i and p_i the energy and momentum of the black holes at the time of production by the cosmic ray.

5.2.1 Accretion slow-down

For the smallest black holes, such as those in the early stage of the accretion, the target particles should be thought of as partons, moving relativistically inside the nucleon. In the black hole rest frame, denoted by a prime, incident partons have energy and momentum

$$E'_p \approx p'_p \approx \frac{E}{M}(E_p - p_p) , \quad (5.6)$$

where E_p and p_p are the parton energy and parallel momentum component in the star rest frame. Note that for the first few collisions $E'_p \sim M$, since $E_i/M \sim M/m_p \sim M/E_p$. But as the black hole slows, E'_p becomes much smaller than M .

If black holes can capture matter via their gravitational fields and accrete within Earth, then their gravitational fields will similarly capture and scatter matter while moving through any astronomical object, and we will consistently work within such a framework. Some general features of gravitational scattering and/or capture of relativistic particles in the field of a D -dimensional black hole are reviewed in Appendix C. There we find the minimum impact parameter, $\hat{b}_{min}R$, below which relativistic particles enter the capture regime. This can be calculated classically, or defined quantum-mechanically in terms of the capture cross section,

$$\sigma_c = \pi(\hat{b}_{min}R)^2 , \quad (5.7)$$

with closely corresponding results in the cases of interest. A capture collision should result in the parton transferring its momentum, and is expected to result in much of the parton energy also being absorbed, although it is also likely that some of the parton energy will be radiated in the process. The change in the black hole mass and momentum are thus parameterized as

$$\Delta p' = c_{ac,p} p'_p \quad ; \quad \Delta M \simeq \Delta E' = c_{ac,M} E'_p . \quad (5.8)$$

We expect $c_{ac,p} \simeq 1$, and have $0 < c_{ac,M} < \text{Min}(1, c_{ac,p})$ parameterizing the fraction of energy absorbed.¹³ Back in the star frame, the momentum change will then be

$$\Delta p = c_{ac,p} p_p - (c_{ac,p} - c_{ac,M}) \frac{E^2}{M^2} (E_p - p_p) \quad (5.9)$$

where the terms proportional to p_p contribute zero when averaged over different parton momenta. One can combine these equations with the capture cross section to determine the

¹³Indeed, we expect that (chromo-)electrostatic effects significantly reduce $c_{ac,M}$, below an energy threshold $E'_p \sim \alpha_s/R$. Notice that any energy that is not absorbed must be re-radiated, thus contributing to black hole momentum loss.

accretion contribution to the momentum and mass variation. For a black hole of velocity $v \sim 1$ in a matter distribution with parton density n , one finds:

$$\left(\frac{dp}{dt}\right)_{ac} = n\pi[\hat{b}_{min}R(\sqrt{s})]^2\Delta p, \quad (5.10)$$

$$\left(\frac{dM}{dt}\right)_{ac} = n\pi[\hat{b}_{min}R(\sqrt{s})]^2\Delta M, \quad (5.11)$$

where

$$s = M^2 + 2(EE_p - pp_p) + m_p^2. \quad (5.12)$$

This leads to the following evolution as a function of path length ℓ :

$$\left(\frac{dp}{d\ell}\right)_{ac} = -(c_{ac,p} - c_{ac,M})\hat{b}_{min}^2\pi\rho\frac{E^2}{M^2}R^2(\sqrt{s}), \quad (5.13)$$

$$\left(\frac{dM}{d\ell}\right)_{ac} = c_{ac,M}\hat{b}_{min}^2\pi\rho\frac{E}{M}R^2(\sqrt{s}), \quad (5.14)$$

where we introduced the energy density $\rho \simeq n\langle E_p \rangle$. We see that in the limit $c_{ac,M} = c_{ac,p}$ (“perfect accretion”), there is no average momentum transfer.

5.2.2 Coulomb slow-down

Consider now the case of gravitational elastic collisions. For the earliest collisions, $R \gg 1/p'_p$, which is the regime of classical particle scattering. Once γ has decreased by a factor of approximately ten, the wavelength becomes longer than R and we enter the quantum regime.

Thus, we consider incident partons outside the capture regime, classically described by impact parameter $b > \hat{b}_{min}R$. The momentum loss of the black hole is

$$\Delta p = -2\frac{E^2}{s}(E_p - p_p)\sin^2\frac{\theta}{2} \quad (5.15)$$

where θ is the CM scattering angle. (For all but the first collisions, the CM frame is well-approximated by the black hole frame.) One can then sum over collisions, as in the accretion case, to obtain the differential momentum loss. In terms of the differential cross section, this takes the form

$$\left(\frac{dp}{d\ell}\right)_{sc} = -\frac{E^2}{s}\rho\int_{\cos\theta_c}^1 d\cos\theta\frac{d\sigma}{d\cos\theta}2\sin^2\frac{\theta}{2}, \quad (5.16)$$

where $\theta_c \sim 1$ represents the maximum angle avoiding capture. Here the parton momenta have averaged to zero. In parallel with (5.13), we write this as

$$\left(\frac{dp}{d\ell}\right)_{sc} = -c_{sc}\hat{b}_{min}^2\pi\rho\frac{E^2}{s}R^2(\sqrt{s}). \quad (5.17)$$

where

$$c_{sc} = \frac{1}{\sigma_c} \int_{\cos\theta_c}^1 d\cos\theta \frac{d\sigma}{d\cos\theta} 2\sin^2\frac{\theta}{2}; \quad (5.18)$$

the corresponding classical expression is

$$c_{sc} = \frac{1}{\hat{b}_{min}^2} \int_{\hat{b}_{min}}^{\infty} d\hat{b}^2 2\sin^2\frac{\theta}{2}. \quad (5.19)$$

The parameter c_{sc} is estimated in Appendix C, yielding for the quantum case the values (0.5, 0.25, 0.17) for $D=5-7$. Note that as a result of $\hat{b}_{min} > 1$, gravitational Coulomb scattering plays a subdominant role.

5.2.3 Slow-down to $\gamma \sim 1$.

We now combine the Coulomb and accretion stopping rates to determine the length required to slow-down the black hole to the non-relativistic regime. As noted, initially $EE_p \sim M^2$, but as the energy falls, the mass term in (5.12) dominates. Then the Coulomb and accretion stopping formulas, (5.17) and (5.13), have the same form. Moreover, dividing (5.14) by their sum, and defining

$$c' = \frac{c_{ac,M}}{c_{ac,p} - c_{ac,M} + c_{sc}}, \quad (5.20)$$

we find in this regime

$$\frac{dM}{dp} = -c' \frac{M}{E}, \quad (5.21)$$

with solution

$$\frac{M}{M_i} = \left(\frac{p}{p_i}\right)^{-c'}, \quad (5.22)$$

This, together with the dependence $R(M) = R_i(M/M_i)^{1/(D-3)}$, then allows us to integrate the sum of (5.17) and (5.13) and deduce the distance d to evolve to a given final momentum p and mass M related by (5.22):

$$\int^d \rho dl \simeq \frac{1}{c_{sc} + c_{ac,p} + c_{ac,M}(D-5)/(D-3)} \frac{1}{\hat{b}_{min}^2} \frac{M}{\pi R^2(M)} \frac{M}{p}. \quad (5.23)$$

The left hand side defines the column density, $\delta(d)$, as a function of d .

The momentum where the black hole becomes near-relativistic, $p \approx M = M_{NR}$, is obtained from eqn. (5.22) as:

$$M_{NR} = M_i \left(\frac{p_i}{M_i}\right)^{c_{ac,M}/(c_{ac,p}+c_{sc})}. \quad (5.24)$$

Since, as we have seen, the initial boost $\gamma_i = p_i/M_i$ is large, growth of the mass in this phase can be significant. The corresponding column density is

$$\delta_R(d) \simeq \frac{1}{c_{sc} + c_{ac,p} + c_{ac,M}(D-5)/(D-3)} \frac{1}{\hat{b}_{min}^2} \frac{M_{NR}}{\pi R^2(M_{NR})}. \quad (5.25)$$

For rough benchmarks we can replace the right hand side by M_0^3/π . If we work with constant density, we see that the stopping distance is then approximated by $d \sim d_0 = M_0^3/\pi\rho$, as defined in (4.21).

In view of the value for Earth $d_0(E) \approx 3 \times 10^{11}$ cm, these mechanisms cannot efficiently slow down neutral CR-produced black holes in Earth, or in other bodies such as planets and ordinary stars¹⁴. For the same reason, typical black holes produced at the LHC are expected not to be captured by the Earth (see Appendix F), posing no risk; however, there is small but finite probability for them to be produced with velocities small enough to become gravitationally bound to the Earth and, in the hypothetical case of stability, to begin accreting.

On the other hand, for a neutron star with densities surpassing 10^{14} gr/cm³, one has $d_0(NS) \lesssim 0.01$ cm. Thus neutron stars can promptly slow down such black holes, and then quickly bring them to below the escape velocity, which for a neutron star is close to $v \sim 1$. Finally, for white dwarfs, whose central density can exceed $\rho = 10^7$ gr/cm³, one finds $d_0(WD) \sim 1.5$ km, compared to radii in the $10^3 - 10^4$ km range. Thus, in order to establish stopping in white dwarfs, we need to make a complete numerical analysis, considering also the nonrelativistic phase of the slow down.

5.3 Stopping in white dwarfs

Stopping scales in white dwarfs are not enormously far from their radii, motivating a more complete treatment. We begin by noting that once a black hole reaches the near-relativistic regime, $p \sim M$, it must be further slowed to below the escape velocity in order to be trapped. Thus we must understand nonrelativistic slowing.

We consider white dwarfs with masses $M \approx M_\odot$, which have radii $R_{WD} \approx 5500$ km. Such a white dwarf has an escape velocity $v_{WD} \sim 2 \times 10^{-2}$. The material in such white dwarfs is described as a fluid of degenerate electrons, in which are embedded atomic nuclei, for example carbon and oxygen. (Later, at time scales \sim Gyr, this material can crystallize.)

¹⁴As a consequence of this, neutral black holes produced during head-on collisions of cosmic rays within the galaxy will freely escape the galaxy, not being trapped by either collisions with the interstellar medium and stars, or by the galactic magnetic field. Therefore arguments such as those used in Ref. [45] to rule out the production of strangelets do not seem to easily apply in this context.

5.3.1 Nonrelativistic stopping

At the end of the relativistic regime, the black hole has a mass $M_{NR} \approx p$ given by (5.24). In addition to R , capture dynamics can in principle be governed by the capture radius for free particles, R/v , or R_{EM} , defined using white dwarf parameters, $a_{WD} \sim 10^{-2}\text{cm}$. However, in the regime $v \gtrsim .02$, these radii are all less than or of order r_N (see Appendix D), so the capture is dominantly subnuclear.

As the black hole moves through the stellar material, it collides with nucleons at a rate

$$\frac{dn}{dl} = \pi \frac{\rho}{m_p} r_n^2. \quad (5.26)$$

When a collision occurs, it moves non-relativistically through the nucleon. As it does so, it is bombarded by the relativistic partons within the nucleon. The average mass and momentum collected during such a transit is given using (5.10), (5.11), times the average time $\Delta t = 4r_n/3v$ of the transit; combining with (5.26) gives

$$\frac{dp}{d\ell} = -(c_{ac,p} - c_{ac,M}) \hat{b}_{min}^2 \pi \rho R^2 \quad (5.27)$$

$$\frac{dM}{d\ell} = c_{ac,M} \hat{b}_{min}^2 \pi \rho \frac{R^2}{v}. \quad (5.28)$$

Note two possible caveats to these formulas. First, in a collision with a single nucleon, ΔM cannot be bigger than m_p . We show that this is true in Appendix D. Second, there could be enhancements of ΔM due to the fact that if the black hole captures a parton, the QCD string can pull in more energy, whether or not it breaks. (Moreover, since most of the nucleons are in nuclei, it may even be that it pulls in more of the nucleus.) Indeed, one might expect a minimum energy captured of ~ 100 MeV if the BH captures one parton. Let us, however, stick with this simple and conservative estimate.

Coulomb stopping may be suppressed in this regime, and we conservatively neglect it. As before, one can find an equation relating M and p :

$$\left(\frac{M}{M_{NR}} \right)^{1-c_{ac,M}/c_{ac,p}} = \left(\frac{p}{M_{NR}} \right)^{-c_{ac,M}/c_{ac,p}}. \quad (5.29)$$

Thus, for ‘‘perfect accretion,’’ p remains a constant. We also find

$$v = \left(\frac{M}{M_{NR}} \right)^{-c_{ac,p}/c_{ac,M}}. \quad (5.30)$$

One can then integrate (5.28) to find the column density to a given final mass M_f :

$$\delta_{NR}(d) = \frac{1}{c_{ac,M} \hat{b}_{min}^2} \int_{M_{NR}}^{M_f} \frac{dM}{\pi R^2} \left(\frac{M_{NR}}{M} \right)^{c_{ac,p}/c_{ac,M}}. \quad (5.31)$$

This can be evaluated using the scaling (3.16) of R with M , to find the distance travelled to reach mass M_f : reformatted to make more readable

$$\delta_{NR}(d) = \frac{1}{c_{ac,p} - c_{ac,M}(D-5)/(D-3)} \frac{1}{\hat{b}_{min}^2} \left\{ 1 - \left(\frac{M_{NR}}{M_f} \right)^{[c_{ac,p}/c_{ac,M} - (D-5)/(D-3)]} \right\} \frac{M_{NR}}{\pi R^2(M_{NR})}, \quad (5.32)$$

an evolution law governed by larger velocities. Note that this gives the same scale as the evolution to M_{NR} , as in (5.25). This is of course a *conservative* scale, since we have completely neglected any momentum loss due to scattering, and also have neglected possible enhancements due to binding effects with nuclear fragments.

5.3.2 Stopping bounds

From these equations we can compute the column densities necessary for stopping. We first note that, by virtue of the fact that $\gamma_i = p_i/M_i$ is large, the stopping distance grows with increasing $c_{ac,M}/c_{ac,p}$, due to the exponential dependence in (5.24). Therefore, we set it to its maximum value, $c_{ac,M} = c_{ac,p}$.¹⁵

Notice also that stopping distance increases with decreasing c_{sc} . Thus, one is tempted to set this to zero. However, even small c_{sc} plays an important role. Specifically, consider the bound on the nonrelativistic stopping,

$$\delta_{NR}(d) < \frac{D-3}{2c_{ac,p}\hat{b}_{min}^2} \frac{M_{NR}}{\pi R^2(M_{NR})}. \quad (5.33)$$

To test its sensitivity to our physical expectation $c_{ac,p} \simeq 1$, let us see how much the column density for given c_{sc} changes if we take $c_{ac,p} = 1/4$, as compared to its value for $c_{ac,p} = 1$ and $c_{sc} = 0$. Note from $c_{ac,M} \leq c_{ac,p}$ that this would correspond to a reduction in the mass accretion rate of 1/4. From (5.33) we easily find less than 25% variation in the resulting bound on δ_{NR} as long as

$$c_{sc} > \frac{1}{4} \frac{1}{(D-5) \ln \gamma_i / [(D-3) \ln(16/5)] - 1}. \quad (5.34)$$

The tightest constraints on stopping parameters arise for largest M_i and thus, as we see from (5.5), large boost. Using that equation, or alternately from fig. 7, we see that there is a large production efficiency for $\gamma_i \lesssim 3M_i/m_p$, or with $M_i = 14$ TeV, around $\gamma_i \sim 4.5 \times 10^4$. Thus, we find the variation of the stopping distance bounded in this fashion so long as $c_{sc} > (.12, .07)$ for $D = 6, 7$. Moreover, this bound neglects the fact that any reduction of $c_{ac,p}$, corresponding to a reduction of accretion, should lead to an *increase* of scattering, parametrized by c_{sc} , thus improving the bound. These features arise from the exponential

¹⁵We note that this appears quite conservative, in that we expect $c_{ac,M}$ to become small below the (chromo-)electrostatic threshold mentioned previously. This in turn would significantly reduce the effective value of M/R^2 that enters the expressions (5.25) and (5.32) for the needed column densities.

Table 1: Column densities δ_T , in units of 10^{15}gr/cm^2 , required to stop a black hole of given masses.

| $\delta_T/10^{15}\text{gr/cm}^2$ | $D = 5$ | $D = 6$ | $D = 7$ | $D = 8$ |
|----------------------------------|---------|---------|---------|---------|
| $M = 7$ TeV | 0.09 | 0.65 | 1.8 | 3.3 |
| $M = 8$ TeV | 0.13 | 1.0 | 2.9 | 5.3 |
| $M = 9$ TeV | 0.19 | 1.5 | 4.3 | 8.2 |
| $M = 10$ TeV | 0.25 | 2.1 | 6.2 | 11.9 |
| $M = 11$ TeV | 0.34 | 2.9 | 8.7 | 16.8 |
| $M = 12$ TeV | 0.44 | 3.9 | 11.8 | 23.0 |
| $M = 13$ TeV | 0.56 | 5.1 | 15.6 | 30.7 |
| $M = 14$ TeV | 0.70 | 6.5 | 20.2 | 40.0 |

dependence in (5.24); a similar statement is slightly stronger for δ_R , as a consequence of its additional dependence on c_{sc} through its denominator. Rough values of c_{sc} for $D = 6, 7$ are given (see Appendix C) by (.25,.17). Thus, in addition to the physical expectation $c_{ac,p} \simeq 1$, we find the statement that even for small c_{sc} , one does not increase the stopping distance by varying $c_{ac,p}$ over a wide range. We thus take $c_{sc} = 0$ and $c_{ac,p} = 1$, and will rely on the resulting column densities to not be more than 25% higher, although we expect that they could be significantly lower.

Taking these values, and combining our bounds from (5.25) and (5.33), we find

$$\delta_T(d) = \delta_R(d) + \delta_{NR}(d) < \frac{(D-3)^2}{2(D-4)} \frac{1}{k_D^{2/(D-3)} \pi \hat{b}_{min}^2} \left(\frac{M_D}{M_0}\right)^3 \left(\frac{\gamma_i M_i}{M_D}\right)^{(D-5)/(D-3)} M_0^3. \quad (5.35)$$

The column density M_0^3 converts to $4.6 \times 10^{12}\text{gr/cm}^2$. For our numerical estimates here we shall confine ourselves to black holes produced with $\gamma_i \lesssim 3M_i/m_p$, as above. Since the evolution is dominated by the phase where the wavelength of the incident particle is large compared to the black hole radius, we use the values of the parameters \hat{b}_{min} corresponding to the quantum absorption, as given in Appendix C.2. To maximize the needed column density, we also use the maximum value of M_D corresponding to a given mass M_i , namely $M_D = M_i/3$. Equation (5.35) then leads to the maximum column densities shown in table 1 for various black hole masses.

Integration of the column density of a $M_{WD} = M_\odot$ white dwarf along a diameter, using the density profiles shown in fig. 1 [46], yields a column density $\delta_{WD} = 2 \int_0^{R_{WD}} \rho dl = 13 \times 10^{15}\text{gr/cm}^2$. This number increases to $\delta_{WD} = 21 \times 10^{15}\text{gr/cm}^2$ for $M_{WD} = 1.1 M_\odot$, and to $\delta_{WD} = 38 \times 10^{15}\text{gr/cm}^2$ for $M_{WD} = 1.2 M_\odot$. The systematic uncertainty on these values, determined by varying the parameters of the white dwarf such as temperature and composition, is of the order of 10% [47].

A comparison between the required stopping column densities, and the available stopping power of white dwarfs, is shown in fig. 2.

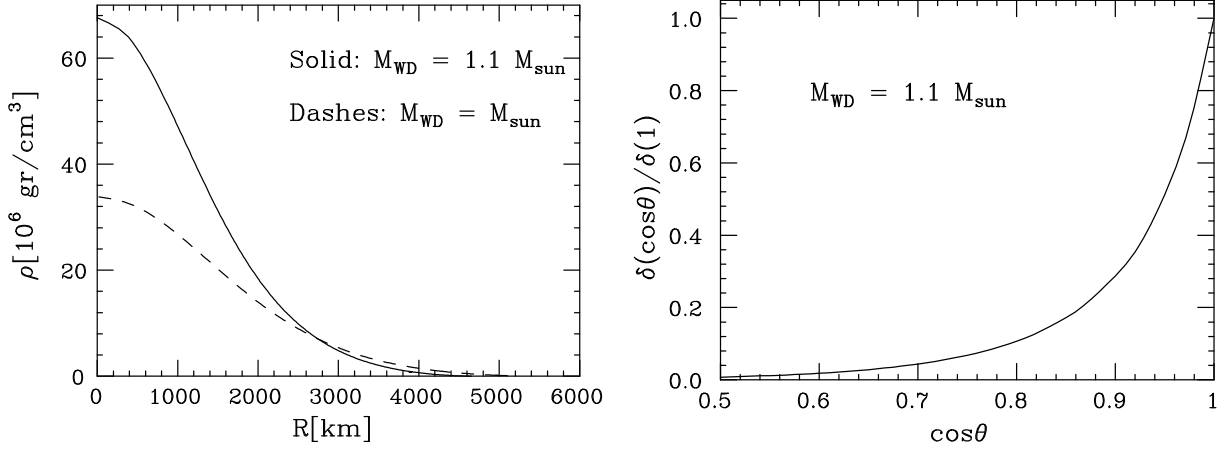


Figure 1: *Left: density profile for a solar-mass white dwarf (courtesy K. Shen). Right: column density, as a function of the penetration angle θ with respect to the zenith, normalized to the column density at $\theta = 0$.*

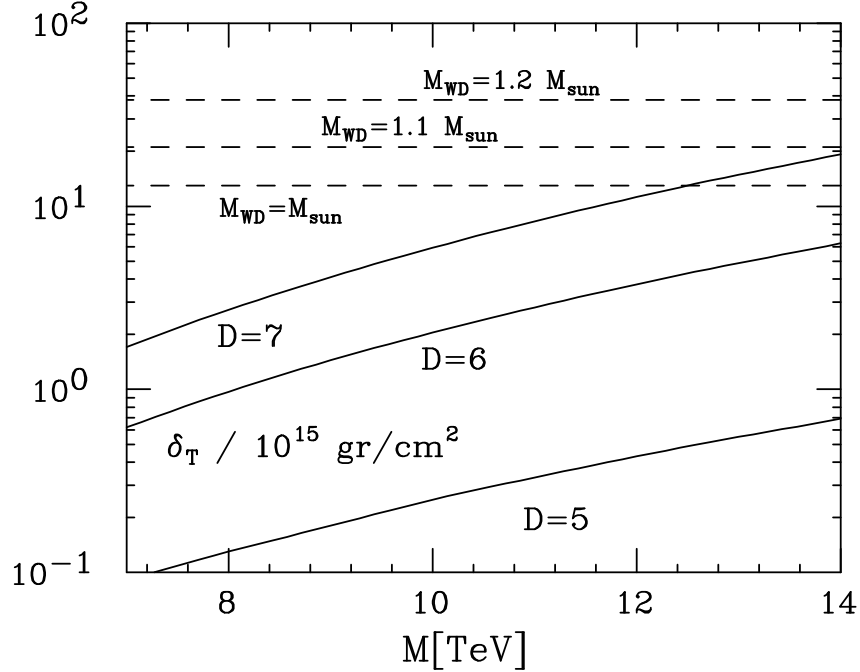


Figure 2: *Column densities required to stop black holes of different masses in different space-time dimensions D (solid lines) and integral column densities for white dwarfs of mass $M_{\text{WD}} = (1, 1.1, 1.2)$ solar masses.*

We thus conclude that a solar-mass white dwarf can efficiently stop black holes. In the case of $D = 5$ and 6, black holes corresponding to the most conservative LHC scenario, with masses up to 14 TeV and M_D accordingly large, will stop within a fraction of the maximum column depth for white dwarfs at or above M_\odot . In the case of $D = 7$, one needs stars heavier than approximately 1.1 solar masses in order to achieve stopping up to 14 TeV. However, as indicated in Section 4.3.5, $D = 7$ black holes above 6 TeV give rise to accretion lifetimes on Earth in excess of 20 billion years. Our calculated stopping column densities for masses below this are well below the column density of a solar mass white dwarf.

As shown in table 1, the column densities required to stop the heaviest black holes for $D \geq 8$ exceed the stopping power of even the most massive white dwarfs, and therefore we shall only state empirical constraints on such scenarios when discussing the neutron stars case.

6 Black hole production on white dwarfs

In this section we briefly describe the expected rates of black hole production on white dwarfs; for more details see Appendix E. Before discussing such production rates, however, we must discuss the effects of magnetic fields.

6.1 Magnetic screening

White dwarfs and neutron stars are known to have significant magnetic fields, which can have important effects on the charged cosmic-ray primaries. (For more details see Appendix G.) For example, in the case of a dipole field of polar strength B_p , an incident ray of charge Ze and momentum p perpendicular to the magnetic axis will have a Larmor radius that depends on the distance r from the center of the object as follows:

$$r_L(r) = \frac{2p}{ZeB_p} \left(\frac{r}{R_0} \right)^3, \quad (6.1)$$

where R_0 is the radius at the surface. While even for neutron stars r_L can be greater than the radius of the star, as shown in Appendix G, with the very high energy cosmic rays required one must consider the effects of synchrotron radiation. This is studied in more detail in Appendix G, with the result that a ray at incident angle θ and with mass number A will have an energy at R_0 determined in terms of its incident energy E_∞ by

$$E_{R_0} = E_{max} \frac{E_\infty}{E_\infty + E_{max}}, \quad (6.2)$$

where

$$E_{max} = \frac{60A^4 m_p^4}{2(Ze)^4 (\sin \theta B_p)^2 R_0}. \quad (6.3)$$

Thus, E_{max} sets an effective maximum energy for cosmic rays that penetrate to the surface of the star; for protons, and normalizing to typical white-dwarf parameters, we find that

$$E_{max}(\theta = \pi/2) = 3.6 \times 10^{18} \text{eV} \frac{5000 \text{km}}{R_0} \left(\frac{10^6 \text{G}}{B_p} \right)^2 . \quad (6.4)$$

Since, as we will find, optimal bounds come from considering cosmic ray energies up to $\sim 10^{20} \text{eV}$, we see that in order to avoid significant magnetic screening, we must consider white dwarfs with magnetic fields $B_p \lesssim \text{few} \times 10^5 \text{ G}$. Bounds from stars with larger fields are still achievable, since cosmic rays incident at angles closer to the magnetic poles will experience reduced energy loss, but this leads to a reduction of rates for acceptable cosmic rays (see Appendix G). We will return to the question of magnetic fields for neutron stars, where we will find them to be somewhat more problematic.

6.2 Production rates

Production rates can be computed using the known fluxes of cosmic rays, together with cross sections obtained by convolving parton-level cross sections with parton distribution functions. We will briefly summarize these calculations here; more details are supplied in Appendix E.

The basic parton level production cross section is of the form $\sigma \approx \pi R^2(\sqrt{\hat{s}})$, where $\sqrt{\hat{s}}$ is the CM energy of the pair of partons forming the black hole. This is only an estimate; one must take into account that not all the collision energy is captured by the black hole, and even less is captured as impact parameters grow comparable to $R(\sqrt{\hat{s}})$. Thus, to be more precise, we account for this via an inelasticity factor, y ; we conservatively summarize trapped-surface calculations of the inelasticity [48–51]¹⁶ by a simple dependence like that in [8]

$$E_{BH} = y\sqrt{\hat{s}} , \quad b < 0.5 R \quad ; \quad E_{BH} = 0 , \quad b > 0.5 R . \quad (6.5)$$

To be conservative for cosmic ray production rates, we use a lower than expected value, $y = 0.5$ [8], for the inelasticity. This corresponds to a limit of 7 TeV for the maximum value of black hole mass that can be produced at the LHC. The actual value of y may be higher, and its reach could be slightly extended due to quantum fluctuations. For this reason we also consider values in the range $0.5 < y < 1$ (the upper limit being an unrealistic extreme [8,51,53]) to allow for black hole production at the LHC all the way up to the largest available energy, namely 14 TeV. In making the estimates of cosmic-ray production rates we shall conservatively choose the value of y corresponding to the smallest possible inelasticity compatible with production of a given mass value at the LHC, namely $y = M_{min}/14 \text{ TeV}$. Furthermore, again to be conservative in our rate estimates, we take the minimum black

¹⁶We also note that the refined estimates in [49], which are based on perturbatively-calculated radiation, have in the case of zero impact parameter recently been checked via numerical relativity techniques [52], with good agreement.

Table 2: *Black hole production rates, per million years, induced by cosmic rays impinging on a $R = 5400$ km white dwarf. N_p refers to the case of 100% proton composition, N_{Fe} refers to 100% Fe. $M_D = M_{min}/3$ and $y = M_{min}/14$ TeV.*

| $D =$ | 5 | 6 | 7 |
|---|-------------------|-------------------|-------------------|
| $N_p/\text{Myr}, M_{min} = 7 \text{ TeV}$ | 2.1×10^7 | 4.3×10^7 | 6.7×10^7 |
| $N_{Fe}/\text{Myr}, M_{min} = 7 \text{ TeV}$ | 7.2×10^4 | 1.6×10^5 | 2.6×10^5 |
| $N_p/\text{Myr}, M_{min} = 14 \text{ TeV}$ | 2.3×10^6 | 5.9×10^6 | 1.0×10^7 |
| $N_{Fe}/\text{Myr}, M_{min} = 14 \text{ TeV}$ | 7.3×10^3 | 2.1×10^4 | 3.8×10^4 |

hole mass to be $M_{min} = 3M_D$; for example, [5] used as a benchmark the less-conservative value $M = 5M_D$.

The resulting cross sections are then convoluted with the CTEQ6M [54] parton distribution functions. The resulting nucleon cross sections are, in turn, convoluted with the measured ultrahigh-energy cosmic ray flux, extracted from the latest Auger spectra [40]. In the case of cosmic ray primaries that are nuclei of mass number A , one must also use a nucleon energy reduced by this factor. The rate calculations of Appendix E are carried out for two test cases: that of incident protons, and that of incident iron nuclei ($A=56$). Partial results are summarized in table 2, for production on a white dwarf of radius 5400 km, and more results are presented in Appendix E. (In that Appendix we also present figures resulting from a 20% hypothesized overestimate of cosmic ray energies, to model the quoted Auger energy resolution of $\pm 20\%$ [40, 55].)

According to the stopping calculations of section 5, not all cosmic-ray produced black holes are stopped by a white dwarf. In order to allow for sufficient column density, we must require the cosmic rays to reach the white dwarf at an angle sufficiently close to the azimuth as to force the black hole to traverse a sufficient fraction of the full column density of the star. The angular dependence of the column density is shown in the right plot of fig. 1. In the case of $D = 5$, our calculated column densities required for stopping are a mere few percent of those available and we can therefore easily accept a reduction to 10% of the available column density. In the cases of $D = 6$ and 7, to be conservative we can allow for at least 30% and 80% of the full available column density, leading to a reduction of the useful cosmic ray flux to a level of 10% and 2%, respectively. Multiplying these efficiencies by the number of events given in table 2, and integrating over a period of 10 million years, leads to total numbers of accumulated black holes larger than 5000, even in the totally extreme case of 100% Fe composition of the cosmic rays. Notice that even in the most conservative case of rates obtained for $M = 14$ TeV with $y = 0.5$ (see table 7 in Appendix E.2), the number of events in 50 million years still exceeds 100 for each value of D .

7 Black hole catalysis of white dwarf decay

The conclusion of the preceding sections is that white dwarfs with solar-size masses, as well as neutron stars, have sufficient ability to stop a cosmic-ray produced black hole, and that significant production rates for such black holes can in particular be achieved on white dwarfs. We will seek bounds from the statement that any stable black holes that could be produced on Earth will be produced and trapped in cosmic ray collisions with these astronomical objects. The remaining problem is to examine the subsequent evolution.

We have in particular argued in section 5.3 that a black hole will be brought to zero velocity, largely through accretion and scattering, deep within a white dwarf. By this time the mass of the black hole may grow significantly from its initial value. The surrounding medium consists of nuclei, for example, carbon and oxygen, embedded in a sea of relativistic degenerate electrons. A lower bound on the relative velocities between the black hole and these nuclei is given by the thermal velocity; for temperatures $\gtrsim 10^7 K$, these are at least of size $v_T \gtrsim 3 \times 10^{-4}$. At times $\mathcal{O}(0.6 \text{ Gyr})$ white dwarf cores begin to crystallize, but we will find accretion to be relevant well before this time.

7.1 Subatomic accretion

A small black hole will only exert an influence when within the nucleus, as described by our “bag-model” discussion in section 5.3.1. However, once larger it will have a longer-scale influence. In general its gravitational force must compete with electrostatic forces between the nuclei and their surroundings. We can estimate these forces as in the discussion of atomic matter on Earth — a displacement of a nucleus from its equilibrium position is expected to produce a dipole force resulting from interactions with the ambient electron cloud, and this is estimated to be of a size given by (4.6), where one uses the typical internuclear separation $a_{WD} \approx 10^{-10} \text{ cm}$ corresponding to $\rho \approx 10^7 \text{ gr/cm}^3$. This leads to a characteristic electromagnetic capture radius R_{EM} as given in (4.10), with β_D given by (4.11), together with the approximate value

$$\frac{K}{mM_0^2} \approx 1.2 \times 10^{-18} . \quad (7.1)$$

For a black hole evolving from $M \sim M_D$, the radius R_{EM} will initially be smaller than both the nuclear scale and the velocity-dominated capture radius R/v . One can readily check when R_{EM} exceeds the latter; this happens at

$$R_{EM} = R/v_T = \sqrt{\frac{(D-3)(D-1)^{D-1}}{2(D-2)^{D-2}}} \sqrt{\frac{m}{K}} v_T^{(D-3)/2} . \quad (7.2)$$

Thus, for $D \geq 6$, by the time R_{EM} reaches $\sim 1 \text{ fm}$ it governs capture, though for $D = 5$ there is a brief phase where $R/v_T > 1 \text{ fm}$ governs the capture rate. Both the subnuclear phases and this phase are governed by very short time scales.

We will focus on cases where $R_D > a_{WD}$, as they include scenarios with short evolution times on Earth. These in particular include the non-warped cases of $D = 6, 7$. The evolution time up to the scale $R_{EM} = a_{WD}$ is then given by d/v_T , with d the electromagnetic evolution distance given in (4.22). This yields time scales for this phase

$$t_{EM} = 1.5 \times 10^{-7} s \left(\frac{M_D}{M_0} \right)^3, \quad D = 5, \quad (7.3)$$

$$t_{EM} = 0.09 s \left(\frac{M_D}{M_0} \right)^4, \quad D = 6, \quad (7.4)$$

$$t_{EM} = 6 \times 10^4 s \left(\frac{M_D}{M_0} \right)^5, \quad D = 7, \quad (7.5)$$

which are quite short.

7.2 Bondi accretion

Once $R_{EM} > a_{WD}$, one enters the Bondi accretion phase. Since, by assumption, $R_D > a_{WD}$, this is initially D -dimensional up to R_D , and then four-dimensional beyond R_C . In cases with warping, there can also be a warped phase intermediate between R_D and R_C .

Consider first the unwarped cases, with $D = 6, 7$. The relevant time scales are given by eqns. (4.43), (4.48) for evolution up to R_D , and from R_C onward. To be conservative, we now model the transition phase between R_D and R_C by assuming the *slowest* evolution, namely a 4-dimensional growth, with a constant Bondi radius equals to R_D , until the mass reaches the value corresponding to $R_B = R_C$. This gives an evolution time scale:

$$t = d_0 c_s \frac{16\pi [4\pi(D-3)k_D]^{1/(D-4)}}{\lambda_D} \left(\frac{M_D}{M_0} \right)^{(D-2)/(D-4)} \left(\frac{M_4}{M_0} \right)^{2(D-5)/(D-4)}, \quad (7.6)$$

The evolution time scales are determined by the white dwarf parameters (for a $M = M_\odot$ white dwarf [56]) $d_0 \approx 1.4 \times 10^{-6} s$ and $c_s \approx 1.4 \times 10^{-2}$. The combination $d_0 c_s$ has a value that is approximately 1.5×10^{-4} times the Earth's value (4.44). The resulting time scales will therefore be comparatively shorter:

$$t(R_B < R_D) = 8 \frac{1}{\lambda_6} \left(\frac{M_D}{M_0} \right)^2 \text{ yr}, \quad D = 6 \quad (7.7)$$

$$t(R_D < R_B < R_C) = 4 \times 10^2 \frac{1}{\lambda_4} \left(\frac{M_D}{M_0} \right)^2 \text{ yr}, \quad D = 6 \quad (7.8)$$

$$t(R_B > R_C) = 15 \frac{1}{\lambda_4} \left(\frac{M_D}{M_0} \right)^2 \text{ yr}, \quad D = 6 \quad (7.9)$$

$$t(R_B < R_D) = 1.3 \times 10^5 \frac{1}{\lambda_7} \left(\frac{M_D}{M_0} \right)^{5/3} \text{ yr}, \quad D = 7 \quad (7.10)$$

$$t(R_D < R_B < R_C) = 6 \times 10^7 \frac{1}{\lambda_4} \left(\frac{M_D}{M_0} \right)^{5/3} \text{ yr}, \quad D = 7 \quad (7.11)$$

$$t(R_B > R_C) = 1.9 \times 10^6 \frac{1}{\lambda_4} \left(\frac{M_D}{M_0} \right)^{5/3} \text{ yr}, \quad D = 7. \quad (7.12)$$

Taking the largest value of relevance for the LHC, $M_D \sim 4.7$ TeV, and using the value of λ_D appropriate for a relativistic electron gas, the longest possible phase of the evolution in $D = 7$ does not exceed 80 million years. We recall that, in this largest- M condition, the Earth's lifetime for $D = 7$ exceeds 10 billion years by a large margin. We also notice that if we consider the case of more massive and thus denser white dwarfs, the timescales are reduced. For example, the central densities of white dwarfs of mass $M = 1.1 M_\odot$ and $M = 1.2 M_\odot$ are 2 and 4 times, respectively, larger than for $M = M_\odot$ [56], leading to accordingly shorter evolution times.

From this analysis we conclude that Bondi accretion time scales for the unwarped $D = 6, 7$ scenarios are quite short, especially as compared to known white dwarf lifetimes that exceed 1 Gyr. We have argued in Appendix B that these are not modified by an Eddington limit, at least until accretion macroscopically disrupts the star. If there were an Eddington limit, Appendix B argues that one is even more likely to find one for Earth. Moreover, as discussed in Appendix B, radiation of an ensemble of black holes at Eddington fluxes would interfere with white dwarf cooling, providing an independent argument against this possibility. We note, parenthetically, that in the true macroscopic regime, when the black hole starts to exert large-scale effects on its host body, the evolution may well not be Bondi, but in any case would disrupt the object in question.

7.3 Generalized scenarios

We next consider a more general warped scenario, with $R_C \gtrsim 15 \text{ \AA}$. In this regime, we find from (3.26) that $R_C/R_D \lesssim 20$, so $R_D > a_{WD}$. The growth will then be governed by Bondi evolution that is D -dimensional up to R_D , warped between R_D and R_C , and four-dimensional between R_C and large mass.

For $R_D \ll R_C$, the bound on the first phase is significantly smaller than the other two. As discussed in the case of accretion in Earth, the evolution in the warped regime in general involves a large change in mass in a relatively small change of radius. For such a slow-growth law, the growth time is governed by the upper limit of the radius range, $R_B = R_C$. This implies that the timescale for growth through this phase is given by

$$t_w \approx \frac{M(R_C)}{\pi \rho c_s R_C^2} = \frac{16\pi c_s d_0}{\lambda_4} \left(\frac{M_4}{M_0} \right)^2 \frac{1}{M_0 R_C}. \quad (7.13)$$

The time for growth from R_C to large mass is the same, from (4.41). For $R_C \gtrsim 15 \text{ \AA}$, this yields timescales $t_{WD} \lesssim 5 \times 10^6 \text{ yr}$. In fact, even in the unrealistic case of evolution via a

constant radius relationship $R_B = R_D$ over the entire warped range up to just below R_C , this would only enhance this time scale by $(R_C/R_D)^2 \sim 400$, and thus the slightly larger value $R_C \gtrsim 30\text{\AA}$ would still be in the range constrained by experimental bounds ($\lesssim 1$ Gyr). Indeed, one can directly compare the white dwarf evolution in the range near $R_B = R_C$ to that on Earth; from (4.41) we find

$$\frac{t_{\text{Earth}}}{t_{\text{WD}}} \approx \frac{d_0(\text{Earth})c_s(\text{Earth})}{d_0(\text{WD})c_s(\text{WD})} \frac{\lambda_4(\text{WD})}{\lambda_4(\text{Earth})}. \quad (7.14)$$

Taking for example $\Gamma = 5/3$ for Earth and $\Gamma = 4/3$ for a white dwarf, this yields a ratio of accretion times

$$\frac{t_{\text{Earth}}}{t_{\text{WD}}} \approx 1.9 \times 10^4. \quad (7.15)$$

7.4 Summary of white dwarf constraints

This and the preceding sections have argued that in the hypothetical TeV-scale gravity scenarios possibly relevant to LHC, 1) cosmic rays will produce significant numbers of black holes on white dwarfs of low ($\lesssim \text{few} \times 10^5 G$) magnetic fields, on time scales short as compared to known white dwarf lifetimes; 2) such black holes, even if neutral and with the highest masses accessible at the LHC, will be stopped on white dwarfs with masses $M \gtrsim M_\odot$, by accreting and scattering the dense matter of the star during their transit; and 3) the white dwarf will then be accreted. Accretion of a white dwarf has been argued to be more rapid than that of Earth. Different considerations reinforce this statement. First, before the \sim Gyr time scale, white dwarf matter is in a liquid form, in contrast to significant solidity of matter in Earth. Secondly, white dwarfs pack the mass of the Sun into a region the size of the Earth, so are much more dense, and have much higher internal pressures, assisting accretion.

Several surveys of low-magnetic-field white dwarfs exist in the literature. The use of Zeeman spectropolarimetry, in particular, has allowed detection of fields down to the level of few kG. White dwarf masses are determined by spectral measurements of surface gravities, with parallax and gravitational redshifts serving as cross-checks; see e.g. [57, 58]. Ages are determined through white dwarf cooling; a textbook account appears in [59], with further discussion in [58, 60, 61]. Several known white dwarfs satisfying our criteria of mass $M \gtrsim M_\odot$, $B_p \lesssim \text{few} \times 10^5 G$, and age $T \gtrsim 100$ Myr can be found, for example, in [62–65]. When not given explicitly, the ages can be inferred from the mass-temperature relations, as discussed e.g. in [60, 61]. Some examples of relevant stars are:¹⁷

- WD0346-011 [62, 64], with parameters $M = 1.25M_\odot$, $B_p < 1.2 \times 10^5$ G, and $T \sim 100$ Myr;
- WD1022-301 [64], with $M = 1.2M_\odot$, $B_p < 1.2 \times 10^5$ G, and $T \gtrsim 100$ Myr;

¹⁷Where B_ℓ appears, it represents the measurement of the average longitudinal field, B_ℓ , whose definition and relation to B_p can be found, e.g. in [62]

- WD1724-359 [64], with $M = 1.2M_\odot$, $B_p < 1.2 \times 10^5$ G, and $T \sim 150$ Myr;
- WD2159-754 [64], with $M = 1.17M_\odot$,¹⁸ $B_p < 3 \times 10^4$ G, and $T \sim 2.5$ Gyr;
- WD0652-563 [64], with $M = 1.16M_\odot$, $B_p < 2.7 \times 10^5$ G, and $T \sim 100$ Myr
- WD1236-495 [64], with $M = 1.1M_\odot$, $B_p < 3 \times 10^4$ G, and $T \gtrsim 1$ Gyr;
- WD2246+223 [62], with $M = 0.97M_\odot$ [65], $B_\ell = 1.5 \pm 13.8 \times 10^3$ G, and $T \sim 1.5$ Gyr.
- WD2359-434 [63], with $M = 0.98M_\odot$ [64], $B_\ell = 3 \times 10^3$ G, and $T \sim 1.5$ Gyr;

The above arguments thus state that comparison of respective accretion rates, together with survival of white dwarfs to observed time scales $\gtrsim 10^8$ years, implies survival of Earth for a significantly longer time, and in particular longer than the natural solar lifetime.

Finally, as in section 4.3.4, we can estimate the lifetime of a white dwarf, should it capture a minimum-mass primordial black hole. With Bondi evolution from the corresponding initial radius, one finds a lifetime ≈ 1.8 Gyr.

8 Bounds from neutron stars

8.1 Production on neutron stars

Neutron stars are very common in the Universe, and in fact provide robust examples of long-lived objects in other galaxies. They also represent the highest known densities of matter that have not undergone gravitational collapse to a black hole. Since they are particularly close to densities beyond which black holes are expected to form, one might expect that introduction of a microscopic stable black hole into a neutron star would rapidly catalyze its decay into a macroscopic black hole. The known stability of NSs, with lifetimes significantly exceeding 10^9 years, therefore offers the prospect of limits on microscopic black hole stability and accretion power.

However, known neutron stars have strong magnetic fields, which are observed to range upwards from $\sim 10^8$ G. In the case of a field of 10^8 G and a radius $R_0 = 10$ km, (6.4) yields a maximum energy 1.8×10^{17} eV for protons impinging perpendicular to the field axis, giving collisions just above the LHC CM energy; the maximum energy is only about sixteen times higher for heavy elements. One can avoid this limit for cosmic rays incident near the magnetic poles, but the acceptance for protons of energies in the optimal range of $\sim 5 \times 10^{18}$ eV is estimated in Appendix G to lead to a reduction of acceptable flux by a factor of approximately 10^{-3} , considerably weakening the resulting bounds.

¹⁸See however [66] for a photometric determination of the surface gravity, leading to a lower mass value. Parallax determinations of the absolute distance are underway to confirm the mass assignment.

Table 3: *Summary of black hole production rates, per million years, induced by proton cosmic rays impinging on a $R = 10$ km neutron star. $M_D = M_{min}/3$ and $y = M_{min}/14$ TeV.*

| $D =$ | 8 | 9 | 10 | 11 |
|--------------------|-----|-----|-----|-----|
| $M_{min} = 7$ TeV | 323 | 422 | 526 | 633 |
| $M_{min} = 10$ TeV | 129 | 172 | 218 | 265 |
| $M_{min} = 12$ TeV | 80 | 109 | 139 | 171 |
| $M_{min} = 14$ TeV | 54 | 74 | 95 | 118 |

8.1.1 Production in binary systems

This suppression suggests we consider a more reliable way to inject CR produced black holes into a neutron star. Many NS binaries are known, and in particular parameters and evolution of low-mass binaries are well-understood. Moreover, in such binaries, the companion to the NS can subtend a significant solid angle in the sky of the NS, as described in Appendix H.1. Cosmic rays which would hit the NS but whose direction intersects the companion will therefore scatter on the companion. In our TeV-scale gravity scenarios, part of the time they will therefore convert to black holes, which then impact the neutron star. Since we only need bounds if stable black holes are neutral, the magnetic field of the NS is irrelevant for these. Such a production mechanism produces a “full-coverage equivalent” (FCE) given by

$$FCE = \int dt \frac{\Delta\Omega(t)}{4\pi}, \quad (8.1)$$

where $\Delta\Omega$ is the solid angle subtended by the companion, and where we allow for time dependence due to evolution of the binary system. In order to compute the actual production rate on the neutron star, we use the uncorrected rates of Appendix E, times the number of years of FCE . A survey of known classes of binary systems (see Appendix H.1) reliably yields FCE’s in the 2 Myr range, resulting from systems with a 1 Gyr lifespan. The neutron star production rates are exhibited in table 9 and in fig. 8 of Appendix E.2. A summary of that table, focusing on the most interesting cases of $D \geq 8$, is shown here in table 3.

We find that in the example of a flux of even only 10% protons, we have a rate for the extreme case of 14 TeV black holes that is $\approx 5/\text{Myr}$, and so 2 Myr of FCE would indicate that typical such systems have experienced sufficient black hole production to initiate the accretion. Less-extreme (and still quite robust) binary scenarios provide significantly higher rates. However, a greater dominance of heavy elements reduces the range of such bounds.

At energies below the GZK cutoff, there are indications of a significant component of heavy elements. There are both theoretical and experimental indications that one transitions to a significant proton component at the GZK cutoff. On the theoretical side one can cite both the match of the observed spectrum to that from models of proton acceleration, and expectations that gamma-ray bursters (GRBs) and active galactic nuclei (AGN) primarily accelerate protons (see [67–69] for more discussion.) On the experimental side, indications

of a predominantly light composition include both measured penetration depths of showers [70, 71] and, most recently, correlations of arrival directions with known AGN [72, 73] (see however [74]). Thus, while not all scenarios are definitively eliminated by such a bound, it appears likely that these bounds will be strengthened with future data on composition.

8.1.2 Production via cosmic neutrinos

Primary cosmic rays propagating through the 3K cosmic microwave background photons will experience significant interactions above the GZK energy $\approx 5 \times 10^{19}$ eV. These interactions produce a “guaranteed” flux of neutrinos (see e.g. [68, 75, 76]), which avoid the synchrotron losses of charged cosmic rays. Using these fluxes, Appendix E calculates production rates on neutron stars. For example, in the very conservative scenario of requiring black holes to have 14 TeV mass, and using both $D = 5$ and our most conservative inelasticity assumptions, $y = 0.5$, one finds production rates $\gtrsim 5000/\text{Myr}$, as shown in table 10.

These thus suggest a very robust bound for production on neutron stars. While we believe it is quite good, we will not take this bound with absolute certainty, for two reasons. First, while the physics of the GZK effect is quite robust, and moreover appears to be in the process of being experimentally confirmed via correlations of the highest energy cosmic rays with AGN [72, 73], experiments have not reached sensitivity sufficient to measure the cosmic neutrino flux.¹⁹ Second, there exist proposals that baryon number conservation is enforced in higher-dimensional brane world models through reduced interactions between neutrinos and quarks by virtue of these living on different branes [78]. While these models are not compelling, they would seem to raise a small possibility that neutrino cosmic rays would not produce black holes the same way that nucleons do.

8.2 Catalysis of neutron star decay

Due to the immense pressures inside a neutron star, one expects introduction of even a microscopic black hole to rapidly catalyze its decay. To understand this process, we note that neutron stars have different layers, a crust extending to a depth of ~ 1 km, and under this, matter at nuclear densities. Since treatment of accretion is simplest in this inner region, we would like to understand whether a BH can penetrate to this distance.

8.2.1 Penetration to core

The slowing distance (5.25), together with a subsequent phase of slowdown to sub-escape velocities, $v \lesssim 0.1c$, may or may not permit penetration to depths $\gtrsim 1$ km, depending on details. Note that the characteristic distance d_0 can be rewritten in appropriate nuclear

¹⁹Suggestions that models with extra dimensions suppress neutrino fluxes [77] do not appear relevant to the scenarios for which we require bounds.

units as

$$d_0(\rho) = 9 \times 10^{-4} \text{cm} / \rho [m_p / \text{fm}^3] , \quad (8.2)$$

and that crustal densities range from 10^{-6} – $10^{-1} m_p / \text{fm}^3$.

Even if penetration does not occur during slowdown, there is a different argument that it takes place on rapid time scales. To see this, instead assume that a sufficiently slow black hole could become temporarily bound in the crust, by absorbing a parton and thus binding to the medium by strong forces. This binding should, however, be temporary, as the scenario we wish to constrain is that where black holes don't remain charged, but instead discharge through Schwinger production. Even ignoring this, if a black hole is bound to a nucleon via the color force, it will absorb the remaining partons of the nucleon, and thus become color neutral, on a relatively short time scale. One can readily estimate this time scale. A nucleon has a parton density of order $1/\text{fm}^3$, and partons within the nucleon travel at speeds $\approx c$. With the smallest possible absorption cross section, of order $\sigma \sim \pi/\text{TeV}^2$, we find a characteristic absorption time $t_{\text{abs}} \sim 10^7 \text{fm}$.

The neutralized black hole will then continue to fall in the net gravitational field of the neutron star until another such binding/neutralization event. The characteristic distance between such events is

$$d_{\text{free}} \approx \frac{8x \times 10^{-7} \text{cm}}{\rho [m_p / \text{fm}^3] r_c^2 [1/\text{TeV}]} , \quad (8.3)$$

where x parameterizes the typical nucleon energy fraction per parton, and we have expressed the capture radius r_c in TeV^{-1} units. The corresponding time between such collisions is given by

$$t_{\text{free}} \approx \sqrt{2d_{\text{free}}/g_{NS}} , \quad (8.4)$$

where g_{NS} is the gravitational acceleration near the surface of the neutron star,

$$g_{NS} \approx \frac{GM_{NS}}{r_{NS}^2} . \quad (8.5)$$

This characteristic time scale is much longer than t_{abs} , and thus sets the speed with which the black hole can penetrate the crust. The corresponding average velocity is

$$v_{\text{av}} \approx \frac{d_{\text{free}}}{t_{\text{free}}} \approx \sqrt{g_{NS} d_{\text{free}}/2} . \quad (8.6)$$

The mean free path d_{free} reaches a minimum near the bottom of the crust, and consequently the average velocity is slowest there. We can therefore bound the crust penetration time by using $\rho = m_p / \text{fm}^3$ to derive a minimum gravitational drift velocity and time:

$$t_{\text{crust}} \lesssim d_{\text{crust}} / v_{\text{av}} [\rho = m_p / \text{fm}^3] \approx 10s r_c [1/\text{TeV}] . \quad (8.7)$$

Thus the black hole should rapidly penetrate the crust and enter the neutron-fluid region of the core.

8.2.2 Accretion from within a neutron star

Like in atomic matter, one might expect different phases for black hole accretion within a NS, depending on the relative range of the black hole's influence as compared to the radii R_D, R_C representing crossover to lower-dimensional behavior, and as compared to 1 fm, the characteristic separation between nucleons, which delineates the crossover from microscopic to macroscopic absorption in the NS context.

To better understand these points, let us begin by comparing the force due to a black hole to typical forces between the neutrons in the NS, which are of size GeV/fm. Specifically, the force on a nucleon of mass m_p at distance r is of order

$$F_G \sim -\frac{m_p}{r} \left(\frac{R}{r}\right)^{D-3} . \quad (8.8)$$

Equating this to the typical nuclear force, we find that gravity beats such a force at scales

$$R_N = R \left(\frac{r_N}{R}\right)^{1/(D-2)} , \quad (8.9)$$

which are only moderately larger than the Schwarzschild radius in the regime $R < r_N$. Thus a conservative (*i.e.*, for the purposes of NS evolution, *slow*) estimate of the evolution is given by simply taking the capture radius in (4.1) to be $r_c = R$ in the subnuclear regime $R < r_N$. To estimate the accretion rate, one needs the flux F . This receives contributions both from the velocity of the black hole, and from the Fermi motion of the partons in the nuclei. The latter produces a flux $F \sim \rho$, in units where $c = 1$, and thus a geometric rate law

$$\frac{dM}{dt} = \pi \rho R^2 . \quad (8.10)$$

The evolution equations are of the same form as eq. 4.31, with the replacements $c_s = 1$, $\lambda_D = 1$, and $R_B \rightarrow R$. The resulting time is analogous to eq. (4.39), and evaluated at $R = r_N \sim 1$ fm gives:

$$t = \frac{d_0}{k_D} \left(\frac{M_D}{M_0}\right)^{D-2} \frac{D-3}{D-5} (r_N M_0)^{(D-5)} , \quad (8.11)$$

leading to timescales ranging from a fraction of a second to at most few weeks for $6 \leq D \leq 11$.

When the black hole enters the regime $R \gtrsim r_N$, the absorption becomes macroscopic – the black hole is capable of absorbing multiple nuclei, and its gravitational range exceeds mean free paths. As Appendix B describes, an Eddington limit would be even more problematic for a neutron star, given its high density and opacity, and so evolution is described as Bondi until the black hole reaches a scale where it disrupts the star.

The corresponding growth laws are those given in section 4. In unwarped scenarios, we find for evolution from $R_B = r_N$ to R_D the growth time (4.43), and for evolution from R_C up to large scales the comparable time scale (4.48), with $\lambda_D \rightarrow \lambda_4$. For the stage in between, we

use, as in the case of the white dwarfs, the conservative time in eq. (7.6). Taking a typical value $\rho = 2 \times 10^{14} \text{gr/cm}^2$ gives $d_0 = 7 \times 10^{-3} s$, and the speed of sound is of magnitude $c_s \sim 0.1$. The time scales are therefore about 10^{-6} times smaller than those of the white dwarf. The longest evolution corresponds to the 4-dimensional phase from R_D to R_C in $D = 11$ dimensions, with a time scale of ~ 10 million years; for $D \leq 7$, times are $\lesssim 50 \text{yr}$.

In the more general warped case, the growth times are, as in the white dwarf case, dominated by the upper end of the warped phase and its crossover to four-dimensional accretion, with time scale (7.13). For neutron star parameters and a value $R_C \geq 5 \text{ \AA}$, this yields times of size $t_{NS,w} \sim 20 \text{yr}$.

Combining the results of this and the preceding subsections, we find that the rate-limiting step to destroy a neutron star is the time required for a black hole to be produced and reach the surface of the neutron star. Once it reaches the core, the accretion times are very rapid compared to the neutron star's lifetime, $\mathcal{O}(\text{Gyr})$. These bounds appear quite challenging to avoid. In order to do so, one would need a significant deficit of light cosmic ray primaries, together with a heavy ($\gtrsim 7 \text{ TeV}$) minimum black hole mass and only systems with low FCE , *and* one would have to have a neutrino flux that is either suppressed by unknown mechanisms or is unusually non-reactive.

As a final note, in our framework we can estimate the lifetime of a neutron star that captures a primordial black hole of mass $\mathcal{O}(10^{15} \text{gr})$. Our parameters yield a time of order $3 \times 10^5 \text{yr}$. We note that such processes have been proposed as the origin of some gamma ray bursts [79], with roughly comparable accretion times. The present analysis, in addition to giving the analogous accretion time scales for Earth and white dwarfs, lends further detail to such a possibility through our description via Bondi accretion, and through our arguments against an Eddington limit.

9 Summary and conclusions

In this paper we have studied accretion of hypothetical stable TeV-scale black holes in two primary contexts: the Earth, and compact stars – white dwarfs and neutron stars.

For Earth, we identified two main evolution domains: that where the black hole's gravitational range of influence is less than the atomic scale, and that where it is greater. An important distinction occurs depending on where the crossover radius R_C to four-dimensional behavior lies relative to the atomic scale. In particular, if R_C is in the subatomic regime, evolution is four-dimensional at both subatomic and macroscopic scales; this case includes unwarped scenarios with $D \geq 8$. In this case we have argued that this evolution occurs on times longer than the expected natural solar lifetime, in two different ways: via a microscopic argument, and via a macroscopic, hydrodynamic argument. In both approaches, we used conservative assumptions, leading to the largest accretion rates and to fastest evolution. At the end of the first phase, at times $\mathcal{O}(10^{11})$ years, the mass of the black hole is still small, with a mass of less than a megaton. Such statements extend to more general warped sce-

narios, and crossover scales up to $\simeq 200\text{\AA}$ lead to accretion times longer than the Earth's natural lifetime.

On the other hand, those cases where $R_C \gtrsim 15\text{\AA}$ have been treated by deriving bounds from white dwarfs, and also from neutron stars. In particular, we have argued that in such scenarios cosmic rays will produce black holes on such astronomical objects, and that these objects will stop even these very high-momentum black holes. We then studied accretion, showing that accreting black holes will disrupt such objects on time scales short as compared to their observed lifetimes. In particular, we found a general relationship (7.15) between accretion times for Earth and for white dwarfs, which, when combined with white dwarf ages exceeding 10^9 years, provides a very strong constraint. Thus, the implication of these arguments is that such scenarios, where Earth would be disrupted on time scales short as compared to its natural lifetime, are ruled out.

We summarize here the origin of our constraints, as a function of dimensionality D and of black hole mass M .

$D = 5$: The evolution scales on Earth for $D = 5$ in the case of maximum allowed crossover radius R_C are quite short. This is a result of the higher-dimensional force law extending well into the macroscopic regime. On the other hand, the greater interactivity of $D = 5$ black holes makes it possible for those produced by cosmic rays to get promptly trapped in both white dwarfs and neutron stars. In white dwarfs they are produced abundantly, with build-up time scales of the order of few thousand years even assuming a cosmic ray composition of 100% Fe, and at the largest Planck mass of interest. After being produced and trapped, in these extreme scenarios they quickly accrete to masses comparable to that of the star on time scales that can be short when measured in years. This would make it impossible for any white dwarf with a mass of the order of one solar masses to have survived longer than few thousand years, contrary to observations. Scenarios with increased warping have correspondingly lower R_C and longer accretion times. In particular, once $R_C \lesssim 200\text{\AA}$, accretion times on Earth exceed its future lifespan.

$D = 6$: The evolution times on Earth for $D = 6$ are of the order tens of thousand years, thus short on geological time scales. Once again the main reason is the large extra-dimensional radius, and the high capture rates. As in the $D = 5$ cases, such black holes produced by cosmic rays can be stopped inside dense stars. The production rates are even larger than in $D = 5$, and the star accretion time scales for unwarped $D = 6$ are comparable to the maximum- R_C version of that scenario. With increased warping, again R_C decreases and accretion times increase.

$D = 7$: The time scale for their macroscopic evolution on Earth is in the range of 6–80 billion years, depending on the black hole mass. Furthermore, $D = 7$ black holes would be produced plentifully by cosmic rays on white dwarfs, and be stopped inside their surface, if the white dwarf mass is larger than 1.1 solar masses. The evolution times would be longer than in $D = 5$ and 6, reflecting the lower growth rate that keeps

them microscopic for billion years inside the Earth. But within the very conservative estimate of 80 million years (for a $M = M_{\odot}$ star, and shorter in the more massive cases) their accretion process of the white dwarf would be completed. Massive white dwarfs older than a few hundred million years would therefore be ruled out in these scenarios, once again contrary to observation. Again, warping decreases R_C , thus increasing accretion times.

$D \geq 8$: For these black holes the evolution time on Earth is extremely long, with times of size 100 billion years. This is due to the radius of the extra dimensions being smaller than 1 \AA , thus forcing most of the evolution to take place in 4 dimensions, where gravity is a totally negligible force. Warping only magnifies this effect. In spite of this slow growth, these black holes would still grow fast enough inside a neutron star to consume it within about ten million years. The significant production rates on neutron stars when $D \geq 8$, and the existence of billion-year old X-ray binary systems, provide therefore additional evidence that such black holes either do not exist, or decay promptly.

We also note that these bounds likely extend in case other objects are imagined that could result from high-energy collisions in the relevant energy ranges, that have weak-scale cross sections, and that could threaten the long-term stability of matter.

We conclude by first summarizing the conditions needed for our bounds to be necessary to rule out a possible risk. In order for our bounds to have relevance, a sequence of unlikely things would have to be true. First, TeV scale gravity, with a Planck scale no higher than a few TeV, would have to be correct, so that black holes can be produced at LHC. Most workers consider this to be a fascinating possibility, but also a somewhat unlikely possibility. Second, black hole radiance, which has been deeply studied from a number of theoretical perspectives, would have to be wrong, *and* more general quantum mechanical arguments for black hole instability would have to be wrong. Most workers consider this to be an exceedingly improbable, if not impossible, scenario. Finally, one would need a mechanism to shut off the quantum effects responsible for Hawking radiation, but still leave intact either the quantum effects responsible for Schwinger discharge, or some other neutralization mechanism that acts to discharge the resulting stable black holes. It is very difficult to conceive of a consistent physical framework that provides such a mechanism.

In the event that all these conditions are satisfied, one can turn to the considerations of this paper to assess the possible impact on Earth. This paper has argued that in order for such a scenario to have an impact on Earth at time scales short as compared to the natural lifetime of the solar system, in the five billion year range, the configuration of extra dimensions would have to be such that gravity doesn't transition to four-dimensional behavior until around the 200 \AA scale. This apparently requires additional fine-tuning, reducing the likelihood even further. But beyond that, this paper has argued that such scenarios are ruled out by the longevity of known white dwarfs, on billion-year time scales. In such a scenario, cosmic ray-produced black holes should have catalyzed white dwarf destruction on significantly shorter time scales.

Moreover, decay of observed neutron stars would also have been catalyzed, unless both of two unlikely possibilities are realized, namely that the composition of ultrahigh-energy cosmic ray primaries is dominantly heavy elements, and ultrahigh energy cosmic ray neutrinos either are not produced, or have suppressed gravitational interactions with partons. To summarize, the present study argues for the following *additional* layers of safety, beyond those that would have to fail to make this study relevant:

- 1. Only in scenarios such that the crossover scale to four-dimensional gravity is larger than about 200 \AA does one have significant accretion at times short as compared to the natural lifetime of Earth. This is a-priori unlikely, due to the additional fine-tuning required to realize such a TeV-scale gravity scenario.**
- 2. In these scenarios where black hole accretion time on Earth is short as compared to natural time scales, white dwarfs would likewise be accreted, on much shorter time scales, in contradiction to observation.**
- 3. Unless cosmic rays have dominantly a very heavy composition, and moreover either the expected neutrino flux doesn't exist or has unusual gravitational couplings to hadronic matter, neutron star decay would likewise be catalyzed on time scales, contradicting observation.**

In short, this study finds no basis for concerns that TeV-scale black holes from the LHC could pose a risk to Earth on time scales shorter than the Earth's natural lifetime. Indeed, conservative arguments based on detailed calculations and the best-available scientific knowledge, including solid astronomical data, conclude, from multiple perspectives, that there is no risk of any significance whatsoever from such black holes.

Acknowledgements We are grateful to many colleagues who helped us in the course of the nine months of this project, providing valuable guidance and advice on the many facets of our study, helping us identify the key issues and pointing us to the relevant literature sources. Among these: J. Arons, J. Ellis, M. Fairbairn, G. Giudice, G. Horowitz, D. Ida, Y. Kanti, G. Landsberg, D. Marolf, J. March-Russell, K.-Y. Oda, S. Park, J. Polchinski, T. Rizzo, S. Rychkov, M. Salaris, M. Srednicki, N. Toro, I. Tkachev, M. Vietri, U. Wiedemann and T. Wiseman. The input of L. Anchordoqui, A. Dar, A. De Rujula, S. Dodelson, D. Hooper and G. Gelmini helped us clarify several issues related to the cosmic ray composition, and that of L. Balents and D. Scalapino, questions of atomic structure relevant to subatomic accretion. We would particularly like to thank O. Blaes for a number of important discussions on Bondi and Eddington accretion, K. Shen and G. Schmidt for guidance on white dwarf structure and populations, and L. Bildsten both for many crucial discussions and for supplying information about neutron-star binary systems. We would also like to thank J. Hartle for earlier collaboration on this work, and for many useful discussions. The work of SBG was supported in part by the U.S. Department of Energy under Contract DE-FG02-91ER40618, and by grant RFPI-06-18 from the Foundational Questions Institute (fqxi.org).

A Bondi accretion

Bondi accretion [33, 59] describes the steady flow of continuous matter into a black hole, assuming spherical symmetry and hydrodynamical conditions. Its basic ingredients are the continuity equation, guaranteeing a conserved matter flow, energy conservation, which gives the accretion velocity, and accretion boundary conditions at the surface of the black hole, which provides the sink for the continuous matter infall. As is well known, many features of accretion depend on matter properties in the non-relativistic region, far from the black hole horizon, and so a non-relativistic treatment is warranted. In particular, one may describe the gravitational dynamics in terms of a general potential $\phi(r)$ that becomes strong in the TeV regime, as discussed in section 3.2.4. Accretion from within a neutron star approaches the relativistic regime; relativistic corrections, which are typically small, are described for example in [59].

The continuity equation is easily expressed as

$$\frac{dM}{dt} = 4\pi \rho(r) r^2 v(r) = \text{constant} \quad (\text{A.1})$$

where $\rho(r)$ and $v(r)$ represent the matter medium density and velocity, with positive $v(r)$ corresponding to radial flow towards the black hole at $r = 0$. The Euler equation,

$$v \frac{dv}{dr} + \frac{1}{\rho} \frac{dp}{dr} = -\partial_r \phi \quad (\text{A.2})$$

describes energy conservation. The first term is clearly the variation of kinetic energy for an element of the medium as it moves. The second term represents the work done by the pressure gradients. As matter falls towards the black hole, its pressure will increase in response to increase in density. This energy, as well as the kinetic energy, are drawn from the gravitational potential of the black hole. Indeed, this equation can be integrated to give the Bernoulli equation,

$$0 = \frac{v^2}{2} - \int_r^\infty \frac{dp}{\rho} + \phi(r) , \quad (\text{A.3})$$

where we neglect the kinetic and gravitational energy densities far away from the black hole.

More highly compressible matter results in a higher accretion rate. We parameterize matter properties via a general polytropic equation of state, assuming adiabatic evolution, as

$$p = K \rho^\Gamma \quad (\text{A.4})$$

where K and Γ are constants. The density change as a function of a pressure variation is related to the sound speed in the medium, according to

$$c_s^2 = \frac{dp}{d\rho} = \frac{\Gamma p}{\rho} . \quad (\text{A.5})$$

This equation of state also provides the value of the integral in the Bernoulli equation:

$$\int_r^\infty \frac{dp}{\rho} = \frac{c_s^2}{\Gamma - 1} \Big|_r^\infty, \quad \Gamma \neq 1 \quad (\text{A.6})$$

$$\int_r^\infty \frac{dp}{\rho} = K \ln \left[\frac{\rho(\infty)}{\rho(r)} \right], \quad \Gamma = 1. \quad (\text{A.7})$$

Using these definitions, ρ can be eliminated by combining the continuity equation and Euler's equation, with the result

$$\frac{1}{2} \partial_r v^2 \left(1 - \frac{c_s^2}{v^2} \right) = -\partial_r \phi + \frac{2c_s^2}{r}. \quad (\text{A.8})$$

As one approaches the black hole, v increases until it reaches the local sound speed c_s ; this equation gives a relation defining the resulting *sonic horizon*, at $r = r_s$:

$$\frac{1}{r_s} = \frac{\partial_r \phi(r_s)}{2c_s^2(r_s)}. \quad (\text{A.9})$$

For example, in the case where the potential transitions from higher-dimensional form

$$\phi(r) = -\frac{k_D M}{2M_D^{D-2} r^{D-3}}, \quad r < R_D \quad (\text{A.10})$$

to four-dimensional form

$$\phi(r) = -\frac{G_4 M}{r}, \quad r > R_C, \quad (\text{A.11})$$

the sonic horizon is given by

$$r_s^{D-3} = \frac{D-3}{4} \frac{k_D M}{M_D^{D-2} c_s^2(r_s)} \quad (\text{A.12})$$

for $r_s < R_D$, and by

$$r_s = \frac{G_4 M}{2c_s^2(r_s)} \quad (\text{A.13})$$

for $r_s > R_C$.

The continuity equation (A.1) implies that the accretion rate is determined by quantities at the sonic horizon as

$$\frac{dM}{dt} = 4\pi \rho(r_s) r_s^2 c(r_s). \quad (\text{A.14})$$

This can then be computed by relating these quantities to those at large distances.

For example, evaluation of Bernoulli's equation (A.3) at $r = r_s$ yields

$$c_s^2(r_s) \left(\frac{1}{2} + \frac{1}{\Gamma - 1} \right) + \phi(r_s) = \frac{c_s^2(\infty)}{\Gamma - 1}. \quad (\text{A.15})$$

In a D -dimensional regime, the formula (A.12) for the sonic radius then gives

$$c(r_s) = \sqrt{\frac{2(D-3)}{D+1-\Gamma(7-D)}} c_s(\infty). \quad (\text{A.16})$$

From the equation of state relation $c_s^2 \propto \rho^{\Gamma-1}$ we then find the D -dimensional relation between asymptotic fluid parameters and those at the sonic horizon:

$$\rho(r_s) = \rho(\infty) \left[\frac{2(D-3)}{D+1-\Gamma(7-D)} \right]^{1/(\Gamma-1)}, \quad p(r_s) = p(\infty) \left[\frac{2(D-3)}{D+1-\Gamma(7-D)} \right]^{\Gamma/(\Gamma-1)} \quad (\text{A.17})$$

Also, define the *Bondi radius* for a given mass by the equation

$$R_B(M) = \left[\frac{(D-3) k_D M}{4c_s^2(\infty) M_D^{D-2}} \right]^{1/(D-3)}. \quad (\text{A.18})$$

Note that the sonic horizon radius and Bondi radius defined in (A.18) also differ by an $\mathcal{O}(1)$ proportionality constant. Combining these quantities gives the Bondi accretion rate,

$$\frac{dM}{dt} = \pi R_B^2(M) \rho(\infty) c_s(\infty) \lambda_D \quad (\text{A.19})$$

where λ_D is a D -dimensional constant,

$$\lambda_D = 4 \left[\frac{2(D-3)}{D+1-\Gamma(7-D)} \right]^{[D+1-\Gamma(7-D)]/[2(\Gamma-1)(D-3)]}. \quad (\text{A.20})$$

In the range $1 \leq \Gamma \leq 5/3$, numerical values fall between $4 \leq \lambda_4 < 18$ for $D = 4$, and $3 < \lambda_D < 6.6$ when $D = 5, \dots, 11$.

Proper understanding of the accretion process also requires knowing the radial dependence of the physical parameters. Eq. (A.17) shows that their values at the sonic horizon are close to their asymptotic values. Within the sonic horizon, where the v becomes supersonic, the relation $v^2 \approx 2\phi$ and the continuity equation give the radial dependence of the density,

$$\rho(r) \simeq \rho(r_s) \frac{r_s^2}{r^2} \sqrt{\frac{\phi(r_s)}{\phi(r)}}, \quad (\text{A.21})$$

from which other quantities follow via the equation of state. In particular, note that in a D -dimensional non-warped regime,

$$\rho(r) \simeq \rho(r_s) \left(\frac{r_s}{r} \right)^{(7-D)/2}. \quad (\text{A.22})$$

From this we see that matter is compressed more strongly at lower D , remains constant density in $D = 7$, and is rarified for $D > 7$. Also, from (3.24), note that in a warped regime, the density scales as

$$\frac{\rho(r)}{\rho(r_0)} \simeq \left(\frac{r_0}{r} \right)^{(8-D)/2} e^{j_D(r-r_0)/2R_D}, \quad (\text{A.23})$$

which implies rarification in the region $R_D < r < R_C$.

B Effects of radiative transport

Acceleration and compression during accretion can cause the infalling medium to radiate. This raises the possibility of new effects. For example, in the case of accretion on Earth, such radiant energy could melt the material surrounding the black hole, and thus has potential to increase the accretion rate. (In our rate bounds for accretion within Earth, we guarantee that we have accounted for melting by treating the problem as accretion from a fluid.) However, pressure from the outgoing radiation also has the potential to decrease the accretion rate, and in particular one should check for the possibility of an Eddington-limited rate.

The actual process of radiation and its reabsorption is somewhat complicated, but can be modeled based on simple considerations. In the microscopic regime, one expects radiation resulting from accelerations of infalling particles. In the macroscopic regime, another reradiation mechanism is heating of the material through its compression, resulting in thermal bremsstrahlung. In general, one can parametrize the reradiation luminosity as

$$L = \eta \frac{dM}{dt} \tag{B.1}$$

where $\eta < 1$ is the fraction of absorbed energy that is reradiated.

B.1 Subatomic regime

In the subatomic context, where accretion is treated as absorption of individual particles, such particles can in general radiate some of their energy via bremsstrahlung during absorption. The precise spectrum depends on details of the capture process, but a characteristic scale is the horizon radius. Thus, for horizon radii below 1fm, one expects nucleons to be broken up, and to emit gluon radiation that hadronizes into pions. For radii above the Fermi scale, one instead expects primarily emission of photons, with typical energies approaching $\sim 1/R$. We expect such radiation effects to be small, due to small couplings of gauge boson amplitudes in the vicinity of the black hole due to spatial wavefunction/gray body factors.

In this limit where individual particles are absorbed one at a time, one certainly doesn't expect an Eddington limit, but can ask whether emitted energy is sufficient to melt atomic matter. Note that if the accretion is driven by black hole motion, then one naturally converts the luminosity (B.1) into an energy deposition per unit length of travel,

$$\frac{dE}{dl} = \eta \sigma \rho , \tag{B.2}$$

with σ the capture cross section of the black hole.

Photons have characteristic absorption lengths in the cm range at sufficiently high energies. Let ℓ_a be the average absorption length for the reradiated photons. In this case, the energy density in the vicinity of the black hole's track has size

$$\mathcal{E} = \frac{\eta \sigma \rho}{\pi \ell_a^2} . \tag{B.3}$$

This can be estimated in the region $R_{\text{EM}} \sim 1 \text{ \AA}$. In this case, one has

$$\mathcal{E} = 10^{-16} \rho \frac{\eta}{\ell_a^2(\text{cm})} . \quad (\text{B.4})$$

For this value of R_{EM} , the Schwarzschild radius for $D = 8-10$ is in the range $10^{-11} - 10^{-12} \text{cm}$, so a characteristic energy is expected to be in the MeV range. In this range, ℓ_a indeed is of order $\gtrsim 1 \text{cm}$. For comparison, the latent heat of fusion for materials such as iron, rock, *etc.* are of size

$$\frac{300 \text{kJ}}{\text{kg}} = 3 \times 10^{-12} . \quad (\text{B.5})$$

To reach a threshold where reradiation could contribute significantly to melting, one should therefore wait until the black hole grows to increase $\sigma/(\pi\ell_a^2)$ by a factor of at least $\sim 10^4$, beyond the atomic scale.

In addition to photons, as noted for sufficiently small R , one can also have some fraction of the energy emitted as strongly interacting particles (mostly pions). These have a longer mean free path than photons, and should therefore contribute even less to melting.

B.2 Macroscopic accretion

When the Bondi radius exceeds the internuclear separation a in atomic matter, or r_N in nuclear matter, accretion transitions to that of a continuous medium.

In this context, for spherically-symmetric accretion, microscopic motion deviating from the overall radial macroscopic flow is parametrized by the temperature of the medium. As the medium is compressed, it heats up, and can radiate through thermal bremsstrahlung; elementary accounts of this mechanism appear in [38, 59]. In particular, the resulting luminosity can be estimated as resulting from free-free scattering. Let Λ_{ff} be the corresponding emissivity; for example, [59] gives the relativistic form of this,

$$\Lambda_{ff} \sim \frac{\alpha^3}{m_e^2 m_p^2} \rho^2 T , \quad (\text{B.6})$$

up to factors of order one. The total luminosity from a range of r is then computed from the integral

$$L_{ff} \approx \int \Lambda_{ff} 4\pi r^2 dr \quad (\text{B.7})$$

over that region. If one integrates this quantity from sonic horizon to event horizon in a four-dimensional accreting medium, using the radial density dependence (A.21), and the temperature dependence of a perfect fluid,

$$T \propto \frac{p}{\rho} \propto \rho^{\Gamma-1} , \quad (\text{B.8})$$

one finds [59] that the integral is dominated near the event horizon,

$$L_{ff} \approx 4\pi R^2 \Lambda_{ff}(R) \text{Min}[l(R), R/3] , \quad (D = 4) , \quad (\text{B.9})$$

where $l(r)$ is the radius-dependent photon mean free path. On the other hand, one can readily check that for a more rapidly increasing potential, *e.g.* $D \geq 5$, and for $\Gamma \leq 5/3$, the integrated luminosity is dominated by the integrand at the *maximum* value of r for the region.

The radiative transfer of the resulting radiation depends on properties of the medium such as its opacity. Particularly relevant is the photon mean free path $l(r)$, as compared to radius r – this determines whether radiation thermalizes, or can instead escape to regions with weaker gravitational potential. (In the regimes we consider, free-free absorption is a typical opacity mechanism.) This ratio is given by

$$\frac{l(r)}{r} = \frac{1}{r\kappa(r)\rho(r)}, \quad (\text{B.10})$$

where $\kappa(r)$ is the opacity. Using the equation (A.21) for the density, we find that this parameter varies like

$$\frac{l(r)}{r} \simeq \frac{1}{r_s\kappa(r)\rho(r_s)} \sqrt{\frac{r^2\phi(r)}{r_s^2\phi(r_s)}} \quad (\text{B.11})$$

in the supersonic region. For constant opacity, we thus find different behaviors at decreasing r , depending on how the potential grows. For four-dimensional growth, $l(r)/r$ decreases as \sqrt{r} , signifying that the medium becomes increasingly optically thick. For $D = 5$, this quantity stays constant at decreasing r , and for faster growth of the potential characteristic of $D > 5$ or warped regimes, $l(r)/r$ increases for decreasing r – the medium becomes more transparent.

The size of the opacity is often approximately given by the Thomson cross section, $\kappa \approx \sigma_T/m$, where m is the medium mass per electron ($\approx Am_p/Z \approx 2m_p$ for non-hydrogenic atomic matter). However, this can vary depending on density and temperature. It also depends on the frequency of the radiation, which will typically be given by the local temperature of the medium.

We will first illustrate these considerations by describing the case of white dwarfs, and then briefly summarize the corresponding story for Earth and for neutron stars.

B.2.1 Radiative effects in white dwarfs

Let us first compare the relevant scales. The ambient mean free path, estimated via the Thomson value for the opacity, at $\rho = 10^7 \text{gr/cm}^3$, is approximately $l_0 \approx 5 \times 10^{-7} \text{cm}$. More careful calculations of the opacity [80] yield a value $l_0 \simeq 5 \times 10^{-8} \text{cm}$ at the temperature $10^8 K$ characteristic of a young white dwarf, and values smaller by about 1/100 for the temperature $10^7 K$ characteristic of the 1 Gyr age.

For the moment we restrict attention to the case $R_D \gtrsim l_0$. From the above values, we find that this covers most situations with R_D larger than the atomic scale, and specifically the cases we particularly would like to bound via white dwarfs, those of $D \leq 7$ and the warped cases such as $D = 5$ with large radius.

This means that there are three regimes for the evolution: first as r_s evolves from the internuclear separation $a_{WD} \sim 10^{-10}\text{cm}$ to l_0 , then on to the scale $R_D \sim R_C$, then the four-dimensional regime $r_s > R_C$. We consider them in turn.

In the first regime, the medium is effectively transparent, and is governed by the higher-dimensional force law. For constant opacity, the preceding arguments indicate that the medium becomes more transparent closer to R . Initially, since the temperature is nonrelativistic, the opacity evolves via a Kramers law, $\kappa \propto \rho/T^{-7/2}$, and thus drops slightly. Then, at the relativistic temperature $\sim 6 \times 10^9\text{K}$, the free-free emissivity (B.6) indicates $\kappa \propto \rho/T^3$, giving an essentially constant value in the degenerate regime $\Gamma = 4/3$. Since the medium is degenerate, one also expects a correction factor due to Fermi blocking of the available energy levels ; this is included in the results of [80], and evolves as $\sim T/\rho^{1/3}$, thus also remaining essentially constant in the degenerate regime.

Accretion is determined by the balance of forces in the vicinity of the sonic horizon. There will be a luminosity pressure from the ambient luminosity of the gas,

$$p_\gamma \sim T^4, \quad (\text{B.12})$$

in the downward direction towards $r = 0$. Below r_s , the medium is being evacuated by the accretion and does not have time to thermalize. It will produce a luminosity, estimated for example by L_{ff} as in the preceding discussion. Since this is higher-dimensional accretion the integral will be dominated at the upper end; however, the result will not produce a value that competes with the downward pressure, since the integral contributes less upward pressure than would be present at the surface $r = r_s$ in the absence of a black hole. Moreover, even if this pressure were competitive with the downward pressure, we can estimate the importance of them both via (B.12). For the early temperature $T_0 \sim 10^8\text{K} \sim 9 \times 10^3\text{eV}$, and a typical pressure, we find

$$\frac{T_0^4}{p_0} \approx \frac{(9 \times 10^3\text{eV})^4}{5 \times 10^{-3}\text{MeV}^4} \approx 10^{-6}. \quad (\text{B.13})$$

Thus these photon pressures cannot not compete with the pressure of the degenerate fluid.

The next regime is evolution from $r_s = l_0$ up to R_D . In this regime, the medium is optically thick when crossing the horizon, and thus approximately thermal. With falling $l(r)/r$, it may become optically thin before reaching the horizon. There, as above, we would find the inward thermal luminosity overcomes the outward luminosity from the thin region at lower r . Any resulting radiation cannot reach $r = r_s$. Moreover, even its effect at $r < r_s$ is small. For example, the ratio of photon pressure to medium pressure scales as

$$\frac{p_\gamma(r)}{p(r)} = \frac{p_\gamma(r_0)}{p(r_0)} \left[\frac{\rho(r)}{\rho(r_0)} \right]^{3\Gamma-4} \quad (\text{B.14})$$

and thus remains relatively small. Furthermore, in the regime $r < r_s$, gravitational attraction dominates over the medium pressure.

As r_s passes R_D, R_C , one reaches the four-dimensional regime. The medium is opaque at the sonic horizon, but, if the true horizon lies below R_C , may or may not become transparent

below that depending on parameters. Once the true horizon reaches R_C , the fluid remains optically thick to the horizon, and thus any outward photon flux thermalizes. Again, by estimating p_γ/p down to the horizon, we see that its effect is small even on the local fluid evolution at $r < r_s$.

As one final check, one can compare the mean outward photon diffusion velocity to the inward flow velocity in the four-dimensional accretion regime. This tells us whether the photons are *trapped*. (For more discussion, see [81].) We find the resulting trapping condition $r^2 < RR_B^3/l_0^2$. This is satisfied for all r out to r_s if $R_B \gtrsim l_0/c_s$. Thus even very small four-dimensional black holes exhibit photon trapping, preventing their escape to the region near the sonic horizon.

From these considerations we conclude that there are good reasons to rule out important radiation effects that could produce an Eddington limit for accretion within a white dwarf, although one cannot state for certain that some form of dissipation would not play such a role. However, we note that even in media that are less optically thick, efforts to produce luminosity that reaches the Eddington limit for spherical black hole accretion in astrophysical contexts have failed, as described in [38,59]. Radiation from spherical accretion onto a black hole seems to be quite inefficient, even in optically thinner situations, which we can find in accretion from Earth.²⁰

B.2.2 Radiative effects in Earth

In the case of Earth, the mean free path is much longer; for a rough estimate, using the Thomson cross section, and a density $\sim 10\text{gr/cm}$ characteristic of the interior of the Earth, one finds a photon mean free path of size $l_0 \sim 0.5\text{cm}$. Thus, in cases relevant to Earth, we must explore another regime, $R_C < l_0$. This changes the discussion as follows.

First, the phase from $r_s = a$ to $r_s = R_D$ is similar to the first phase for white-dwarf accretion: the medium begins in the optically thin regime, and can get thinner as it nears the horizon. Thus the upward luminosity pressure should not be competitive with the downward pressure. Estimating relative sizes of photon vs. medium pressures for material near the center of the Earth, we find

$$\frac{T_0^4}{p_0} \sim \frac{(.5\text{eV})^4}{2 \times 10^{10}\text{eV}^4} \sim 4 \times 10^{-12} . \quad (\text{B.15})$$

Thus, radiation pressure is negligible.

The next possible regime is from $r_s = R_C$ to $r_s = l_0$, and is new: it involves four-dimensional accretion from an optically thin medium. In this case, the contribution to the luminosity from the integral (B.7) is dominated by its lower limit, as long as that is in the four-dimensional regime. Thus, initially it will be dominated by $r \approx R_C$. However, as the

²⁰In certain low-collisionality contexts, magnetic fields can change this situation; see *e.g.* [39]. However, one can check that inside the low-magnetic field white dwarfs we consider, the dynamics is collisional, with typical Larmor radii greatly exceeding mean free paths.

black hole grows, the opacity at $r = R_C$ typically grows. Before R reaches R_C , the optical thickness $\tau(R_C)$ from R_C to r_s , defined via

$$\tau(r) = \int_r^{r_s} \frac{dr}{l(r)} = \int_r^{r_s} dr \kappa(r) \rho(r) , \quad (\text{B.16})$$

reaches unity. Subsequently the radius r_T defined by $\tau(r_T) = 1$ increases past R_C . This means that the medium is optically thick and thermalizes inside this radius. Thus, the integral (B.7) should be cut off at the greater of R_D, r_T . The net luminosity can be estimated as due to the contribution of that integral, dominated by the resulting radius, plus the luminosity of the thermal region inside r_T ,

$$L_T \approx 4\pi r_T^2 T^4(r_T) . \quad (\text{B.17})$$

This case is similar to the case of accretion of an optically thin gas onto a black hole, treated for example in [38, 59]. This situation, in which radiation can readily propagate from regions of high compression and temperature, seems to have the highest prospect of producing an Eddington limit among the scenarios we consider. However, while a significant amount of luminosity can be generated, it appears difficult to attain an Eddington limit, due to the cutoff on free-propagation of photons at the radius r_T . In particular, if one assumes an Eddington limit with a small efficiency η , this implies that $r_T \approx R/\eta^2$. This thus requires r_T to be large, which in turn limits the temperature at the last-scattering surface. This basic inconsistency is related to those explained for example in [38]. Thus, presence of an Eddington limit would require satisfying a non-trivial set of consistency conditions, in the absence of other dissipative mechanisms in the medium. (One can incidentally check that there is not sufficient infall time for neutronization to provide a *cooling* mechanism.)

Finally, ultimately r_s reaches l_0 . Above this value, the accreting medium is optically thick at the sonic horizon, and typically gets thicker as r decreases. If the true horizon is still inside R_D , there is a possibility that the medium might become optically thin in a region before reaching R . Whether or not this happens, the significant optical depth in the regime just inside the sonic horizon apparently precludes an Eddington limit.

B.2.3 Radiative effects in neutron stars

A rough estimate of the photon mean free path in the neutron star case, using the Thomson cross section, yields $l_0 \lesssim 1\text{fm}$. Thus in all cases where we seek a bound (namely, if $R_D \gtrsim 1 \text{ \AA}$), we are in a situation analogous to that of the second and third regimes for a white dwarf, but with an even higher opacity. Moreover, the range of r between the sonic radius and the horizon is quite limited; in general, we have

$$\frac{R_B}{R} \lesssim \frac{1}{c_s^2} , \quad (\text{B.18})$$

with a typical sound speed $c_s \gtrsim 0.17$. Thus we typically don't expect the medium to ever become optically thin. Finally, asymptotic interior temperatures are expected to be in the

range $10^4 - 10^5 \text{eV}$, and pressures are in the range of MeV/fm^3 . Thus, asymptotically, $p_\gamma/p \lesssim 10^{-11}$, and from (A.21) and (B.14) we find that the radiation pressure remains negligible down to the horizon.

The relative unimportance of radiative pressure, and its inability to stream outward, thus indicate that the neutron star evolution should also be governed by Bondi accretion, without an Eddington limit.

We also note here that our arguments against an Eddington limit in subsections B.2.1-B.2.3, and therefore for a Bondi description of accretion, likewise apply to the case of primordial four-dimensional black holes, which are expected to have masses $\gtrsim 10^{15} \text{gr}$.

B.3 Eddington evolution

For completeness, we will give a rudimentary account of accretion in the presence of an Eddington limit. We model this effect as follows.²¹ The reradiation luminosity leads to a flux of energy

$$S = \frac{\eta \dot{M}}{4\pi r^2} \quad (\text{B.19})$$

through the spherical surface at radius r from the BH. As described, the reradiation consists of light particles such as photons, pions, etc. These outgoing particles scatter on the accreting matter, producing an effective outward force. If the scattering cross section on a given infalling particle of mass m is σ , the average force on this incident particle takes the form

$$F_L = \frac{\eta \dot{M} \sigma}{4\pi r^2} . \quad (\text{B.20})$$

For Earth, the incident matter is atoms. In the case of a white dwarf or neutron star interior, generally the incident matter is a degenerate electron liquid or the n-p-e liquid of neutron star interiors. For horizon sizes above the scale 1fm, the radiation is expected to be primarily photons, and thus its force can be estimated using the Thomson cross section for photon-electron scattering.

This reradiation force has the effect of modifying the Euler equation (A.2) to

$$v \frac{dv}{dr} + \frac{1}{\rho} \frac{dP}{dr} = -\partial_r \phi + \frac{\eta \dot{M} \sigma}{4\pi m r^2} . \quad (\text{B.21})$$

This yields a modified Bernoulli equation; for a D-dimensional potential,

$$\frac{1}{2} v^2 + \frac{1}{\Gamma - 1} c_s^2 = \left[\frac{1}{2} \left(\frac{R}{r} \right)^{D-3} - \frac{\eta \dot{M} \sigma}{4\pi m r} \right] + \frac{1}{\Gamma - 1} c_s^2(\infty) . \quad (\text{B.22})$$

²¹For a textbook treatment of some aspects of the Eddington limit, see [59].

This equation provides an important constraint on accretion flows. In particular, notice that its left hand side is positive semidefinite. Therefore, if the right hand side vanishes for some r , the density and velocity of the accreting fluid must go to zero, effectively shutting off accretion. There are two cases, depending on whether the Bondi radius R_B defined in equation (A.18) is greater or less than the crossover radius to four-dimensions, R_C .

Notice that the two positive terms on the RHS of (B.22) are of the same size when

$$r = \left[\frac{2(\Gamma - 1)}{D - 3} \right]^{1/(D-3)} R_B , \quad (\text{B.23})$$

and consider first the case $R_B \gg R_C$. Then the gravitational term dominates in the range $R_B \gtrsim r > R_C$. The condition that the negative Eddington term not negate the four-dimensional gravitational force is then the usual Eddington limit,

$$\dot{M} \leq \frac{4\pi m G}{\eta \sigma} M . \quad (\text{B.24})$$

In the case $R_B < R_C$, the positive terms become of comparable size in the higher-dimensional regime. If the negative term is smaller than the other two terms at the radius given by (B.23), then it will also clearly be subdominant for both larger and smaller r . This yields the relevant higher-dimensional Eddington limit,

$$\dot{M} \leq f(\Gamma, D) \frac{8\pi m R_B}{\eta \sigma} c_s^2(\infty) , \quad (\text{B.25})$$

where for $D \geq 5$

$$f(\Gamma, D) = 2 \left(\frac{2}{\Gamma - 1} \right)^{(D-4)/(D-3)} \left(\frac{1}{D - 3} \right)^{1/(D-3)} \quad (\text{B.26})$$

is an $\mathcal{O}(1)$ coefficient. In the case of $D = 4$, (B.25) subsumes (B.24) with $f(\Gamma, 4) = 1$.

The Eddington limit becomes relevant when the Bondi accretion rate (A.19) exceeds the Eddington rate (B.25). This occurs for

$$R_B \gtrsim R_{Edd} = \frac{8m c_s(\infty)}{\lambda_D \eta \sigma \rho} , \quad (\text{B.27})$$

defining the *Eddington radius* R_{Edd} . Growth of the mass at the four-dimensional Eddington limit (B.24) is exponential, with a time constant

$$t_{Edd} = \eta \frac{\sigma}{4\pi m G} . \quad (\text{B.28})$$

We have given arguments about the difficulty of achieving such an Eddington limit in Earth, and even more so in white dwarfs, at least until one reaches large black hole sizes which disrupt the large-scale structure of the body in question. Moreover, if such a mechanism were to become operative in white dwarfs, then each black hole within the dwarf would be

emitting at the characteristic Eddington luminosity $L_{Edd} \simeq 8\pi m R_B c_s^2 / \sigma$. This would also be evident through interference with white dwarf cooling. Typical cooling rates are in the range $10^{-1} - 10^{-3} L_\odot$, where the solar luminosity is $L_\odot = 4 \times 10^{33} \text{ erg/s}$. As an example, we find that the Eddington output of N black holes of Bondi radii R_B would exceed $10^{-2} L_\odot$ for

$$NR_B/\text{cm} \gtrsim 60 . \quad (\text{B.29})$$

Given the large numbers of black holes that would be produced, on relatively short time scales one would find a buildup of black holes that have a major impact on cooling, even for a relatively large value like $\eta = .01$.

C Gravitational scattering of relativistic particles in a Schwarzschild field

This Appendix focuses on the dynamics of a test particle in the background of a D -dimensional black hole. In the classical context, we consider the trajectory of a test particle in motion with positive energy with respect to a D -dimensional black hole. The goal is to establish the features of the particle's dynamics as a function of the initial energy and impact parameter, and to define the conditions under which the test particle, in the encounter with the black hole, is scattered or is absorbed. We shall be interested in applying this discussion to the study of energy loss, slow-down and stopping of black holes produced by cosmic rays. In this phase the black hole is still sufficiently small that it only interacts, microscopically, with the partons inside the nucleon. Since these are in relativistic motion, we need to consider the case of relativistic test particles. Two kinematical regimes are then potentially relevant: the classical one, in which the de Broglie wavelength of the test particle is small in comparison to the black hole radius, and the quantum regime, where the black hole itself is small compared to the probe's wavelength. In the context of black holes produced by cosmic rays, the classical regime is relevant early on, when the Lorentz γ factor of the black hole is very large, and later on, when its size has grown significantly. If we consider first the problem in the rest frame of the black hole, the momentum of the infalling parton is of order γm_p . At production, $\gamma > M/m_p$ (see eq. (5.5)), and therefore the wavelength of the projectile is indeed smaller than $1/M$, and thus smaller than the D -dimensional black hole radius, which is larger than $1/M$. As the black hole slows down, γ drops, and we enter the quantum regime, where we stay until the black hole grows to a size of > 1 fm. In the quantum case, we can use the known total quantum scattering cross section. Where we need the differential cross section as a function of angle, outside the capture regime, we will use the classical result; the two are known to agree for $D = 4$ Rutherford scattering.

C.1 Classical trajectories and capture

The equation of the particle's trajectory, in the rest frame of a D -dim Schwarzschild potential, is given by:

$$\varphi = \int \frac{L}{r^2} \left\{ E^2 - \left(m^2 + \frac{L^2}{r^2} \right) \left[1 - \left(\frac{R}{r} \right)^n \right] \right\}^{-1/2} dr \quad (\text{C.1})$$

where $n = D - 3$, E is the projectile energy at infinity, and $L = pb$ is the angular momentum at infinity (b being the impact parameter). Setting $E = m\gamma$, $p = mv\gamma$ and defining $\hat{r} = r/R$ and $\hat{b} = b/R$ gives:

$$\varphi = \int \frac{v\hat{b}}{\hat{r}^2} \left[1 - \left(\frac{1}{\gamma^2} + v^2 \frac{\hat{b}^2}{\hat{r}^2} \right) \left(1 - \frac{1}{\hat{r}^n} \right) \right]^{-1/2} d\hat{r}. \quad (\text{C.2})$$

In the relativistic limit, $\gamma \rightarrow \infty$, this becomes:

$$\varphi = \int \frac{\hat{b}}{\hat{r}^2} \left[1 - \frac{\hat{b}^2}{\hat{r}^2} + \frac{\hat{b}^2}{\hat{r}^{n+2}} \right]^{-1/2} d\hat{r}. \quad (\text{C.3})$$

The orbit is thus entirely defined by the initial impact parameter \hat{b} . Scattering states only exist if the impact parameter is large enough that the term in square brackets admits a zero for $\hat{r} > 0$, defining the point of closest approach, \hat{r}_{min} , of the trajectory. At this point,

$$\hat{b}^2 = \frac{\hat{r}_{min}^{2+n}}{\hat{r}_{min}^n - 1}, \quad \hat{r} > 1. \quad (\text{C.4})$$

It is straightforward to prove that this relation admits a real-valued solution for \hat{r}_{min} only if

$$\hat{b} > \hat{b}_{min} = \frac{(2+n)^{(2+n)/2n}}{\sqrt{n} 2^{1/n}}. \quad (\text{C.5})$$

Thus $b_{min} = \hat{b}_{min}R$ represents the minimum impact parameter for scattering, below which the projectile falls inside the event horizon. This therefore defines the classical *capture radius*²². Approximate values for $D = 5, \dots, 11$ are given by $\hat{b}_{min} = (2, 1.8, 1.6, 1.5, 1.5, 1.4, 1.4)$.

C.2 Quantum capture

The absorption cross section of 4-dimensional spin-1/2 and spin-1 fields in the field of a D -dimensional black hole has been calculated in [82–86], generalizing the $D = 4$ results of [87–89]. Considering spin-1/2 fields, the largest contribution is given by the s -wave states, resulting in capture cross sections σ_c given by the following equation:

$$\sigma_c = 2^{(3D-13)/(D-3)} \pi R^2. \quad (\text{C.6})$$

²²For the $D = 4$ case, we recover the usual results, $b_{min} = 3\sqrt{3}R/2$, and $r_{min} = 3R$, leading to a capture cross section of $27\pi R^2/4$.

These can be thought of as determining the capture impact parameter $\hat{b}_{min,q}$, like in the classical case, via the equation

$$\sigma_c = \pi \hat{b}_{min,q}^2 R^2 . \quad (C.7)$$

The quantum capture radius $\hat{b}_{min,q}$ grows from $\sqrt{2}$ for $D = 5$ to $\sim 2\sqrt{2}$ for large D . The approximate values in the range of interest are given by $\hat{b}_{min,q} = (1.4, 1.8, 2.0, 2.1, 2.2, 2.3, 2.4)$. Notice that, with the exception of $D = 5$, these are slightly larger than the classical capture radii given above.

C.3 Coulomb scattering

Outside the capture region, the projectile is deflected by the gravitational field. In the large- \hat{b} approximation, the approximate expression for the classical scattering angle $\theta \equiv \pi - 2\varphi$ is given by:

$$\theta_{app} = -\frac{1}{\hat{b}^n} \sqrt{\pi} \frac{\Gamma[(n+3)/2]}{\Gamma[(n+2)/2]} \equiv -\frac{1}{\hat{b}^n} \alpha_{n+2} , \quad (C.8)$$

which correctly reproduces the classical deflection of light in $D = 4$, $\theta = -2R/b$. Notice that this approximate result underestimates the exact deflection angle in the region around $b \sim b_{min}$, as shown fig. 3. Notice also in the figure that, as D grows, large-angle scattering only takes place for projectiles with impact parameter very close to the minimum value b_{min} , as a result of the rapidly falling gravitational field.

As discussed in the main text, for the momentum loss due to elastic scattering we need the quantity

$$c_{sc} = \frac{1}{\sigma_c} \int_{\cos\theta_c}^1 d \cos\theta \frac{d\sigma}{d \cos\theta} 2 \sin^2 \frac{\theta}{2} . \quad (C.9)$$

Without an explicit formula for the quantum differential cross section, we will estimate it using the classical expression (5.19), combined with the small-angle formula (C.8). This yields the approximate value

$$c_{sc} \approx \frac{\theta_c^2}{2(D-4)} . \quad (C.10)$$

If $\theta_c \sim 1$, we find the approximate values $c_{sc} = (.5, .25, .17)$ for $D = 5 - 7$.

D Nonrelativistic accretion checks

The discussion in section 5.3 assumes the validity of two facts, which we establish here:

1. the mass accreted per nucleon-crossing should not exceed the proton mass.
2. the capture radius remains smaller than 1 fm throughout this phase.

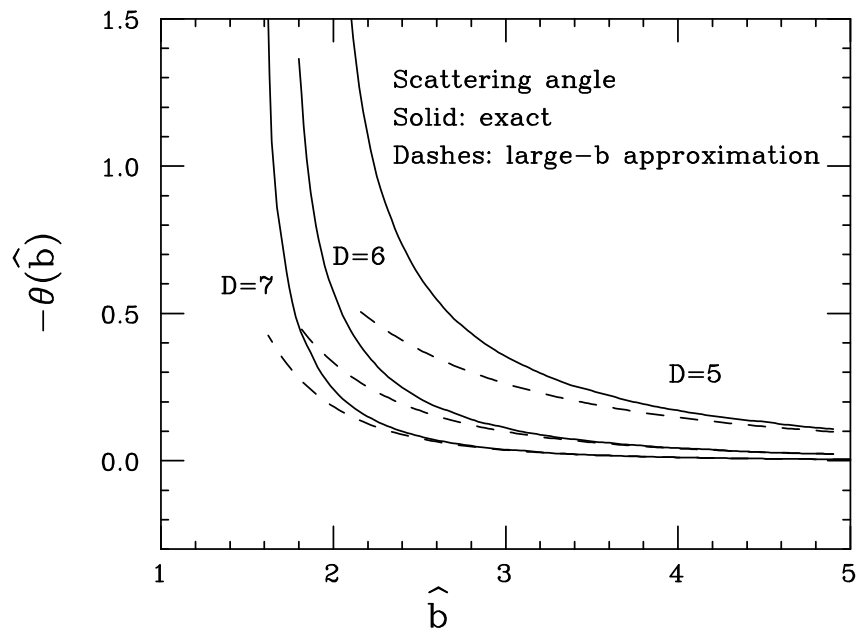


Figure 3: Comparison of exact (solid) and approximate (dashes) relations between the scattering angle (which for an attractive force is negative) and the normalized impact parameter $\hat{b} = b/R$, for $D = 5, 6, 7$.

The first statement is stronger than the second one. If the first is true, the second one is also true. Here is the proof:

The first statement requires the following:

$$\Delta M = \pi \rho_n \frac{r_n}{v} R_c^2 < m_p \quad (\text{D.1})$$

where R_c is the capture radius, $R_c = \hat{b}_{min} R$. Writing $m_p = (4\pi/3)\rho_n r_n^3$, we obtain $R_c < \sqrt{4v/3} r_n \lesssim r_n$. Thus, we just need to be show that the accretion rate during a single crossing does not saturate m_p .

The maximal mass relevant to nonrelativistic stopping in a white dwarf is the mass at the gravitational trapping velocity, which is bounded by $M < M_{NR}/v$, where we recall from (5.24) that $M_{NR} < \gamma_i M_i$, and where $v \simeq .02$. Thus, our condition becomes

$$\hat{b}_{min} R(\gamma_i M_i/v) < r_n \sqrt{\frac{4v}{3}}. \quad (\text{D.2})$$

Recall also that a typical boost for a large initial black hole, $M = 14\text{TeV}$, is $\gamma_i \approx 4.5 \times 10^4$. For $D \geq 6$, this inequality can then easily be checked to hold for all $v > .02$ and $M_D > 1\text{TeV}$. For $D = 5$, even for the extreme case $M_D = 1\text{TeV}$, the condition holds for black holes well above $M_i = 5M_D$ (with corresponding reduction in initial boost), down to the low end of the velocity range, $v \simeq .05$ and of course is easier to satisfy at larger M_D .

E Black hole production rates

E.1 Elementary cross sections

In the scenarios considered here, black holes are formed in the collisions of partons with center-of-mass energies $\sqrt{\hat{s}} \gg M_D$, and with impact parameters comparable to the Schwarzschild radius $R = R(\sqrt{\hat{s}})$ [5, 6, 48, 90]. The resulting cross section estimate, $\sigma \sim \pi R(\sqrt{\hat{s}})^2$, should be improved to account for two effects. On one side, the fraction y of partonic energy $\sqrt{\hat{s}}$ that is absorbed by the black hole is expected to be less than unity. The rest is radiated off [48–51]. Furthermore, the maximum impact parameter b of the partonic collision that can lead to a black hole formation above the threshold mass M_{min} for black holes to exist is typically smaller than the radius $R(\sqrt{\hat{s}})$. Recent estimates [8], based on [51], give inelasticity y of the order of 0.6–0.7, depending on D , dying off beyond impact parameters of about half the radius $R(\sqrt{\hat{s}})$. We implement these constraints by allowing black hole production only for partonic collisions with impact parameter $b < 0.5 R$, and considering inelasticities as small as 0.5.

For a given inelasticity y , the LHC would only be able to make black holes at masses $M_{min} \leq y E_{LHC}$. When one calculates rates for cosmic rays to produce black holes, those rates increase with y . Thus, for the purposes of setting lower bounds on those rates, for a

given M_{min} , a conservative choice is to take the inelasticity to be the smallest value that would be compatible with LHC black hole production,

$$y = M_{min}/E_{LHC} . \quad (\text{E.1})$$

If indeed the inelasticity took this value, that would correspond to *zero* production at LHC, due to lack of kinematical range. For example, if the actual inelasticity were 0.5, LHC would produce no black holes above 7 TeV. For purposes of exploring the possible range of y , we will where appropriate let y range from 0.5 up to unity.

A related issue is what is the minimum black hole mass that can arise for a given value of the extra-dimensional Plank mass M_D . Several criteria are discussed in [5]; there it was advocated that one particularly useful criterion is that the entropy of the black hole be large, so that a thermal approximation begins to make sense. A non-rotating hole of mass M has entropy:

$$S_{BH} = \frac{R^{D-2} \Omega_{D-2}}{4G_D} = \left[\frac{2M}{(D-2)M_D} \right]^{(D-2)/(D-3)} \left[\frac{(2\pi)^{(2D-7)}}{\Omega_{D-2}} \right]^{1/(D-3)} . \quad (\text{E.2})$$

For example, for the representative cases of $D = 6$ and $D = 10$, a black hole with mass $M = 5M_D$ has entropy $S_{BH} \sim 24$, a plausible threshold to assume a semiclassical behaviour. Since for a fixed value of M the black hole radius, and thus the production cross sections, decrease with increasing M_D , to be conservative in our estimates of production rates by cosmic rays we shall loosen this constraint, and allow for M_{min}/M_D to be as small as 3. In the primary cases of interest for cosmic ray bounds, $D \leq 7$, this lowest value corresponds to a Schwarzschild radius that is less than twice the Planck radius, $1/M_D$.

The production cross sections at the LHC are then obtained from the simple formula:

$$\sigma_{BH}(M > M_{min}) = \sum_{ij} \int_{\tau_{min}}^1 d\tau \int_{\tau}^1 \frac{dx}{x} f_i(x) f_j(\tau/x) \hat{\sigma}(\sqrt{\hat{s}}) , \quad (\text{E.3})$$

where $\hat{s} = x_1 x_2 s$, and, as discussed above, $\hat{\sigma}(\sqrt{\hat{s}}) = \pi R^2(\sqrt{\hat{s}})/4$, $M_{min} = 3M_D$, and

$$\tau = x_1 x_2 > \tau_{min} = M_{min}^2/(y^2 s) . \quad (\text{E.4})$$

$x_{1,2}$ are the momentum fractions of the colliding nucleons carried by the partons i and j , which are taken to span the full set of quarks, antiquarks and gluons. For the numerical evaluations throughout this work we shall use the CTEQ6M set of parton distribution functions [54], calculated at the factorization scale $Q = 1/R$ [5].

The event rates at the LHC, integrated over the 1000 fb⁻¹ luminosity expected to be collected during the experiments lifetime, are given in fig. 4. We show here both the cases of $y = 1$ and of $y = 0.5$. We use $y = 1$ only to overcompensate for uncertainty in the precise value of this parameter; the value $y = 1$ is an extreme case, and recent analyses [8] have argued for the more realistic value $y = 0.6 - 0.7$, or even a lower value [53].

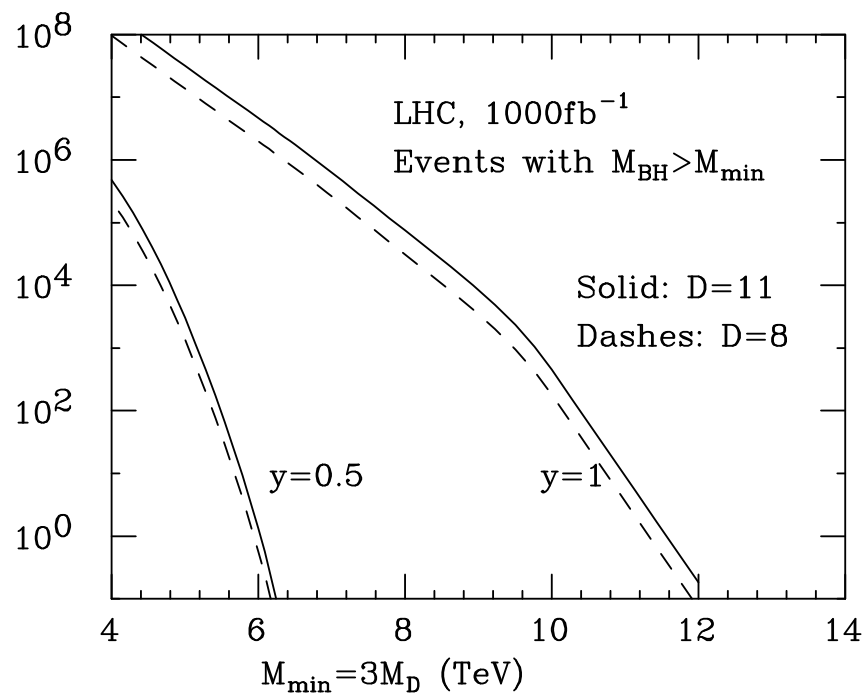


Figure 4: Black hole production rates at the LHC, with inelasticity $y = 1$ (upper curves) and $y = 0.5$ (lower curves), and for $D = 8, 11$.

E.2 Black hole production by cosmic rays

We present here the estimates of production rates and properties of black holes produced by cosmic rays hitting the surface of astronomical bodies. The rates presented in this section refer to the exposure of the full area of the star to cosmic rays coming from zenith angles between 0° and 90° . Possible sources of reduction of acceptance must be considered: the stellar magnetic fields, and the need for the black hole to traverse a sufficient amount of material in order to stop inside the star. These effects will be discussed in appropriate parts of the main text.

We assume cosmic rays to be composed of nuclei with atomic number A , and will consider the two extreme cases of $A = 1$ (protons) and $A = 56$ (Fe). When $A > 1$, only a fraction $1/A$ of the primary energy is available for the nucleon entering the hard collision that will produce the black hole, thus leading to a significant reduction in rate. The kinematics of the production is therefore as follows:

$$A(E) + N(m_p) \rightarrow i(x_1 E/A) + j(x_2 m_p) \rightarrow BH(M^2 = 2y^2 x_1 x_2 m_p E/A) \quad (\text{E.5})$$

where E is the energy of the cosmic ray primary; $N(m_p)$ is a nucleon in the target, with rest energy m_p . For each value of the primary energy E , the kinematics for the production of a black hole with minimum mass M_{min} is defined by the constraints $E > E_{min} \equiv M_{min}^2 \times A/(2m_p y^2)$ and $\tau = x_1 x_2 > \tau_{min} \equiv E_{min}/E$. The resulting number of produced black holes (per area, per time) is then expressed in terms of the cosmic ray flux $d\Phi/dE$ and by the total nucleon-nucleon inelastic cross section, $\sigma_{NN} = 100$ mb, as follows:

$$N_{BH}(M > M_{min}) = A \frac{1}{\sigma_{NN}} \int_{E_{min}}^{E_{max}} \frac{d\Phi}{dE} dE \sum_{ij} \int_{\tau_{min}}^1 d\tau \int_{\tau}^1 \frac{dx}{x} f_i(x) f_j(\tau/x) \hat{\sigma}(\sqrt{\hat{s}}). \quad (\text{E.6})$$

We describe the cosmic ray energy spectrum $d\Phi/dE$ using the latest results by Auger [40], using the reported values of the flux, and linearly interpolating in energy. We allow E_{max} to extend only up to the largest value for which data exist, namely $E_{max} = 2 \times 10^{20}$ eV.

We are interested in excluding the existence of stable black holes with masses within the reach of the LHC. The presence of an inelasticity y limits the mass reach to the range $M \lesssim y \times 14$ TeV. We allow y to take values in the range $(0.5, 1)$ in order to cover the full kinematic range up to 14 TeV, and calculate the cosmic ray rates corresponding to the smallest possible inelasticity compatible with production at a given mass value at the LHC, given by (E.1), and with the largest possible value of M_D , namely $M_D = M_{min}/3$. By so doing we obtain the lowest possible cosmic-ray-induced rates for black holes of any given mass that can be produced at the LHC.

As a reference, we shall consider the case of a white dwarf, with radius of 5400 km. The production rates, as a function of the energy of the primary cosmic ray, and integrated over an exposure of the full star surface of 1 million years, are shown in fig. 5. They are given for the case where the production rate is the lowest, namely $D = 5$, and for the values of $M_{min} = 7$ TeV, corresponding to inelasticity $y = 0.5$, and $M_{min} = 14$ TeV, with $y = 1$. The

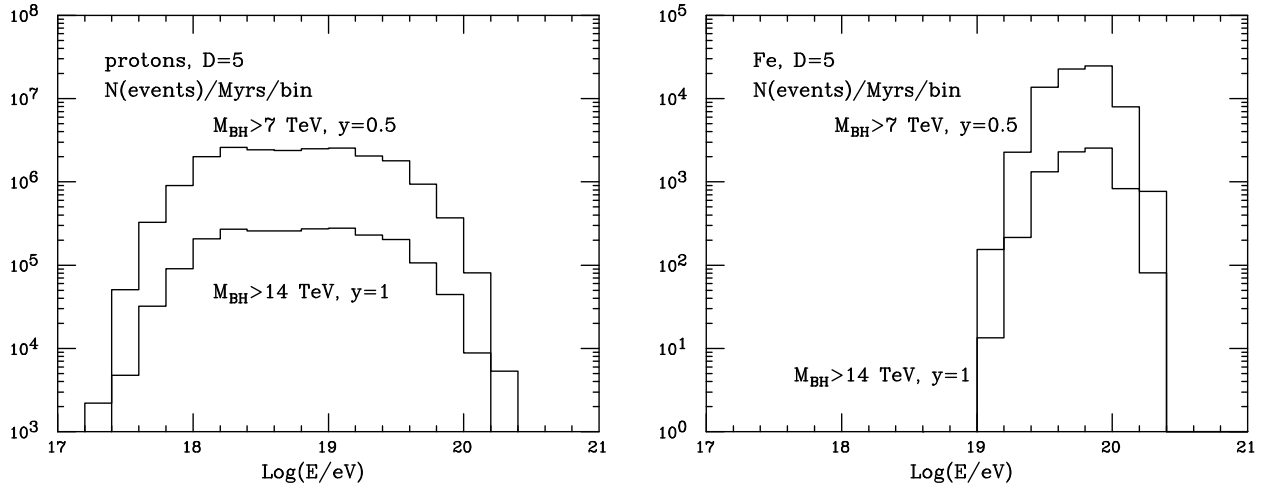


Figure 5: *Black hole production rates by cosmic rays impinging on a 5400 km radius white dwarf. The rates correspond to number of events, in one million years, in each energy bin. On the left we have a pure-proton cosmic ray composition, on the right pure Fe. The two curves correspond to minimum mass values of 7 and 14 TeV. In all cases, $M_D = M_{min}/3$ and $y = M_{min}/14$ TeV.*

Table 4: *Black hole production rates, per million years, induced by proton cosmic rays impinging on a $R = 5400$ km white dwarf. $M_D = M_{min}/3$ and $y = M_{min}/14$ TeV.*

| $D =$ | 5 | 6 | 7 |
|--------------------|-------------------|-------------------|-------------------|
| $M_{min} = 7$ TeV | 2.1×10^7 | 4.3×10^7 | 6.7×10^7 |
| $M_{min} = 8$ TeV | 1.4×10^7 | 2.9×10^7 | 4.7×10^7 |
| $M_{min} = 10$ TeV | 6.7×10^6 | 1.5×10^7 | 2.6×10^7 |
| $M_{min} = 12$ TeV | 3.7×10^6 | 9.1×10^6 | 1.6×10^7 |
| $M_{min} = 14$ TeV | 2.3×10^6 | 5.9×10^6 | 1.0×10^7 |

integrated rates for $D = 5 - 7$ are shown in Table 4 (for a pure proton composition) and in Table 5 (for a pure Fe composition). The rates increase due to the increasing black hole radius (for a given M , M_D) with larger D .

As expected the rates for pure protons are much larger, since in the case of Fe, to achieve sufficient energy for the nucleon-nucleon collisions, one is forced to use cosmic rays in the tail of the data distribution. Compositions intermediate between protons and Fe will lead to distributions contained within these two extremes. In particular, it is straightforward to evaluate the production rates resulting from some specified fraction of cosmic-ray protons, by convoluting the rates we show in fig. 5, bin-by-bin, with the experimental determination of the proton fraction as a function of energy. Current experimental data on the penetration and development of the shower (see e.g. [70,71]) provide evidence for a mixed composition, at

Table 5: *Black hole production rates, per million years, induced by Fe cosmic rays impinging on a $R = 5400$ km white dwarf. $M_D = M_{min}/3$ and $y = M_{min}/14$ TeV.*

| $D =$ | 5 | 6 | 7 |
|--------------------|-------------------|-------------------|-------------------|
| $M_{min} = 7$ TeV | 7.2×10^4 | 1.6×10^5 | 2.6×10^5 |
| $M_{min} = 8$ TeV | 4.6×10^4 | 1.1×10^5 | 1.8×10^5 |
| $M_{min} = 10$ TeV | 2.2×10^4 | 5.5×10^4 | 9.7×10^4 |
| $M_{min} = 12$ TeV | 1.2×10^4 | 3.2×10^4 | 5.9×10^4 |
| $M_{min} = 14$ TeV | 7.3×10^3 | 2.1×10^4 | 3.8×10^4 |

Table 6: *Black hole production rates, per million years, induced by cosmic rays impinging on a $R = 5400$ km white dwarf, with the cosmic ray energies rescaled such that $E_{exp} = 1.2 \times E_{true}$. $y = M_{min}/14$ TeV.*

| $D =$ | 5 | 6 | 7 |
|---------------------------------------|-------------------|-------------------|-------------------|
| $N_p/\text{Myr}, M_{min} = 7$ TeV | 1.2×10^7 | 2.5×10^7 | 3.9×10^7 |
| $N_{Fe}/\text{Myr}, M_{min} = 7$ TeV | 3.2×10^4 | 7.0×10^4 | 1.2×10^5 |
| $N_p/\text{Myr}, M_{min} = 14$ TeV | 1.3×10^6 | 3.4×10^6 | 6.0×10^6 |
| $N_{Fe}/\text{Myr}, M_{min} = 14$ TeV | 3.2×10^3 | 9.0×10^3 | 1.7×10^4 |

least in the region where such data are statistically significant, namely below 4×10^{19} eV. Data are inconsistent with being fully protons, or fully Fe, and provide an estimate of $\langle A \rangle \sim 5$ [41]. On the other hand, the uncertainty of these analyses is such that one cannot separate the individual components that contribute to the average of $\langle A \rangle$. Phenomenological descriptions or theoretical models of the highest energy cosmic ray sources, fitted [68, 69, 91, 92] using the latest Auger spectra, as well as the Auger data [72, 73] on the correlation between the origin of cosmic rays around the GZK cutoff and remote AGN, point to a significant proton fraction, of the order of at least 10%, and higher at super-GZK energies.

Proton fractions as low as only 10% lead to huge black hole production rates, with sufficient accumulation inside a white dwarf within a few years.

We point out that even assuming the most pessimistic scenario in which 100% of the cosmic rays are made of Fe, a scenario that is inconsistent with both data and with the modeling of cosmic ray sources, there would still be a large number of black holes that can be accumulated on the timescale of a few thousand years, very short compared to the natural lifetime of a white dwarf. As a further robustness check, we provide in Table 6 the rates obtained if one assumes a 20% systematic overestimate in the extraction of the primary energy, to simulate the possible impact of the Auger $\pm 20\%$ energy resolution [55].

Finally, we note that the production rates are still significant even if we set the inelasticity $y = 0.5$ in the calculation of the cosmic ray rates for black holes of 14 TeV. Notice that with $y = 0.5$ the black hole mass reach at the LHC drops to zero at around $M = 7$ TeV. The

Table 7: *Black hole production rates, per million years, induced by cosmic rays impinging on a $R = 5400$ km white dwarf. N_p refers to the case of 100% proton composition, N_{Fe} refers to 100% Fe. $M_D = M_{min}/3$ and inelasticity $y = 0.5$.*

| $D =$ | 5 | 6 | 7 |
|---|-------------------|-------------------|-------------------|
| $N_p/\text{Myr}, M_{min} = 7 \text{ TeV}$ | 2.1×10^7 | 4.3×10^7 | 6.7×10^7 |
| $N_{Fe}/\text{Myr}, M_{min} = 7 \text{ TeV}$ | 7.2×10^4 | 1.6×10^5 | 2.6×10^5 |
| $N_p/\text{Myr}, M_{min} = 14 \text{ TeV}$ | 2.8×10^5 | 5.7×10^5 | 9.1×10^5 |
| $N_{Fe}/\text{Myr}, M_{min} = 14 \text{ TeV}$ | 35 | 80 | 135 |

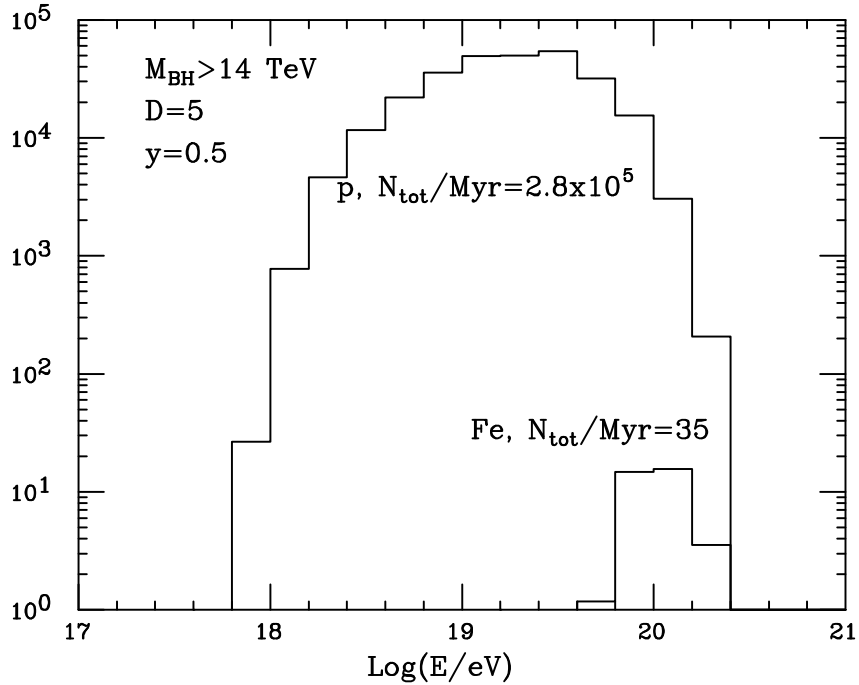


Figure 6: *Black hole production rates by cosmic rays impinging on a 5400 km radius white dwarf in the extreme case of $M > 14$ TeV and with the inelasticity parameter $y = 0.5$. The upper curve corresponds to a pure proton cosmic-ray composition, the lower one to pure Fe.*

number of produced black holes on our reference white dwarf is given in table 7, and the distribution as a function of the cosmic ray energy is shown in fig. 6.

For the discussion of slow-down and stopping of the black hole inside the white dwarf, we also present here some relevant kinematical distributions. Figure 7 shows the distributions of the Lorentz factor, $\gamma = E/M$, of the produced black hole, in the case of proton (left) and of Fe (right) primaries. We present in table 8 the rate-suppression factors due to requiring that the produced black hole has a Lorentz factor $\gamma < 3M_{min}/m_p$, and a mass $M < M_{min} + 1 \text{ TeV}$,

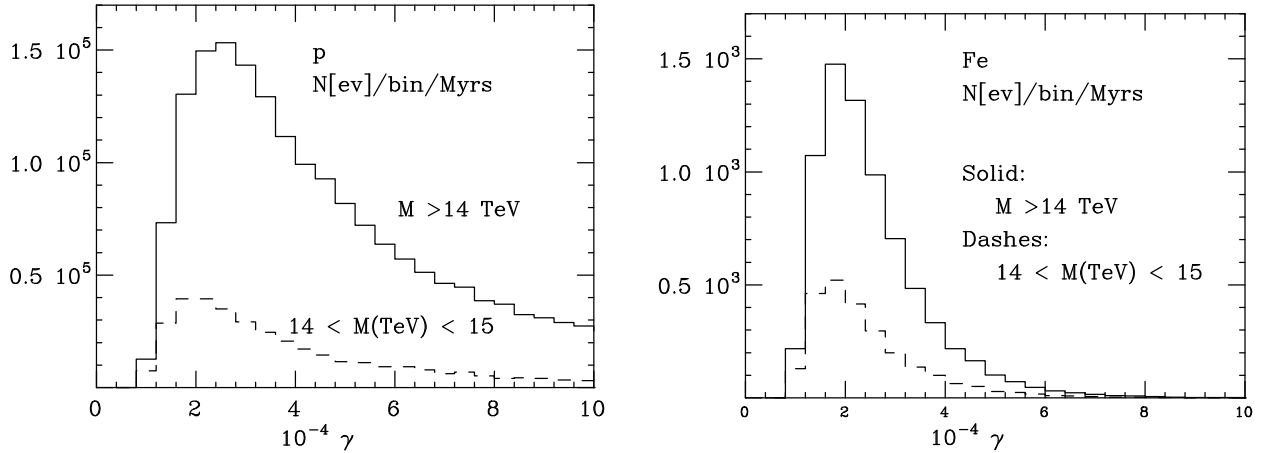


Figure 7: The Lorentz factors γ , in units of 10^4 , for black holes with $M > 14$ TeV produced by proton (left) and Fe (right) cosmic rays. The lower curves represent the distributions relative to the events with $14 < M(\text{TeV}) < 15$.

Table 8: Efficiency factors ϵ_p (100% proton flux) and ϵ_{Fe} (100% Fe flux) for the production of black holes with $M < M_{min} + 1$ TeV and $\gamma < 3M_{min}/m_p$. $M_D = M_{min}/3$, and inelasticity $y = M_{min}/14$ TeV for all columns except the last one, which has $y = 0.5$.

| $M(\text{TeV})$ | 7 | 8 | 10 | 12 | 14 | 14 ($y = 0.5$) |
|-----------------|----------------------|----------------------|----------------------|------|------|----------------------|
| ϵ_p | 6.9×10^{-2} | 8.3×10^{-2} | 9.8×10^{-2} | 0.10 | 0.10 | 4.4×10^{-2} |
| ϵ_{Fe} | 0.28 | 0.32 | 0.35 | 0.34 | 0.32 | 0.47 |

the criteria we used in section 5.3, to determine the stopping power of white dwarfs. Notice that in all cases these efficiencies are large enough to ensure abundant rates of produced black holes.

The production rates on a neutron star (neglecting the magnetic screening) can be obtained from the white dwarf's ones by rescaling by the surface area. Assuming a 10 km radius, the proton rates in Table 4 are reduced by a factor of 3.4×10^{-6} , leading to the numbers in Table 9. The distributions as a function of the cosmic ray energy have the same shape as those in the white dwarf cases, fig. 5. The results for $D = 5, 8$ are summarized in fig. 8, where the corresponding rates for Fe cosmic rays are also shown.

We conclude our discussion of production properties by showing in fig. 9 the x spectrum of the partons engaged in the production of black holes with $M > 14$ TeV, for various cosmic ray components and different inelasticity assumptions. Notice that the bulk of the production is always obtained for $x \lesssim 0.6$, namely the region where the knowledge of the PDFs is accurate to better than 10% [54].

Table 9: *Black hole production rates, per million years, induced by proton cosmic rays impinging on a $R = 10$ km neutron star. $M_D = M_{\min}/3$ and $y = \max(0.5, M_{\min}/14 \text{ TeV})$.*

| M_{\min} | $D = 5$ | $D = 6$ | $D = 7$ | $D = 8$ | $D = 9$ | $D = 10$ | $D = 11$ |
|------------|-------------------|-------------------|-------------------|-------------------|-------------------|-------------------|-------------------|
| 3 TeV | 1.3×10^4 | 2.5×10^4 | 4.0×10^4 | 5.6×10^4 | 7.4×10^4 | 9.2×10^4 | 1.1×10^5 |
| 4 TeV | 2.2×10^3 | 4.5×10^3 | 7.0×10^3 | 9.9×10^3 | 1.3×10^4 | 1.6×10^4 | 1.9×10^4 |
| 5 TeV | 570 | 1100 | 1800 | 2500 | 3300 | 4100 | 5000 |
| 6 TeV | 190 | 380 | 590 | 830 | 1100 | 140 | 1600 |
| 7 TeV | 72 | 146 | 231 | 323 | 422 | 526 | 633 |
| 8 TeV | 47 | 99 | 161 | 229 | 301 | 378 | 457 |
| 10 TeV | 23 | 52 | 88 | 129 | 172 | 218 | 265 |
| 12 TeV | 13 | 31 | 54 | 80 | 109 | 139 | 171 |
| 14 TeV | 8 | 20 | 36 | 54 | 74 | 95 | 118 |

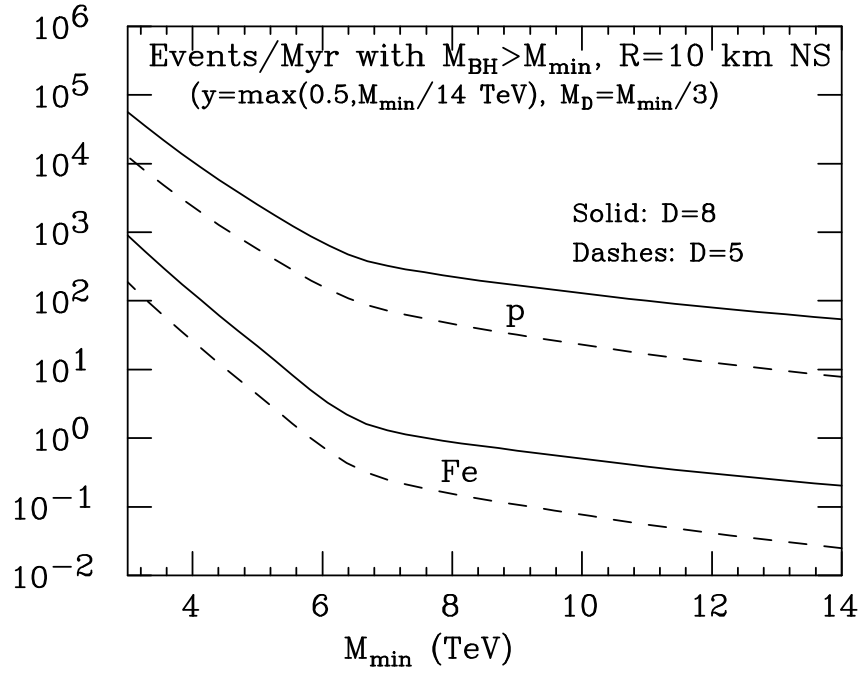


Figure 8: *Black hole production rates by cosmic rays impinging on a 10 km radius neutron star, for the inelasticity parameter $y = \max(0.5, M_{\min}/14 \text{ TeV})$ and with $M_D = M_{\min}/3$. The upper curves correspond to a pure proton cosmic-ray composition, the lower ones to pure Fe.*

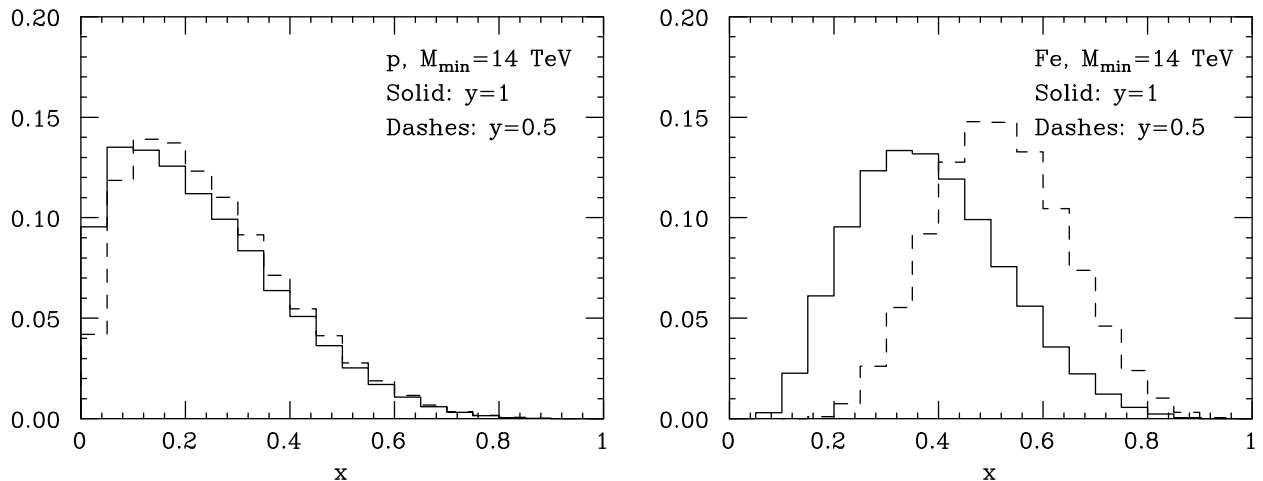


Figure 9: *The normalized spectra of the partonic momentum fraction x , for proton (left) and Fe (right) cosmic rays, and for $y = 1$ and $y = 0.5$. $M_{min} = 14$ TeV.*

E.3 Black hole production by cosmic neutrinos

High-energy neutrinos have a black hole production rate much bigger than nuclear cosmic rays of the same energy (see e.g. [7, 93–98]). Two reasons justify this statement. The first one is that all the energy carried by the neutrino can be used for the production of the black hole (contrary to protons or nuclei, where the partons carry a small fraction of the primary energy). The second reason is that the fraction of neutrino interactions that lead to black hole production is much bigger than the similar fraction of nuclear interactions: most collisions with a star atmosphere result in generic strong-interaction processes, and the rate of black hole production is proportional to the ratio of the black hole cross section to the total inelastic cross section. In the case of neutrinos, black hole production only competes against the total electroweak cross section [99], which turns out to be of the same size as the black hole cross section, when neutrino energies exceed 10^{17} eV.

While no experimental evidence is as yet available for the existence of such high-energy neutrinos, any modeling of cosmic ray production and evolution predicts their presence, with rates that are consistent with the current non-observation. Neutrinos can be produced directly at the source of the highest energy cosmic rays, where they emerge as decay products of the charged pions produced during the acceleration of the primary charged cosmic rays [100, 101]. And they also would appear in the decay of pions produced by the collision of protons with energy above the GZK cutoff with the cosmic microwave background: $\gamma p \rightarrow \Delta^+ \rightarrow n\pi^+$ (the so-called *cosmogenic neutrino flux* [102–104]). The observation of cosmic rays above the GZK cutoff, and the assumption that even only a tiny fraction of these are protons, automatically leads to the presence of neutrinos in the region above 10^{14} eV. Several groups have extracted predictions for the cosmogenic neutrino flux, most recently [75, 76] and [68]. The latter based their analysis on the Auger study of the highest-energy cosmic ray

Table 10: *Black hole production rates, per million years, induced by neutrino cosmic rays impinging on a $R = 10$ km neutron star. $M_{min} = 14$ TeV, $M_D = M_{min}/3$ and $y = 0.5$.*

| $D =$ | 5 | 6 | 7 | 8 | 9 | 10 | 11 |
|-------|-------------------|-------------------|-------------------|-------------------|-------------------|-------------------|-------------------|
| $N =$ | 4.5×10^3 | 1.1×10^4 | 2.0×10^4 | 3.0×10^4 | 4.0×10^4 | 5.1×10^4 | 6.2×10^4 |

composition [70], and considered a broad range of single and mixed compositions, including the extreme case of a Fe-only spectrum at injection, in which case the spectrum of protons dissociated from the Fe nuclei would be soft enough to strongly suppress pion photoproduction, and thus the neutrino flux. For our calculations we use the following parameterization of the neutrino flux:

$$\frac{d\Phi_\nu(E_\nu)}{dE_\nu} = 10^{-7} \left(\frac{\text{GeV}}{E_\nu} \right)^2 \text{ m}^{-2}\text{s}^{-1}\text{sr}^{-1}\text{GeV}^{-1}. \quad (\text{E.7})$$

This provides a lower limit to the acceptable fits of the worse-case, Fe-only, scenarios considered in [68], in the region $10^{17} \lesssim E_\nu(\text{eV}) \lesssim 10^{19}$. We stress that this is a very conservative assumption, and does not include the contribution from neutrinos originating directly at the cosmic ray sources. A recent evaluation of this contribution from AGN and GRBs [105], for example, leads to a flux between 10 and 100 times larger than (E.7), over and beyond the range $10^{17} \lesssim E_\nu(\text{eV}) \lesssim 10^{20}$.²³ We also notice that the flux in (E.7) is over three orders of magnitude below the Waxman-Bahcall upper bound [100, 101].

The corresponding black hole production rate for a 10 km-radius neutron star is shown in fig. 10, for $D = 5$, $M_{min} = 14$ TeV and $y = 0.5$, as a function of the neutrino energy. The rates as a function of D are given in table 10. Accumulation over more than several hundred million years of the life of a neutron star would lead to immense rates, even if the cosmic neutrino flux turned out to be suppressed by several orders of magnitude relative to our most conservative assumption. The direct detection of high-energy neutrinos in the next generation of neutrino telescopes [107] will make it possible to strengthen these estimates.

F LHC production of gravitationally bound black holes

In this Appendix we estimate the number of LHC-produced black holes that could in these hypothetical scenarios become gravitationally trapped by the Earth. This in particular addresses questions about whether there could be multi-black hole effects. For a black hole to get trapped, and start its accretion, its speed should not exceed the escape velocity from Earth, namely $v_E \sim 11 \text{ km s}^{-1} \sim 3.7 \times 10^{-5}c$. In the central LHC collisions, the black hole acquires a speed along the beam axis because of an imbalance in the longitudinal momenta

²³See also [106], where the decay of muons produced in the interactions of π^0 photons with the CMB photons leads to a flux of comparable size.

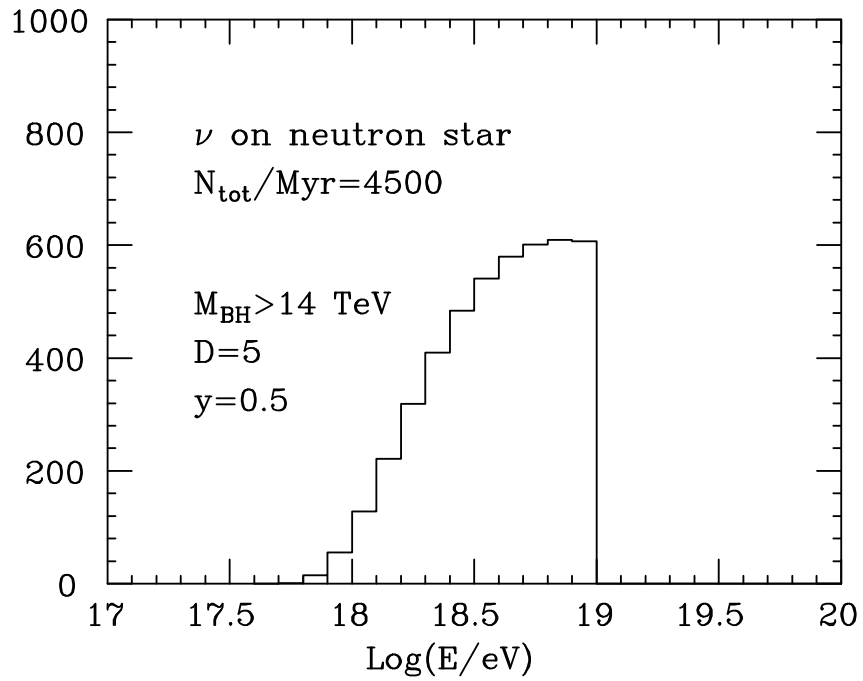


Figure 10: *Production rates for black holes of mass $M > 14 \text{ TeV}$, created by cosmic neutrinos impinging on a 10 km radius neutron star. The rates correspond to number of events, in one million years, in each energy bin. $D = 5$ and $y = 0.5$.*

Table 11: *Maximum velocities at production for gravitational trapping.*

| $M(\text{TeV})$ | 4 | 6 | 8 | 10 | 12 |
|-------------------------------|-----|-----|-----|------|------|
| $v_{max} \times 10^3, D = 8$ | 9.1 | 2.7 | 1.1 | 0.58 | 0.34 |
| $v_{max} \times 10^3, D = 11$ | 15 | 4.5 | 1.9 | 0.96 | 0.56 |

of the colliding partons, and a transverse speed because of the bremsstrahlung emitted from the initial state. These velocities are typically much larger than v_E . One should however also account for the slow-down caused by the interactions with matter as the black hole crosses the Earth. Such a slow-down will increase the chances that a black hole will be captured in the Earth's gravitational field. In this Appendix we study in detail the velocity spectrum resulting at production, and convolute it with the stopping power of the Earth, to obtain an estimate of the trapping probability, as a function of the black hole mass.

We start by analyzing the slow-down due to accretion. As pointed out in the main text, the Earth's density does not provide enough material to stop a highly relativistic black hole, such as those produced by cosmic rays. Indeed, the Earth's column density $\delta_E = 1.1 \cdot 10^{10} \text{gr/cm}^2 \sim 2 \text{GeV/TeV}^{-2}$ leads, for $v \sim 1$, to the accretion of at most a few GeV. This number will however increase significantly at low velocity, where the accretion per unit length traveled goes like $1/v$, as shown in eq. (5.28). Therefore some slow-down will typically arise for non-relativistic black holes produced at the LHC. Repeating the analysis of the slow-down in the non-relativistic regime given in section 5.3, we derive the following relation for the maximum velocity at production, v_{max} , that can be stopped before the black hole exits the Earth:

$$v_{max} = \frac{2\pi k_D \hat{b}_{min}^2}{(D-3)M_D^3} \left(\frac{M_D}{k_D M} \right)^{(D-5)/(D-3)} \delta_E. \quad (\text{F.1})$$

For a given mass, v_{max} is the largest in $D = 11$. We give some reference values for v_{max} in table 11, using the largest allowed value for M_D corresponding to a given mass, $M_D = M/3$. Notice that these velocities can be significantly larger than the escape velocity. Black holes pointing away from the center of the Earth will travel across a smaller column density, and their velocity should therefore be smaller than $v_{max} \ell/D$, where ℓ is the length of the path inside the Earth, and D is the Earth's diameter. This condition can be written as

$$v < v_{max} \cos \theta = v_{max} \frac{v_z}{v}, \quad (\text{F.2})$$

where θ is the angle with respect to the vertical axis \hat{z} . The stopping condition becomes:

$$v^2 = y^2 + v_{\perp}^2 < v_{max} v_{\perp} \cos \phi, \quad (\text{F.3})$$

where y is the black hole rapidity (equal to its longitudinal velocity in the non-relativistic limit), v_{\perp} its velocity in the plane transverse to the beam direction, and ϕ is the angle between the velocity direction in the transverse plane and \hat{z} .

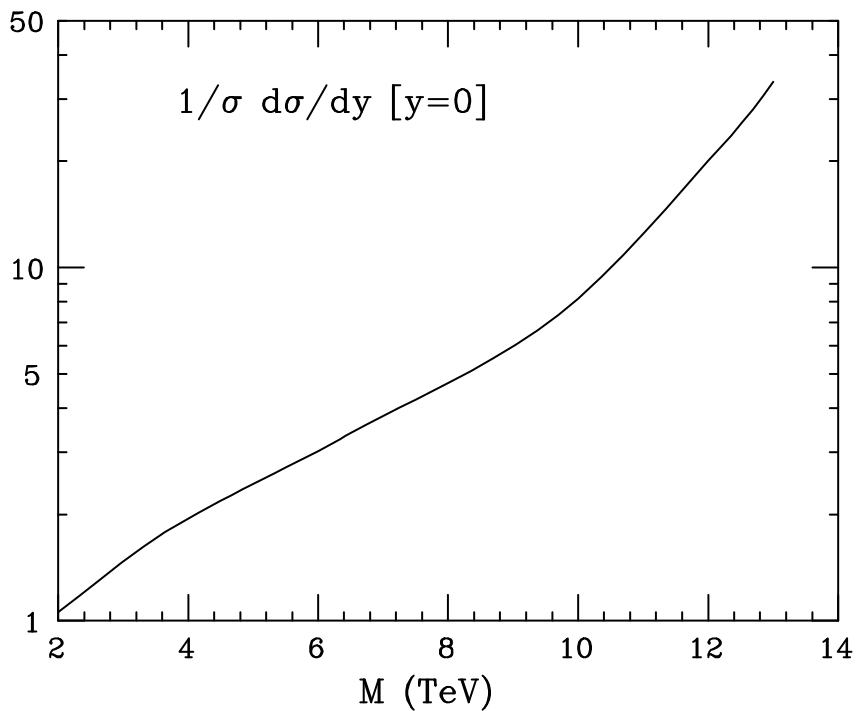


Figure 11: *Rapidity spectrum at $y = 0$ for production at the LHC.*

For $y \ll 1$, $d\sigma/dy$ is approximately flat, and independent of the black hole transverse momentum, since at small velocity that longitudinal and transverse dynamics decouple. For a given value of $v_{\perp} < v_{max}$,

$$y < y_0 = \sqrt{v_{max} v_{\perp} \cos \phi - v_{\perp}^2}, \quad (\text{F.4})$$

and the fraction of events that satisfy the stopping condition is therefore given by:

$$\frac{1}{2\pi} \int_{-\phi_v}^{\phi_v} d\phi \int_{-y_0}^{y_0} \frac{1}{\sigma} \frac{d\sigma}{dy} \Big|_{y=0} dy = \frac{2}{\pi} \frac{d\sigma}{dy} \Big|_{y=0} v_{max} \sqrt{\frac{v_{\perp}}{v_{max}}} \int_0^{\phi_v} d\phi \left(\cos \phi - \frac{v_{\perp}}{v_{max}} \right)^{1/2}, \quad (\text{F.5})$$

where $\phi_v = \arccos(v_{\perp}/v_{max})$. To excellent approximation, this can be written as:

$$\frac{2}{\pi} \frac{d\sigma}{dy} \Big|_{y=0} v_{max} \sqrt{\frac{v_{\perp}}{v_{max}}} 1.2 \times \left(1 - \frac{v_{\perp}}{v_{max}} \right) \quad (\text{F.6})$$

The normalized rapidity spectra of black holes at $y = 0$, as a function of M , is shown in fig. 11.

Convolution of this probability with the v_{\perp} spectrum obtained, as a function of the black hole mass, from the Herwig Monte Carlo [108], leads to the stopping probabilities shown in table 12. We then convolute these trapping probabilities with the black hole production

Table 12: *Stopping probabilities for typical M values.*

| $M(\text{TeV})$ | 4 | 6 | 8 | 10 | 12 |
|-------------------------|-----|-----|------|------|------|
| $P \times 10^4, D = 8$ | 5.7 | 1.2 | 0.37 | 0.20 | 0.24 |
| $P \times 10^4, D = 11$ | 14 | 3.4 | 1.2 | 0.71 | 0.92 |

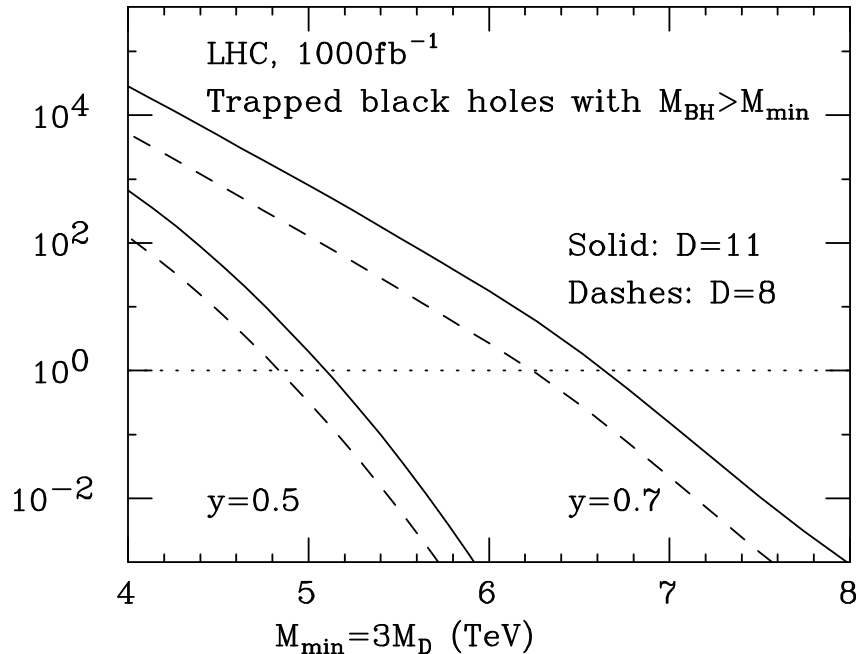


Figure 12: *Number of trapped black holes, for inelasticity $y = 0.5$ and $y = 0.7$, as a function of the black hole mass M , and for an integrated luminosity of 1000 fb^{-1} .*

rates derived assuming inelasticity in the realistic range from $y = 0.5$ to $y = 0.7$ (we trust that the coincidence of notation here of y for the rapidity and for the inelasticity will not be a source of confusion!). The results are shown in fig. 12, for the standard integrated luminosity of 1000 fb^{-1} . As soon as $M \gtrsim 7 \text{ TeV}$ the expected number of trapped black holes falls below 1 even with the looser inelasticity value of $y = 0.7$. We notice that mass values where the build up of multiple black holes could significantly exceed the value one are firmly excluded for $8 \leq D \leq 11$ by the neutron stars, and for $D \leq 7$ by the white dwarfs.

Some of the hypothesized black holes from LHC could reach the Sun or the Moon. In the case of the Sun, its core is the only part that has a significant stopping power. The density in the core, whose radius is about $R_{core} \sim 0.2R_{\odot} \sim 1.4 \times 10^5 \text{ km}$, reaches 150 gr/cm^3 , giving a column density hundreds of times greater than the Earth, allowing to stop black holes proportionally faster. On the other hand, the geometric probability that an LHC-produced black hole reaches the Sun's core is only about 2.2×10^{-7} , a number that by itself is much smaller than the probability of trapping inside the Earth. The Moon has

the same geometrical suppression than the Sun, but a much higher suppression due to the limited stopping power, and the smaller escape velocity. We also note that the parameter controlling macroscopic accretion, $d_0 c_s$, is for the Sun approximately four times its value on Earth (with $\rho = 150 \text{ gr/cm}^3$ and $c_s = 500 \text{ km/s}$), implying accretion time scales that are four times longer.

G Synchrotron losses in magnetic fields

In this Appendix we briefly summarize the limitations on cosmic ray penetration to stellar surfaces resulting from synchrotron radiation losses.

We assume a dipole magnetic field, with polar intensity B_p defined by:

$$\vec{B}(\theta, r) = B_p \left(\frac{R_0}{r} \right)^3 \frac{3 \cos \theta \hat{r} - \hat{z}}{2} \quad (\text{G.1})$$

where R_0 is the star radius, \hat{z} points along the field axis, and θ is the angle with respect to \hat{z} . We consider an incident nucleus with charge Z and mass A , with radial momentum p at an angle θ from the direction of the magnetic axis. One easily finds the Larmor radius as a function of r ,

$$r_L(r, \theta) = \frac{2p}{ZeB_p \sin \theta} \left(\frac{r}{R_0} \right)^3. \quad (\text{G.2})$$

To ensure that the cosmic ray reaches the star's surface, we require that $r_L(r, \theta) > r$ for all values of the distance r . If we consider the trajectories subject to the largest field ($\sin \theta = 1$), this corresponds to requiring: $p > ZeB_p R_0/2$, or:

$$p \gtrsim 0.75 \times 10^{17} \text{ eV} \frac{R_0}{5000 \text{ km}} \frac{ZB_p}{10^6 \text{ G}} = 1.5 \times 10^{17} \text{ eV} \frac{R_0}{10 \text{ km}} \frac{ZB_p}{10^9 \text{ G}}. \quad (\text{G.3})$$

The two expressions correspond to typical radii of white dwarfs and neutrons stars, and to reference magnetic fields chosen to be in the range of actual measured values [64, 109]. For the energies we are dealing with, in the range of 10^{18} eV or more, we see therefore that magnetic fields of 1MG (WD) or 1000MG (NS) correspond to relatively small deflections (and even smaller at lower fields), which are compatible with our criterion.

While typical magnetic fields do not seem to induce sufficient deflection in the trajectory, they may nevertheless lead to great energy losses due to synchrotron radiation emission. The synchrotron power loss for relativistic cosmic rays corresponding to the above Larmor radius is given by:

$$\frac{dE}{dt} = -\frac{1}{6} \frac{(Ze)^4 B_p^2 \sin^2 \theta R_0^6}{A^4 m_p^4 r^6} E^2. \quad (\text{G.4})$$

Integrating along a cosmic ray trajectory from $r = \infty$, where $E = E_\infty$, to $r = R_0$, where $E = E_{R_0}$, gives:

$$E_{R_0} = E_{max} \frac{E_\infty}{E_\infty + E_{max}}, \quad (\text{G.5})$$

where

$$E_{max} = \frac{30A^4m_p^4}{(Ze)^4(\sin\theta B_p)^2R_0} . \quad (\text{G.6})$$

Notice that E_{R_0} is always smaller than E_{max} , regardless of the initial cosmic ray energy. This is therefore a maximum energy that can be retained by a cosmic ray impinging on the star. For initial energies above E_{max} , the higher the energy, the more is radiated off, ending up always with the same limiting energy. Introducing numbers appropriate for a neutron star, we get:

$$E_{max} \approx 1.8 \times 10^{17} \text{eV} \frac{A^4}{Z^4} \frac{10\text{km}}{R_0} \left(\frac{10^8 G}{B_p \sin\theta} \right)^2 . \quad (\text{G.7})$$

In a strong field, cosmic rays of the highest energies are therefore allowed to penetrate only within an angle $\theta(E)$ from the northern/southern hemispheres of the star, with:

$$\sin\theta(E) < \sin\theta_{max} = \sqrt{\left(\frac{1.8 \times 10^{17} \text{eV}}{E} \right) \left(\frac{10\text{km}}{R_0} \right) \frac{A^2}{Z^2} \left(\frac{10^8 G}{B_p} \right)} . \quad (\text{G.8})$$

Notice that the reduction factor is less harmful for nuclei, since $A/Z \sim 2$. The lowest magnetic fields that have been measured for neutron stars are of the order of 100 MG [109], and this is therefore the lowest field that we can assume for our study. In the case of proton cosmic rays, penetration to the star's surface with energies in the range of $5 \times 10^{18} \text{eV}$, as required for efficient production of $M > 14 \text{TeV}$ black holes (see fig. 5), would require $\theta \lesssim 0.2$. Combining the reduction in the star surface area that can be reached (just the polar caps, of area $\sim \pi(\theta_{max}R_0)^2$) with the limited angular acceptance (cosmics with $\theta < \theta_{max}$ from the polar zenith), we obtain an approximate rate suppression of order θ_{max}^4 , and thus of order 10^{-3} for the case considered. These numbers are too small to allow sufficient rate for all cases, and specifically those at the highest black hole masses.

H Production on background objects

Given the self-screening behavior resulting from neutron-star magnetic fields, one is naturally led to consider production of neutral black holes on background objects, such as on a binary companion of the star, or on the interstellar medium. We here outline some such considerations.

H.1 On lifetimes and solid angles in X-ray binaries

We would like to understand the range of possible values for the full coverage equivalent (FCE), defined in (8.1), for neutron star binary systems. A number of such systems have been well-studied and modeled. Thus, deviations from the FCEs given below would require substantial revision of our theoretical description of the formation and evolution of these systems.

Specifically, neutron stars are often found in binaries tight enough for mass transfer to occur from the donor to the NS. These X-ray binaries (see [110] for an overview) are well studied systems, and are also known to exist in other galaxies. The range of possible donor masses, M_d , is large [110], from $M_d = 0.01M_\odot$ Helium white dwarfs in ultracompact binaries to $30M_\odot$ stars around accreting X-ray pulsars. The closest possible distance is when the donor star fills its Roche lobe (e.g. the tidal radius), yielding the largest value for $f = \Delta\Omega/4\pi = (1 - \cos\theta)/2$, where [111] $\tan\theta = R_{RL}/a = 0.49[0.6 + q^{-2/3} \ln(1 + q^{1/3})]^{-1}$ is only a function of the mass ratio $q = M_d/M_{NS}$. For $M_d = 0.01 - 10M_\odot$ (and a fixed NS mass of $M_{NS} = 1.4M_\odot$), we find $f = 0.002 - 0.06$.

Massive X-ray binaries (see [112] for an overview) have donor masses $M_d > 5M_\odot$ and range up to $50M_\odot$. The longest time that such a system can live as a mass transferring system (and thereby visible in X-rays) is when the donor always underfills the Roche Lobe, and the NS accretes some of the stellar wind leaving the companion. Such a system lives for at most the hydrogen burning main sequence lifetime [113], $T_{MS} \approx 10\text{Gyr}(M_\odot/M)^{2.5}$ of the massive star, which is $< 10^8$ years for $M_d > 5M_\odot$. Such a star has $f = 0.05$, yielding ≈ 5 Myr of FCE. More massive main sequence companions would have slightly larger values of f , but their much shorter main sequence lifetimes make them less constraining.

A well-known class is that of NSs accreting from a $M \approx M_\odot$ red giant that result in millisecond radio pulsars orbiting the remaining He WD core. While the Roche-lobe filling mass transfer is occurring, $f \approx 0.03$, and the lifetime in this phase is set by the nuclear evolution rate of the red giant. Those that start Roche-lobe filling at orbital periods less than 10 days can have a mass transfer lifetime of 10^9 years [110], giving ≈ 30 Myr of FCE.

The best examples are traditional low-mass X-ray binaries (those with $M_d < M_\odot$) that have shorter $10^8 - 10^9$ year lifetimes set by the mass transfer rates of $\dot{M} \approx 10^{-8} - 10^{-9}M_\odot \text{ yr}^{-1}$. However, at very short orbital periods, the donors become so low in mass, $M_d \approx 0.05M_\odot$ ($f = 0.006$), as to be brown dwarfs (e.g. SAX J1808.4-3658 [114]) with mass transfer rates of $10^{-11}M_\odot \text{ yr}^{-1}$, consistent with that expected from gravitational wave losses. These are certainly mass-transferring for over a Gyr, giving 6 Myr of FCE

The lowest mass companions are in ultracompact binaries where a He white dwarf donates material to a NS at a rate set by gravitational wave losses (see [115] for an overview). The most constraining of these systems are those at the longest orbital period of 40 minutes, where $T = 10^9\text{yr}$ and $M_d \approx 0.01M_\odot$ ($f = 0.002$) and ≈ 2 Myr of FCE.

In closing, the exposures of known systems are in the range of 2 – 30 Myr of FCE, and one can be very confident in those scenarios in the 2-6 Myr range [116]. Even the NSs accreting from red giants that give 30 Myr are relatively robust, and plausibly could be used in improving bounds.

H.2 Production on the interstellar medium

We study here the possibility that black holes are produced by the collision of cosmic rays with the interstellar medium (ISM). This is not meant to be a fully robust study, but to

provide an indication of further directions that could be undertaken to produce additional constraints, largely complementary to ours. We first estimate the column density that cosmic rays travel through as they reach a star. We consider stars in the disk as embedded in a disk of ISM of height h and radius L , where reasonable values are given by $h \sim 6 \times 10^2$ light years, the disk width, and $L \sim 60h$. The average ISM density n_{ISM} is about 1 proton/cm³. The average column density for cosmic rays pointing toward the star is given by $n_{ISM} (h/2) \log(2L/h) \sim 1.4 \times 10^{-4}$ protons/(100 mb). This means an interaction probability of about 1.4×10^{-4} for each nucleon in the cosmic rays. When the cosmic ray is pointing directly toward the star, and when it produces a black hole, this will end up hitting the star. The star's magnetic field has no influence, and therefore both neutron stars and white dwarfs of arbitrary magnetic field can be considered as targets. The number of black holes is obtained by applying this reduction factor to the rates calculated for the production of black holes via cosmic rays directly hitting a star. This suppression is too large to give acceptable rates on neutron stars. In the case of white dwarfs, and for $D = 5$, $M_{min} = 14$ TeV and $y = 1$, this means a rate of over 30/Myrs for a 10% proton composition (see table 4), and of about 1/Myrs for 100% Fe (see table 5). Even in the latter, most conservative, case, this means 100 black holes produced over 100Myrs. Any white dwarf with mass in the range 1–1.2 solar masses, independently of the magnetic field, will absorb and stop such black holes, which will then catalyze its decay on time scales short as compared to observed (\gtrsim Gyr) lifetimes. A white dwarf like Sirius-B, for example, with a mass of exactly one solar mass and an age of about 120 Myrs [117], would not have escaped destruction by $D = 5, 6$ black holes up to minimum mass 14 TeV, or by $D = 7$ black holes up to around 10 TeV (see fig. 2).

Finally, we point out the possible use of massive weakly-interacting dark matter as a target for black hole production by cosmic rays [118]. While lack of direct experimental evidence for it makes it insufficient today for our purposes, the expected densities [119] of about 0.3 GeV/cm³ could provide sufficient to generate large numbers of black holes to be absorbed by white dwarfs. The much lower γ factor due to production on such a heavy target would extend the range of capture of even the highest black holes to lighter white dwarfs, and extend the stopping potential to black holes significantly heavier than those accessible at the LHC.

I Useful conventions, conversion factors, and reference quantities

Conversion factors:

$$1 \text{ yr} = 3.2 \times 10^7 \text{ s} \quad (\text{I.1})$$

$$1 \text{ gr} = 0.56 \times 10^{24} \text{ GeV} \rightarrow 1 \text{ GeV} = 1.78 \times 10^{-24} \text{ gr} \quad (\text{I.2})$$

$$\rightarrow 1 \text{ TeV} = 1.78 \times 10^{-21} \text{ gr} \quad (\text{I.3})$$

$$1 \text{ fm}^{-1} = 197 \text{ MeV} \rightarrow 1 \text{ GeV} = 5.1 \times 10^{13} \text{ cm}^{-1} \quad (\text{I.4})$$

$$\rightarrow 1 \text{ TeV}^{-1} = 1.97 \times 10^{-17} \text{ cm} \quad (\text{I.5})$$

$$1 \text{ K} = 8.6 \times 10^{-5} \text{ eV} = 4.5 \times 10^{-8} \text{ \AA} \quad (\text{I.6})$$

Fundamental constants:

$$M_4 = 1/\sqrt{8\pi G_N} = 2.4 \times 10^{18} \text{ GeV} = 2.4 \times 10^{15} \text{ TeV} = 4.3 \times 10^{-6} \text{ gr} \quad (\text{I.7})$$

$$m_p = 1.84 \times 10^3 m_e = 9.4 \times 10^2 \text{ MeV} \quad (\text{I.8})$$

Astronomical quantities:

$$M_E = 6.0 \times 10^{27} \text{ gr} = 3.3 \times 10^{51} \text{ GeV} \quad (\text{I.9})$$

$$R_E = 6.4 \times 10^8 \text{ cm} \quad (\text{I.10})$$

$$\rho_E = 5.5 \text{ gr/cm}^3 \quad (\text{I.11})$$

$$\langle A_E \rangle = 4 \times 10^1 \quad (\text{I.12})$$

$$v_E = 1.12 \times 10^6 \text{ cm/s} = 3.7 \times 10^{-5} \quad (\text{I.13})$$

$$M_{NS} \approx 1.5 M_\odot = 3 \times 10^{33} \text{ gr} = 2 \times 10^{57} \text{ GeV} \quad (\text{I.14})$$

$$R_{NS} \approx 10 \text{ km} \quad (\text{I.15})$$

$$\rho_{NS} \gtrsim 2 \times 10^{14} \text{ gr/cm}^3 \approx \frac{0.1 m_p}{\text{fm}^3} \sim 10^{-3} \text{ GeV}^4 \quad (\text{I.16})$$

References

- [1] N. Arkani-Hamed, S. Dimopoulos and G. R. Dvali, “The hierarchy problem and new dimensions at a millimeter,” *Phys. Lett. B* **429**, 263 (1998) [arXiv:hep-ph/9803315].
- [2] I. Antoniadis, N. Arkani-Hamed, S. Dimopoulos and G. R. Dvali, “New dimensions at a millimeter to a Fermi and superstrings at a TeV,” *Phys. Lett. B* **436**, 257 (1998) [arXiv:hep-ph/9804398].
- [3] L. Randall and R. Sundrum, “A large mass hierarchy from a small extra dimension,” *Phys. Rev. Lett.* **83**, 3370 (1999) [arXiv:hep-ph/9905221].

- [4] S. B. Giddings, S. Kachru and J. Polchinski, “Hierarchies from fluxes in string compactifications,” *Phys. Rev. D* **66**, 106006 (2002) [arXiv:hep-th/0105097].
- [5] S. B. Giddings and S. D. Thomas, “High energy colliders as black hole factories: The end of short distance physics,” *Phys. Rev. D* **65**, 056010 (2002) [arXiv:hep-ph/0106219].
- [6] S. Dimopoulos and G. L. Landsberg, “Black holes at the LHC,” *Phys. Rev. Lett.* **87**, 161602 (2001) [arXiv:hep-ph/0106295].
- [7] S. B. Giddings, “Black hole production in TeV-scale gravity, and the future of high energy physics,” in *Proc. of the APS/DPF/DPB Summer Study on the Future of Particle Physics (Snowmass 2001)* ed. N. Graf, *In the Proceedings of APS / DPF / DPB Summer Study on the Future of Particle Physics (Snowmass 2001), Snowmass, Colorado, 30 Jun - 21 Jul 2001, pp P328* [arXiv:hep-ph/0110127].
- [8] S. B. Giddings, “High-energy black hole production,” *AIP Conf. Proc.* **957**, 69 (2007) [arXiv:0709.1107 [hep-ph]].
- [9] S. W. Hawking, “Particle Creation By Black Holes,” *Commun. Math. Phys.* **43**, 199 (1975) [Erratum-ibid. **46**, 206 (1976)].
- [10] W. G. Unruh and R. Schutzhold, “On the universality of the Hawking effect,” *Phys. Rev. D* **71** (2005) 024028 [arXiv:gr-qc/0408009].
- [11] G. A. Vilkovisky, “Backreaction of the Hawking radiation,” *Phys. Lett. B* **638**, 523 (2006) [arXiv:hep-th/0511184].
- [12] G. ’t Hooft, “The scattering matrix approach for the quantum black hole: An overview,” *Int. J. Mod. Phys. A* **11**, 4623 (1996) [arXiv:gr-qc/9607022].
- [13] S. M. Christensen and S. A. Fulling, “Trace Anomalies And The Hawking Effect,” *Phys. Rev. D* **15**, 2088 (1977).
- [14] C. G. Callan, S. B. Giddings, J. A. Harvey and A. Strominger, “Evanescent black holes,” *Phys. Rev. D* **45**, 1005 (1992) [arXiv:hep-th/9111056].
- [15] S. P. Robinson and F. Wilczek, “A relationship between Hawking radiation and gravitational anomalies,” *Phys. Rev. Lett.* **95**, 011303 (2005) [arXiv:gr-qc/0502074].
- [16] T. Jacobson, “Introduction to quantum fields in curved spacetime and the Hawking effect,” arXiv:gr-qc/0308048.
- [17] C. Barcelo, S. Liberati and M. Visser, “Analogue gravity,” *Living Rev. Rel.* **8**, 12 (2005) [arXiv:gr-qc/0505065].
- [18] W. Unruh, “Where do the particles come from?” talk at the workshop *Effective models of quantum gravity*, Perimeter Institute, November 2007.

- [19] S. W. Hawking, “Breakdown Of Predictability In Gravitational Collapse,” *Phys. Rev. D* **14**, 2460 (1976).
- [20] S. B. Giddings, “Quantum mechanics of black holes,” arXiv:hep-th/9412138.
- [21] A. Strominger, “Les Houches lectures on black holes,” arXiv:hep-th/9501071.
- [22] S. B. Giddings, “The Black hole information paradox,” arXiv:hep-th/9508151.
- [23] W. Busza, R. L. Jaffe, J. Sandweiss and F. Wilczek, “Review of speculative ‘disaster scenarios’ at RHIC,” *Rev. Mod. Phys.* **72**, 1125 (2000) [arXiv:hep-ph/9910333].
- [24] J.P. Blaizot et al, “Study of potentially dangerous events during heavy-ion collisions at the LHC : report of the LHC safety study group”, CERN-2003-001 (2003).
- [25] J. S. Schwinger, *Phys. Rev.* **82**, 664 (1951).
- [26] W. M. Yao *et al.* [Particle Data Group], “Review of particle physics,” *J. Phys. G* **33**, 1 (2006).
- [27] D.E. Groom, N.V. Mokhov and S.I. Striganov, “Muon stopping power and range tables, 10 MeV – 100 TeV”, *Atomic data and Nuclear Data Tables*, Vol, 76, No. 2, July 2001.
- [28] G. Giacomelli and L. Patrizzii, “Magnetic monopole searches,” arXiv:hep-ex/0506014.
- [29] R. C. Myers and M. J. Perry, “Black Holes In Higher Dimensional Space-Times,” *Annals Phys.* **172**, 304 (1986).
- [30] R. Gregory and R. Laflamme, “Black strings and p-branes are unstable,” *Phys. Rev. Lett.* **70**, 2837 (1993) [arXiv:hep-th/9301052].
- [31] S. Kachru, R. Kallosh, A. Linde and S. P. Trivedi, “De Sitter vacua in string theory,” *Phys. Rev. D* **68**, 046005 (2003) [arXiv:hep-th/0301240].
- [32] S. B. Giddings, “High energy QCD scattering, the shape of gravity on an IR brane, and the Froissart bound,” *Phys. Rev. D* **67**, 126001 (2003) [arXiv:hep-th/0203004].
- [33] F. Hoyle and R.A. Lyttleton, *Proc. Camb. Phil. Soc.*, **35**, 405, 1939; *ibid.* **36**, 325, 1940; *ibid.* **36**, 424, 1940; H. Bondi and F. Hoyle, *Mon. Notic. Roy. Astron. Soc.*, **104**, 273, 1944; H. Bondi, *Mon. Notic. Roy. Astron. Soc.*, **112**, 195, 1952.
- [34] F. Birch, in “Solids under pressure”, W. Paul, D.M. Warschauer, Eds. (McGraw-Hill, New York, 1963), p. 137; *Geophys. J. R. Astron. Soc.* **4**, 295 (1961).
- [35] J.M. Brown and R.G. McQueen, “Phase transitions, Grueneisen parameter, and elasticity for shocked iron between 77 GPa and 400 GPa”, *J. Geophys. Res.* **91**, 7485 (1986).
- [36] G. Fiquet et. al., “Sound velocities in iron to 110 GPa”, *Science* **291**, 468 (2001).

- [37] O. Aharony, S. Minwalla and T. Wiseman, “Plasma-balls in large N gauge theories and localized black holes,” *Class. Quant. Grav.* **23**, 2171 (2006) [arXiv:hep-th/0507219].
- [38] J. Frank, A. King, and D. Raine, “Accretion Power in Astrophysics”, 3rd edition, Cambridge University Press (2002).
- [39] P. Sharma, E. Quataert and J. M. Stone, “Spherical Accretion with Anisotropic Thermal Conduction,” arXiv:0804.1353 [astro-ph].
- [40] T. Yamamoto [Pierre Auger Collaboration], “The UHECR spectrum measured at the Pierre Auger Observatory and its astrophysical implications,” arXiv:0707.2638 [astro-ph].
- [41] G. Matthiae [Pierre Auger Collaboration], “High-energy cosmic rays,” *AIP Conf. Proc.* **957**, 107 (2007).
- [42] R. Abbasi *et al.* [HiRes Collaboration], “Observation of the GZK cutoff by the HiRes experiment,” *Phys. Rev. Lett.* **100**, 101101 (2008) [arXiv:astro-ph/0703099].
- [43] K. Greisen, “End To The Cosmic Ray Spectrum?,” *Phys. Rev. Lett.* **16**, 748 (1966).
- [44] G. T. Zatsepin and V. A. Kuzmin, “Upper limit of the spectrum of cosmic rays,” *JETP Lett.* **4**, 78 (1966) [*Pisma Zh. Eksp. Teor. Fiz.* **4**, 114 (1966)].
- [45] A. Dar, A. De Rujula and U. W. Heinz, “Will relativistic heavy ion colliders destroy our planet?,” *Phys. Lett. B* **470**, 142 (1999) [arXiv:hep-ph/9910471].
- [46] K. Shen, private communication; see http://mesa.sourceforge.net/micro_physics.html#eos for codes used.
- [47] L. Bildsten and K. Shen, private communication.
- [48] D. M. Eardley and S. B. Giddings, “Classical black hole production in high-energy collisions,” *Phys. Rev. D* **66**, 044011 (2002) [arXiv:gr-qc/0201034].
- [49] P. D. D’Eath and P. N. Payne, “Gravitational radiation in high speed black hole collisions. 3. Results and conclusions,” *Phys. Rev. D* **46**, 694 (1992).
- [50] H. Yoshino and Y. Nambu, “Black hole formation in the grazing collision of high-energy particles,” *Phys. Rev. D* **67**, 024009 (2003) [arXiv:gr-qc/0209003].
- [51] H. Yoshino and V. S. Rychkov, “Improved analysis of black hole formation in high-energy particle collisions,” *Phys. Rev. D* **71**, 104028 (2005) [arXiv:hep-th/0503171].
- [52] U. Sperhake, V. Cardoso, F. Pretorius, E. Berti and J. A. Gonzalez, “The high-energy collision of two black holes,” arXiv:0806.1738 [gr-qc].
- [53] P. Meade and L. Randall, “Black Holes and Quantum Gravity at the LHC,” *JHEP* **0805**, 003 (2008) [arXiv:0708.3017 [hep-ph]].

- [54] J. Pumplin, D. R. Stump, J. Huston, H. L. Lai, P. Nadolsky and W. K. Tung, “New generation of parton distributions with uncertainties from global QCD analysis,” *JHEP* **0207**, 012 (2002) [arXiv:hep-ph/0201195].
- [55] J. Ridky [Pierre Auger Collaboration], “Measurement of cosmic ray energy with the Pierre Auger Observatory,” *AIP Conf. Proc.* **928**, 39 (2007).
- [56] K. Shen, private communication.
- [57] S.O. Kepler and P.A. Bradley, “Structure and evolution of white dwarfs,” *Baltic Astro.* **4**, 166 (1995).
- [58] G. Fontaine, P. Brassard, and P. Bergeron, “The potential of white dwarf cosmochronology,” *Publications of the Astro. Soc. of the Pacific*, **113**, 409 (2001).
- [59] S.L. Shapiro and S.A. Teukolsky, *Black Holes, White Dwarfs, and Neutron Stars*, John Wiley and Sons, 1983.
- [60] J. Liebert, P. Bergeron and J. B. Holberg, “The Formation Rate, Mass and Luminosity Functions of DA White Dwarfs from the Palomar Green Survey,” *Astrophys. J. Suppl.* **156**, 47 (2005) [arXiv:astro-ph/0406657].
- [61] L. G. Althaus, E. Garcia-Berro, J. Isern, A. H. Corsico and R. D. Rohrmann, “The age and colors of massive white dwarf stars,” *Astron. Astrophys.* **465**, 249 (2007) [arXiv:astro-ph/0702024].
- [62] G. D. Schmidt and P. S. Smith, “A Search for magnetic fields among DA white dwarfs,” *Astrophys. J.* **448**, 305 (1995).
- [63] R.A. Cuadrado et. al, “Discovery of kilogauss magnetic fields in three DA white dwarfs,” *Astron. Astrophys.* **423**, 1081 (2004).
- [64] A. Kawka et. al, “Spectropolarimetric survey of hydrogen-rich white dwarf stars,” *Astrophys. J.* **654**, 499 (2007).
- [65] M. Nalezyty and J. Madej, “A catalogue of isolated massive white dwarfs”, *Astron. Astrophys.* **420**, 507 (2004).
- [66] J. P. Subasavage, T. J. Henry, P. Bergeron, P. Dufour and N. C. Hambly, “The Solar Neighborhood. XX. Discovery and Characterization of 21 New Nearby White Dwarf Systems,” arXiv:0805.2515 [astro-ph].
- [67] T. Kashti and E. Waxman, “Searching for a Correlation Between Cosmic-Ray Sources Above 10^{19} eV and Large-Scale Structure,” arXiv:0801.4516 [astro-ph].
- [68] L. A. Anchordoqui, H. Goldberg, D. Hooper, S. Sarkar and A. M. Taylor, “Predictions for the Cosmogenic Neutrino Flux in Light of New Data from the Pierre Auger Observatory,” *Phys. Rev. D* **76**, 123008 (2007) [arXiv:0709.0734 [astro-ph]].

- [69] D. Hooper, S. Sarkar and A. M. Taylor, “The Intergalactic Propagation of Ultra-High Energy Cosmic Ray Nuclei: An Analytic Approach,” arXiv:0802.1538 [astro-ph].
- [70] M. Unger [The Pierre Auger Collaboration], “Study of the Cosmic Ray Composition above 0.4 EeV using the Longitudinal Profiles of Showers observed at the Pierre Auger Observatory,” arXiv:0706.1495 [astro-ph].
- [71] G. Hughes et al. [HiRes Collaboration], “A Measurement of the Average Longitudinal Development Profile of Cosmic Ray Air Showers from 10^{17} eV to 10^{20} eV,” Proc. 30th ICRC, Merida (2007).
- [72] J. Abraham *et al.* [Pierre Auger Collaboration], “Correlation of the highest-energy cosmic rays with the positions of nearby active galactic nuclei,” *Astropart. Phys.* **29**, 188 (2008) [arXiv:0712.2843 [astro-ph]].
- [73] J. Abraham *et al.* [Pierre Auger Collaboration], “Correlation of the highest energy cosmic rays with nearby extragalactic objects,” *Science* **318**, 938 (2007) [arXiv:0711.2256 [astro-ph]].
- [74] D. S. Gorbunov, P. G. Tinyakov, I. I. Tkachev and S. V. Troitsky, “On the interpretation of the cosmic-ray anisotropy at ultra-high energies,” arXiv:0804.1088 [astro-ph].
- [75] R. Engel, D. Seckel and T. Stanev, “Neutrinos from propagation of ultra-high energy protons,” *Phys. Rev. D* **64**, 093010 (2001) [arXiv:astro-ph/0101216].
- [76] Z. Fodor, S. D. Katz, A. Ringwald and H. Tu, “Bounds on the cosmogenic neutrino flux,” *JCAP* **0311**, 015 (2003) [arXiv:hep-ph/0309171].
- [77] J. Lykken, O. Mena and S. Razzaque, “Ultrahigh-energy neutrino flux as a probe of large extra-dimensions,” *JCAP* **0712**, 015 (2007) [arXiv:0705.2029 [hep-ph]].
- [78] D. Stojkovic and G. D. Starkman, “Why black hole production in scattering of cosmic ray neutrinos is generically suppressed,” *Phys. Rev. Lett.* **96**, 041303 (2006) [arXiv:hep-ph/0505112].
- [79] E. V. Derishev, V. V. Kocharovskiy and V. V. Kocharovskiy, “Cosmological gamma-ray bursts from a neutron star collapse induced by a primordial black hole,” *JETP Lett.* **70**, 652 (1999) [*Pisma Zh. Eksp. Teor. Fiz.* **70**, 642 (1999)].
- [80] D.P. Kilcrease and N.H. Magee, “Plasma non-ideality effects on the photon-electron scattering contribution to radiative opacities,” *J. of Spectroscopy and Radiative Transfer*, **71**, 445 (2001).
- [81] M.C. Begelman, “Black holes in radiation-dominated gas- An analogue of the Bondi accretion problem,” *Mon. Not. Astr. Soc.*, **184**, 53 (1978).

- [82] P. Kanti and J. March-Russell, “Calculable corrections to brane black hole decay. II: Greybody factors for spin 1/2 and 1,” *Phys. Rev. D* **67**, 104019 (2003) [arXiv:hep-ph/0212199].
- [83] P. Kanti and J. March-Russell, “Calculable corrections to brane black hole decay. I: The scalar case,” *Phys. Rev. D* **66**, 024023 (2002) [arXiv:hep-ph/0203223].
- [84] D. Ida, K. y. Oda and S. C. Park, “Rotating black holes at future colliders: Greybody factors for brane fields,” *Phys. Rev. D* **67**, 064025 (2003) [Erratum-ibid. *D* **69**, 049901 (2004)] [arXiv:hep-th/0212108].
- [85] D. Ida, K. y. Oda and S. C. Park, “Rotating black holes at future colliders. III: Determination of black hole evolution,” *Phys. Rev. D* **73**, 124022 (2006) [arXiv:hep-th/0602188].
- [86] D. Ida, K. y. Oda and S. C. Park, private communication.
- [87] D. N. Page, “Particle Emission Rates From A Black Hole: Massless Particles From An Uncharged, Nonrotating Hole,” *Phys. Rev. D* **13**, 198 (1976).
- [88] W. G. Unruh, “Absorption Cross-Section Of Small Black Holes,” *Phys. Rev. D* **14**, 3251 (1976).
- [89] N. G. Sanchez, “Absorption And Emission Spectra Of A Schwarzschild Black Hole,” *Phys. Rev. D* **18**, 1030 (1978).
- [90] T. Banks and W. Fischler, “A model for high energy scattering in quantum gravity,” arXiv:hep-th/9906038.
- [91] K. Arisaka, G. B. Gelmini, M. Healy, O. Kalashev and J. Lee, “Composition of UHECR and the Pierre Auger Observatory Spectrum,” *JCAP* **0712**, 002 (2007) [arXiv:0709.3390 [astro-ph]].
- [92] A. Dar and A. De Rujula, “A theory of cosmic rays,” arXiv:hep-ph/0606199.
- [93] J. L. Feng and A. D. Shapere, “Black hole production by cosmic rays,” *Phys. Rev. Lett.* **88**, 021303 (2002) [arXiv:hep-ph/0109106].
- [94] L. A. Anchordoqui, J. L. Feng, H. Goldberg and A. D. Shapere, “Black holes from cosmic rays: Probes of extra dimensions and new limits on TeV-scale gravity,” *Phys. Rev. D* **65**, 124027 (2002) [arXiv:hep-ph/0112247].
- [95] M. Kowalski, A. Ringwald and H. Tu, “Black holes at neutrino telescopes,” *Phys. Lett. B* **529**, 1 (2002) [arXiv:hep-ph/0201139].
- [96] A. Ringwald and H. Tu, “Collider versus cosmic ray sensitivity to black hole production,” *Phys. Lett. B* **525**, 135 (2002) [arXiv:hep-ph/0111042].

- [97] C. Tyler, A. V. Olinto and G. Sigl, “Cosmic neutrinos and new physics beyond the electroweak scale,” *Phys. Rev. D* **63**, 055001 (2001) [arXiv:hep-ph/0002257].
- [98] S. I. Dutta, M. H. Reno and I. Sarcevic, “On black hole detection with the OWL/Airwatch telescope,” *Phys. Rev. D* **66**, 033002 (2002) [arXiv:hep-ph/0204218].
- [99] S. I. Dutta, M. H. Reno and I. Sarcevic, “Ultrahigh energy neutrinos,” *Int. J. Mod. Phys. A* **18**, 4085 (2003) [arXiv:hep-ph/0302178].
- [100] E. Waxman and J. N. Bahcall, “High energy neutrinos from astrophysical sources: An upper bound,” *Phys. Rev. D* **59**, 023002 (1999) [arXiv:hep-ph/9807282].
- [101] J. N. Bahcall and E. Waxman, “High energy astrophysical neutrinos: The upper bound is robust,” *Phys. Rev. D* **64**, 023002 (2001) [arXiv:hep-ph/9902383].
- [102] V. S. Beresinsky and G. T. Zatsepin, “Cosmic rays at ultrahigh-energies (neutrino?),” *Phys. Lett. B* **28**, 423 (1969).
- [103] F. W. Stecker, “Diffuse Fluxes Of Cosmic High-Energy Neutrinos,” *Astrophys. J.* **228**, 919 (1979).
- [104] C. T. Hill and D. N. Schramm, “Ultrahigh-energy cosmic ray neutrinos,” *Phys. Lett. B* **131**, 247 (1983).
- [105] L. A. Anchordoqui, D. Hooper, S. Sarkar and A. M. Taylor, “High-energy neutrinos from astrophysical accelerators of cosmic ray nuclei,” *Astropart. Phys.* **29**, 1 (2008) [arXiv:astro-ph/0703001].
- [106] Z. Li and E. Waxman, “EeV neutrinos associated with UHECR sources,” arXiv:0711.4969 [hep-ph].
- [107] F. Halzen and D. Hooper, “High-energy neutrino astronomy: The cosmic ray connection,” *Rept. Prog. Phys.* **65**, 1025 (2002) [arXiv:astro-ph/0204527].
- [108] G. Corcella *et al.*, “HERWIG 6: An event generator for hadron emission reactions with interfering gluons (including supersymmetric processes),” *JHEP* **0101**, 010 (2001) [arXiv:hep-ph/0011363].
- [109] D. R. Lorimer, “Binary and Millisecond Pulsars,” *Living Rev. Rel.* **8**, 7 (2005) [arXiv:astro-ph/0511258].
- [110] F. Verbunt and E.P.J. van den Heuvel, “Formation and evolution of neutron stars and black holes in binaries”, in “X-Ray Binaries”, W.H.G. Lewin, J. van Paradijs, and E.P.J. van den Heuvel eds., (1995).
- [111] P.P Eggleton, “Approximations to the radii of Roche lobes”, *Astrophys. J.* **268**, 368 (1983).

- [112] L. Bildsten *et al.*, “Observations of Accreting Pulsars,” *Astrophys. J.* **113**, 367 (1997), arXiv:astro-ph/9707125.
- [113] C.J. Hansen and S.D. Kawaler, ” *Stellar Interiors*” (New York: Springer), 1994
- [114] L. Bildsten and D. Chakrabarty, “A Brown Dwarf Companion for the Accreting Millisecond Pulsar SAX J1808.4-3658”, *Astrophys. J.* **557**, 292 (2001), arxiv:astro-ph/0104153.
- [115] C. J. Deloye and L. Bildsten, “White Dwarf Donors in Ultracompact Binaries: The Stellar Structure of Finite Entropy Objects”, *Astrophys. J.* **598**, 1217 (2003) [arXiv:astro-ph/0308233].
- [116] L. Bildsten, private communication.
- [117] J. Liebert, P. A. Young, D. Arnett, J. B. Holberg and K. A. Williams, “The Age and Progenitor Mass of Sirius B,” *Astrophys. J.* **630**, L69 (2005) [arXiv:astro-ph/0507523].
- [118] P. Draggiotis, M. Masip and I. Mastromatteo, “Hawking evaporation of cosmogenic black holes in TeV-gravity models,” arXiv:0805.1344 [hep-ph].
- [119] M. Kamionkowski and A. Kinkhabwala, “Galactic halo models and particle dark matter detection,” *Phys. Rev. D* **57**, 3256 (1998) [arXiv:hep-ph/9710337].